Experimental High Energy Physics at Colliders
Lecture 3: Reconstruction of Objects - 1

1. Calorimeters, electrons, Jets
2. Muons
3. MET & Co

Tile Calorimeter (TileCal)

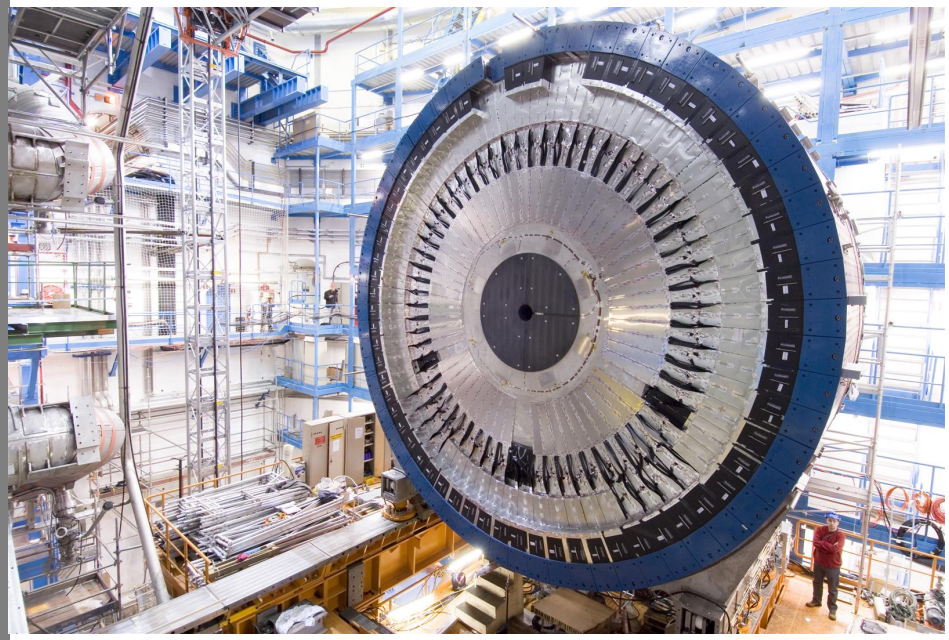

Liquid Argon (LAr) Calorimeter

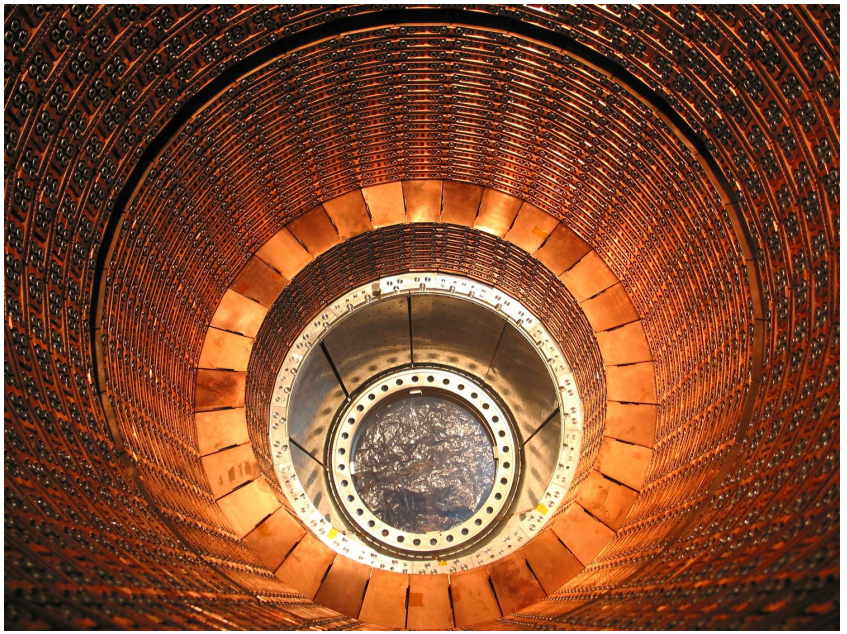

Calorimeters: Energy Calibration and Resolution

Calorimetry

Design goals:

Precise energy measurement of electrons,photons, jets & measurement of missing transverse energy, MET.

Partial Particle-ID via shower reconstruction

Needs:

Good intrinsic energy resolution

High granularity, hermetic detector (“no cracks”)

Large depth to contain full shower

Trigger capabilities, i.e. fast identification of high energy deposits

Calorimeter energy resolution:

[complementary to tracker: resolution improves with energy]

$$\frac{\sigma(E)}{E} = \frac{a}{\sqrt{E}} + b + \frac{c}{E}$$

Stochastic term: shower fluctuations

Shower leakage, calibration

Electronics noise

ATLAS Calorimeter System

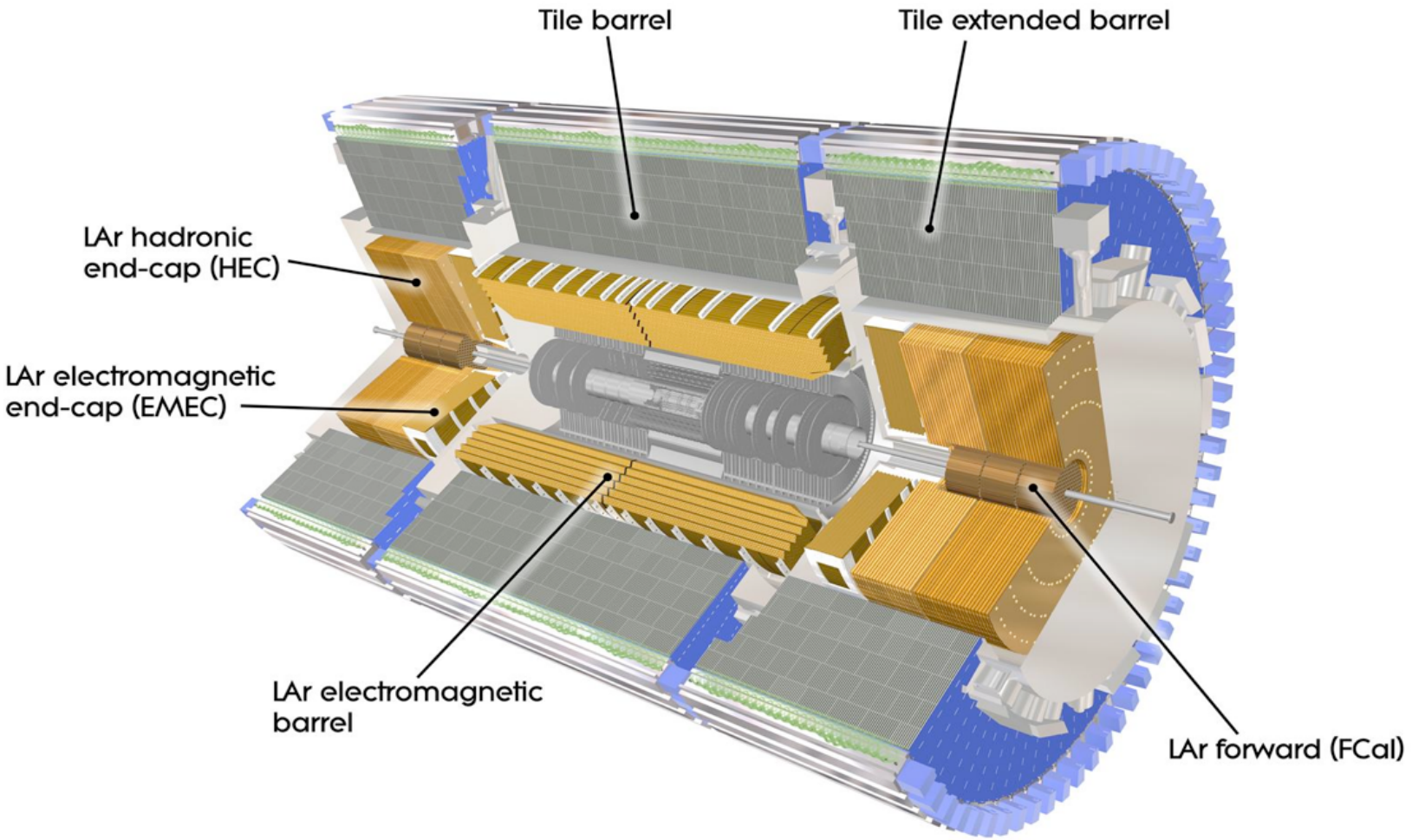

ATLAS & CMS Calorimeters

Issue	ATLAS	CMS
Position	Outside solenoid coil i.e. up to 4 X_0 dead material in front of ECAL	Inside solenoid coil i.e. limited calorimeter depth [HCAL: only 7.2 λ at η=0]
ECAL	Lead/liquid argon (LAr) sampling calorimeter i.e. excellent granularity and longitudinal segmentation	Homogeneous crystal calorimeter [$PbWO_4$] excellent intrinsic energy resolution for e/γ
HCAL	Sampling Calorimeter Barrel: iron/scintillating tiles End-caps: copper/LAr	Sampling Calorimeter brass/scintillating tiles

Energy Calibration

ATLAS Test Beam Results

Fixed energy electron beam

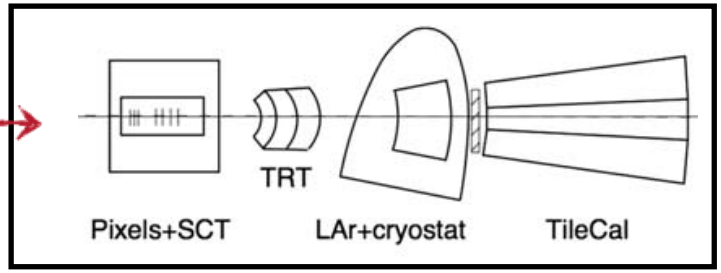

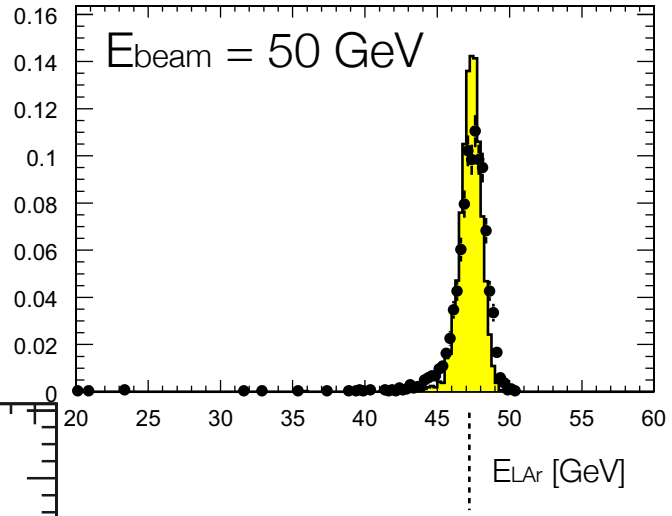

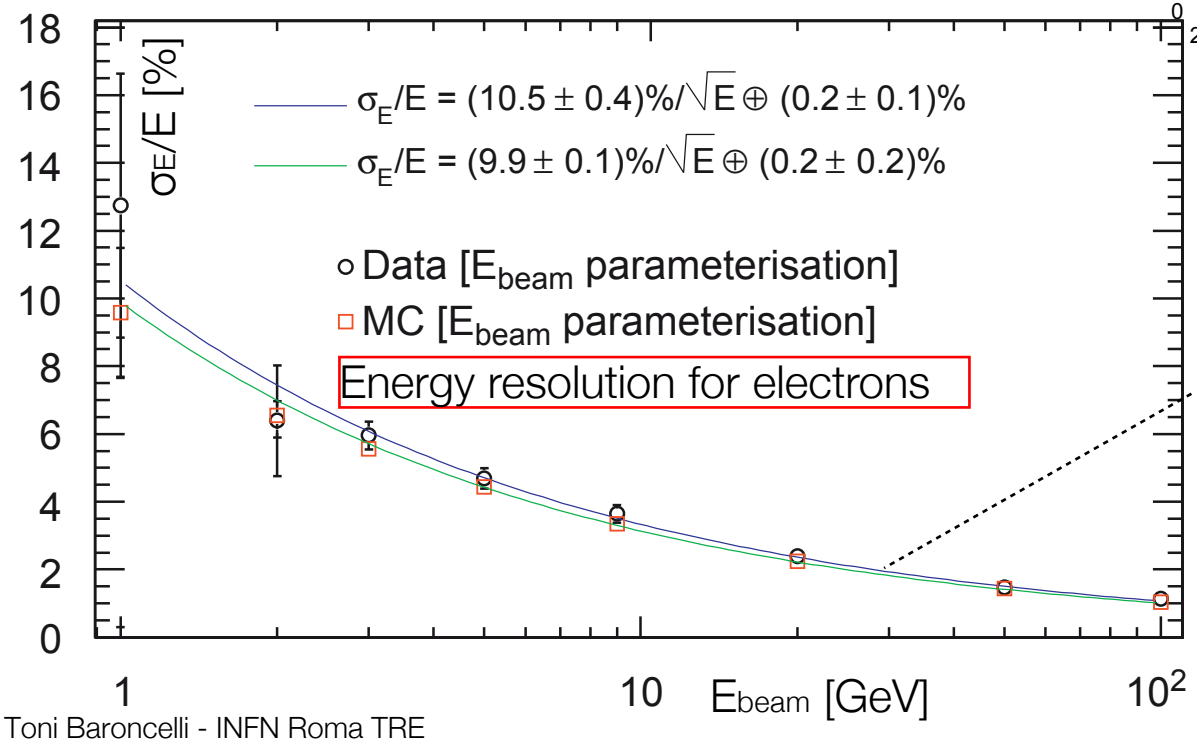

Position yields calibration factor

Width yields energy resolution

Nominal:

ATLAS : $\sigma_E/E \sim 10\%/\sqrt{E}$

CMS : $\sigma_E/E \sim 13\%/\sqrt{E}$

Testing the Electromagnetic Energy Scale

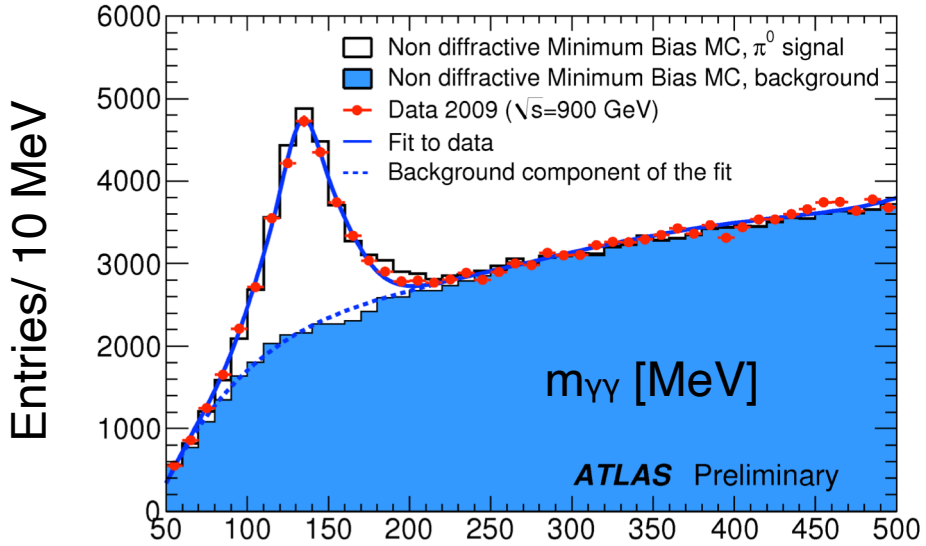

$\pi^0 \rightarrow \gamma\gamma$

$\Xi_T > 0.4$ GeV, $P_{T,pair} > 0.9$ GeV, $f_1 > 0.1$

Dedicated calibration for low E_T photons]

Data: $m_\pi = 134.0 \pm 0.8$ (stat) MeV; $\sigma = 24.0$ MeV

MC: $m_\pi = 132.9 \pm 0.2$ (stat) MeV; $\sigma = 25.2$ MeV

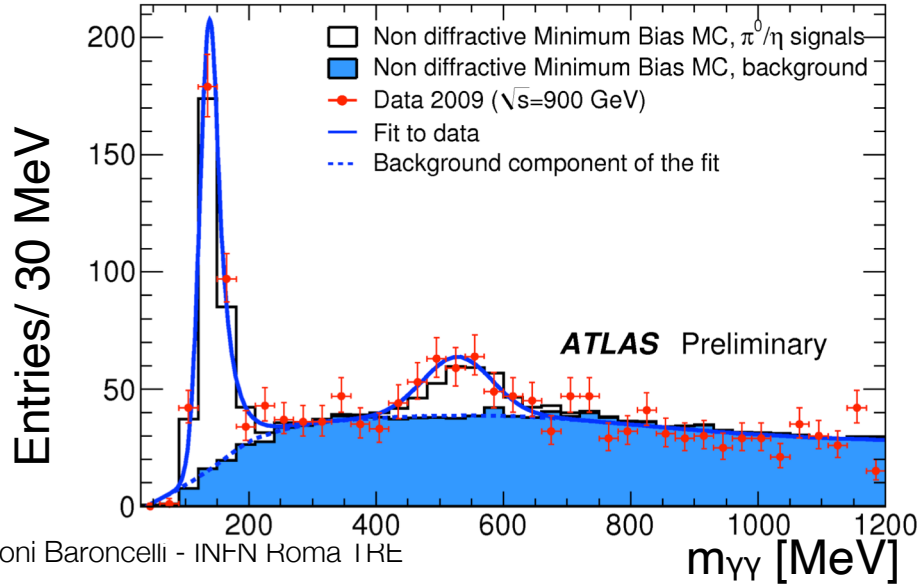

$\pi^0 \rightarrow \gamma\gamma$

$\eta \rightarrow \gamma\gamma$

$E_T > 0.8$ GeV, $P_{T,pair} > 2.2$ GeV track veto

[Dedicated calibration for low E^T photons]

Data: $m_\eta = 527 \pm 11$ (stat) MeV

MC: $m_\eta = 544 \pm 3$ (stat) MeV

Physics with Electrons & Photons

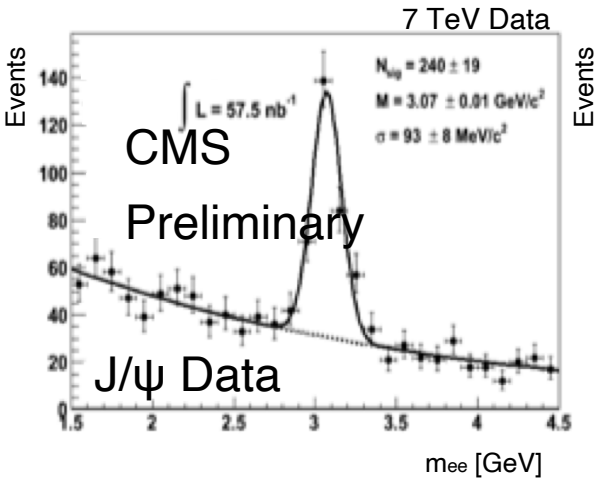

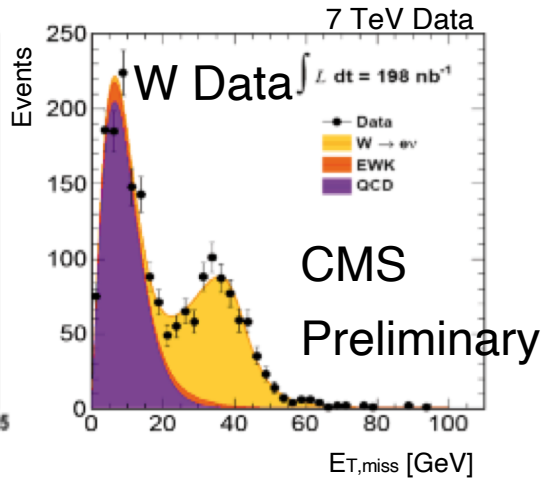

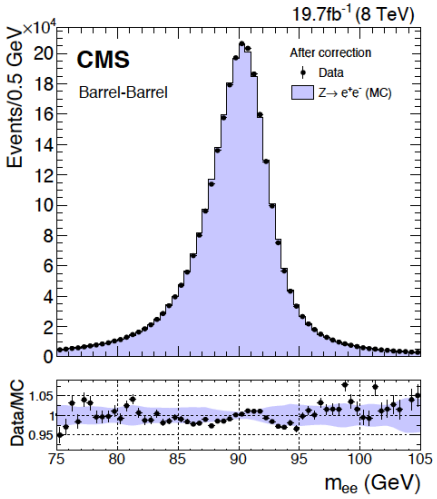

Electrons

Future

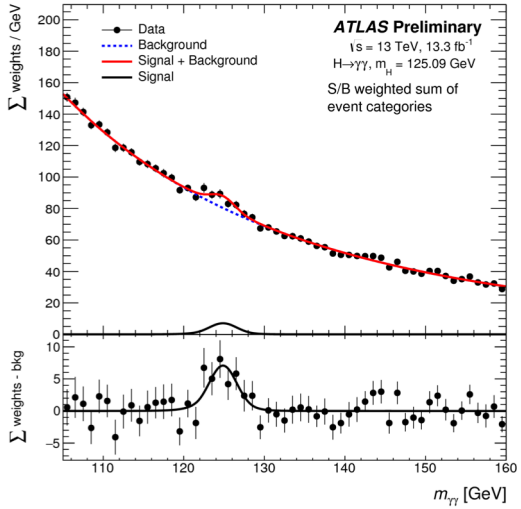

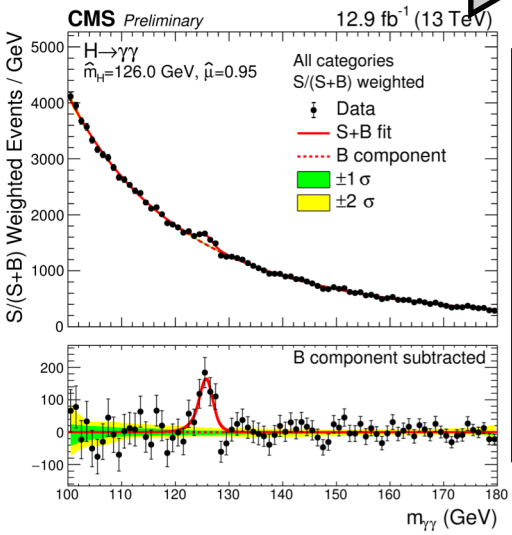

Photons

Jets & Jet Energy Measurement

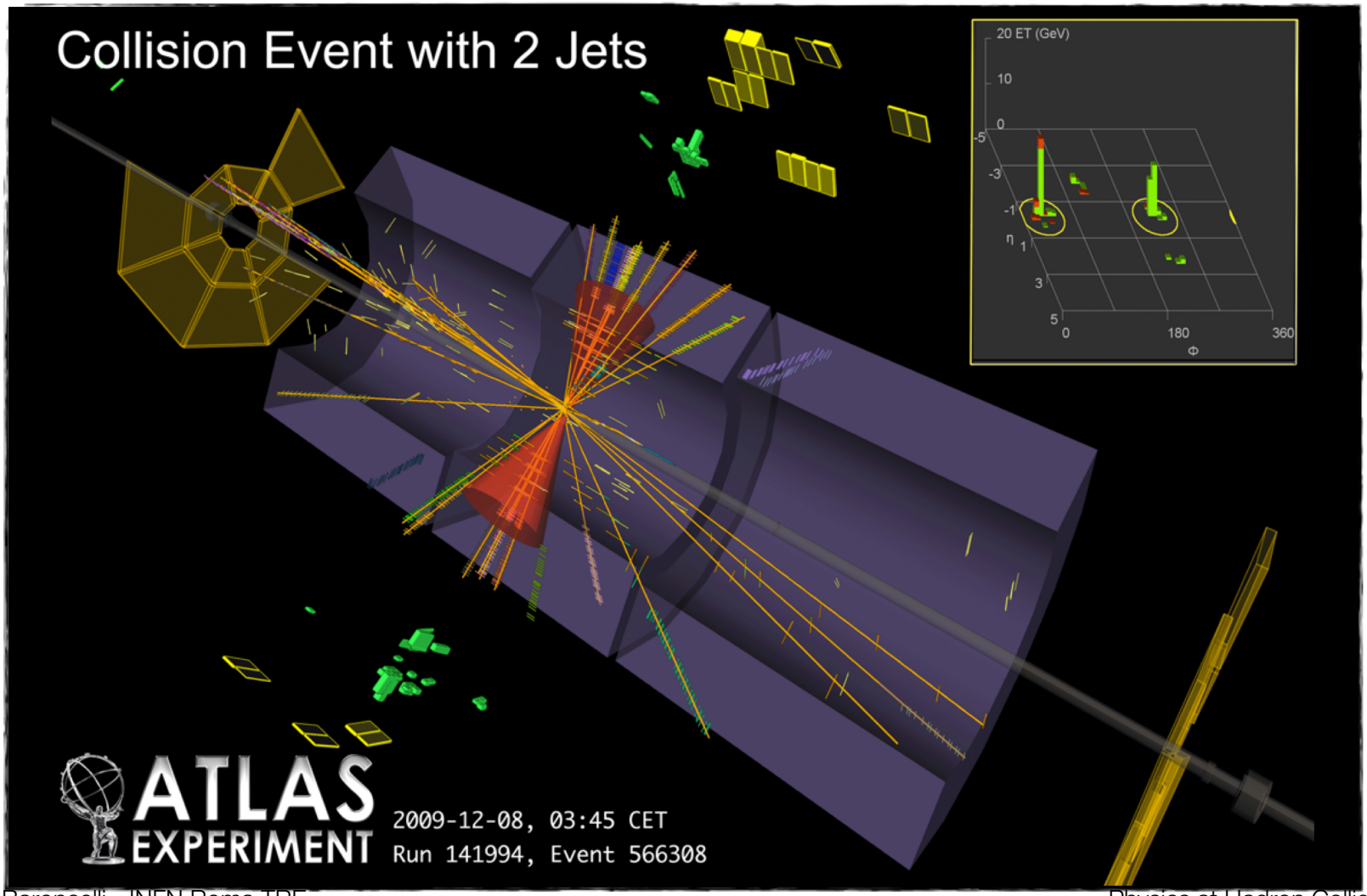

Jet Energy Measurement

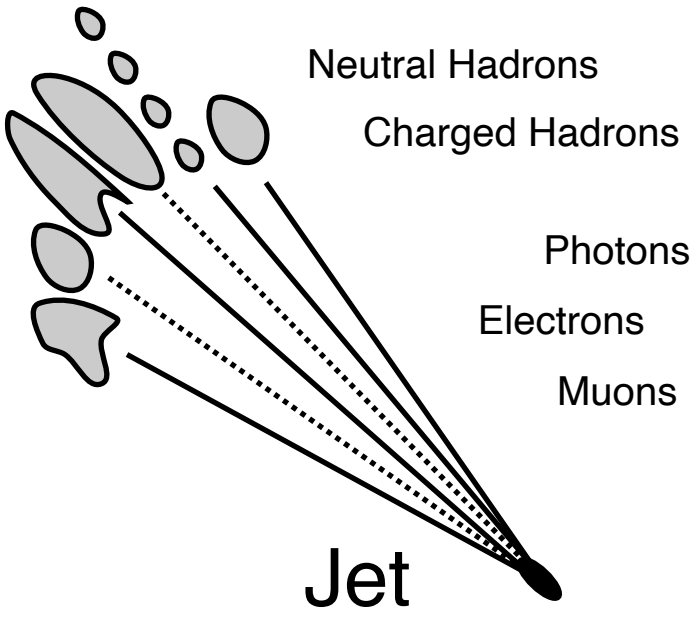

Hadronic showers may develop across EM + HC !!

Problems:

- Non-compensation
  [hadronic vs. electromagnetic energy]
- Missing energy
  [e.g. muon tracks]
- Double counting
  [when using track momenta]

A Particle Flow Calorimetry

Reduce role of 'hadron' calorimetry to measurement of n, K^0

B Compensating Calorimetry

Correcting hadronic energy for nuclear-binding energy loss.

Jet Energy Measurement, which Jet?

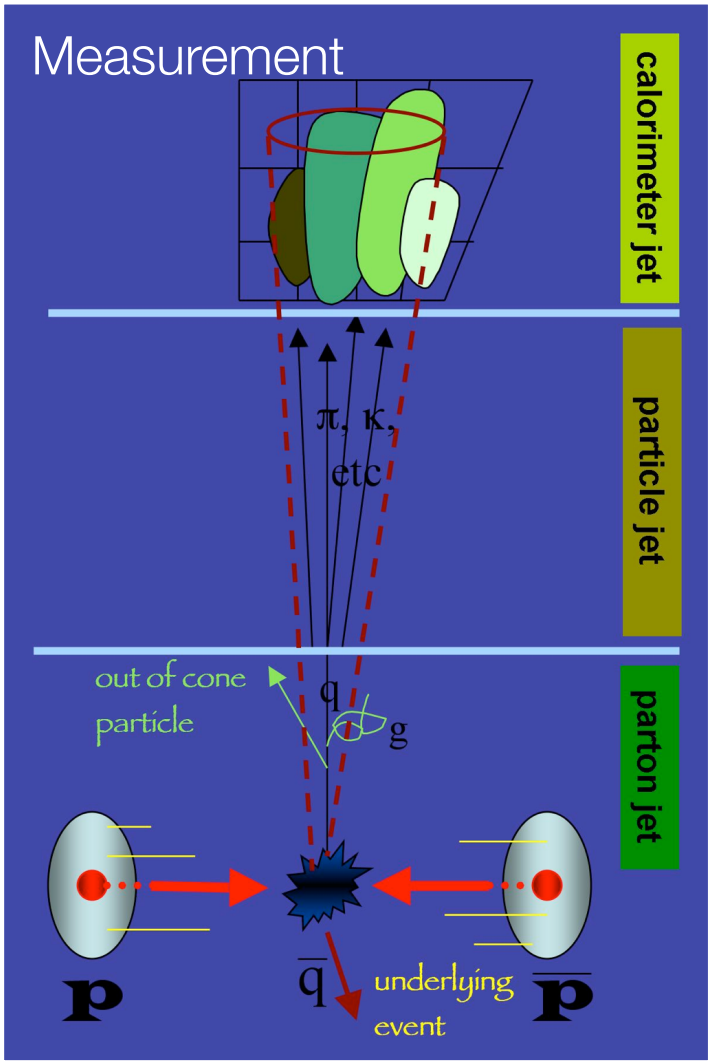

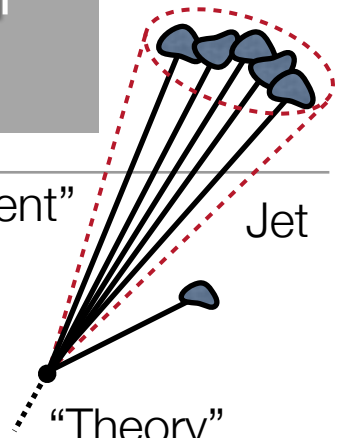

"Measurement" Jet

"Theory"

Calorimeter Jet

[extracted from calorimeter clusters]

Understanding of detector response

Knowledge about dead material

Correct signal calibration

Potentially include tracks

From measured energy to particle energy

Hadron Jet

[might include electrons, muons ...]

Hadronization

Fragmentation

Parton shower

Particle decays

Compensate energy loss due to neutrinos, nuclear excitation ...

From particle energy to original parton energy

Parton Jet

[quarks and gluons]

Compensate hadronization; energy in/outside jet cone ...

Proton-proton interactions

Initial and final state radiation

Underlying event

Needs Calibration

Jet Energy Measurement

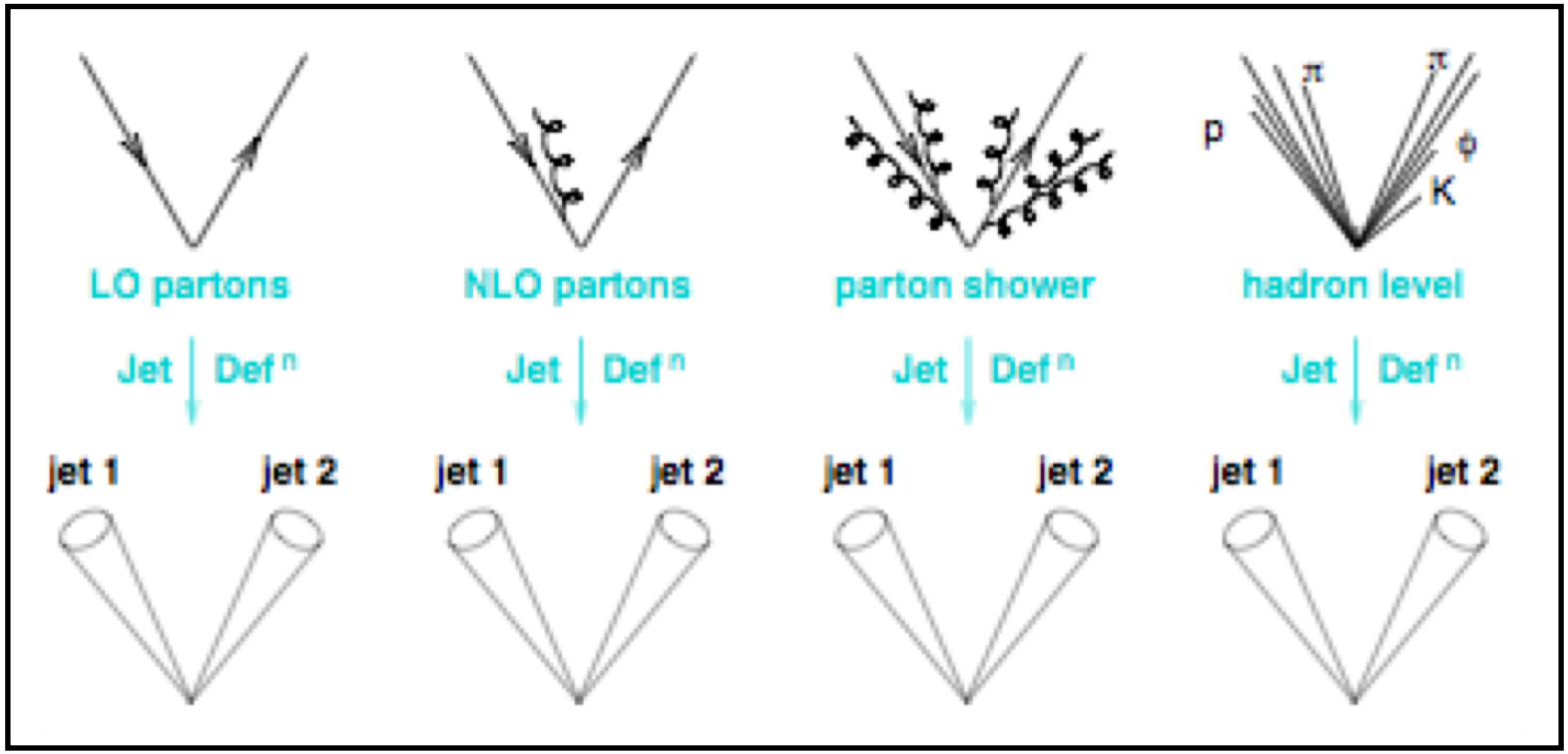

Jets may look different at different levels

Robust jet definition ➛ stable on all jet levels

Jet Reconstruction

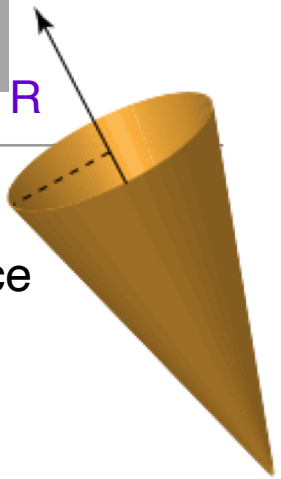

Iterative cone algorithms:

Jet defined as energy flow within a cone of radius R in (y,ϕ) or (η,ϕ) space:

$$R = \sqrt{(y - y_0)^2 + (\phi - \phi_0)^2}$$

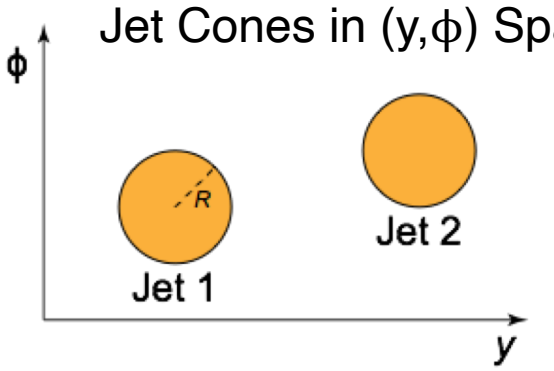

Sequential recombination algorithms:

Define distance measure d_{ij} ...
Calculate d_{ij} for all pairs of objects ...
Combine particles with minimum d_{ij} below cut ...
Stop if minimum d_{ij} above cut ...

e.g. k_T-algorithm:
[see later]

$$d_{ij} = \min\left(k_{T,i}^2, k_{T,j}^2\right) \frac{\Delta R ij}{R}$$

Sequential recombination

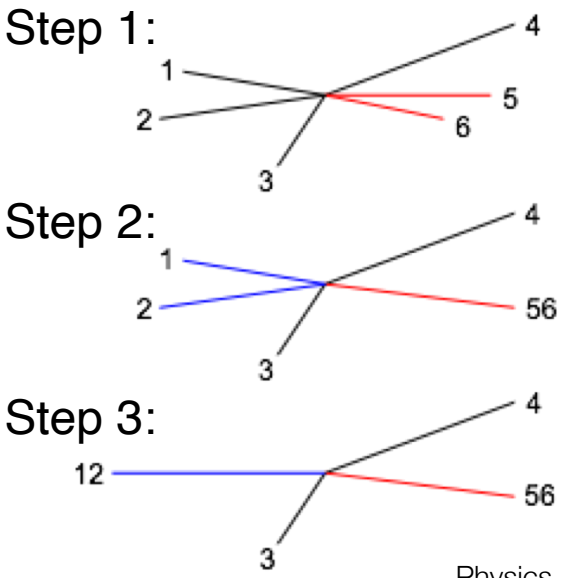

(Anti-) k_t jet clustering

The anti-k_t jet clustering algorithm

Matteo Cacciari and Gavin P. Salam
LPTHE
UPMC Université Paris 6,
Université Paris Diderot – Paris 7,
CNRS UMR 7589, Paris, France

Gregory Soyez
Brookhaven National Laboratory, Upton, NY, USA

Abstract: The k_t and Cambridge/Aachen inclusive jet finding algorithms for hadron-hadron collisions can be seen as belonging to a broader class of sequential recombination jet algorithms, parametrised by the power of the energy scale in the distance measure. We examine some properties of a new member of this class, for which the power is negative. This "anti-k_t" algorithm essentially behaves like an idealised cone algorithm, in that jets with only soft fragmentation are conical, active and passive areas are equal, the area anomalous dimensions are zero, the non-global logarithms are those of a rigid boundary and the Milan factor is universal. None of these properties hold for existing sequential recombination algorithms, nor for cone algorithms with split–merge steps, such as SISCone. They are however the identifying characteristics of the collinear unsafe plain "iterative cone" algorithm, for which the anti-k_t algorithm provides a natural, fast, infrared and collinear safe replacement.

1 Introduction and definition

Jet clustering algorithms are among the main tools for analysing data from hadronic collisions. Their widespread use at the Tevatron and the prospect of unprecedented final-state complexity at the upcoming Large Hadron Collider (LHC) have stimulated considerable debate concerning the merits of different kinds of jet algorithm. Part of the discussion has centred on the relative advantages of sequential recombination (k_t [1] and Cambridge/Aachen [2]) and cone (e.g. [3]) jet algorithms, with an issue of particular interest being that of the regularity of the boundaries of the resulting jets. This is related to the question of their sensitivity to non-perturbative effects like hadronisation and underlying event contamination and arises also in the context of experimental calibration.

Recently [4], tools have been developed that allow one, for the first time, to support the debate with analytical calculations of the contrasting properties of boundaries of jets within different algorithms. One of the main results of that work is that all known infrared and collinear (IRC) safe algorithms have the property that soft radiation can provoke irregularities in the boundaries of the final jets. This is the case even for SISCone [5], an IRC-safe jet algorithm based on the search for stable cones, together with a split–merge step that disentangles overlapping stable cones. One might describe current IRC-safe algorithms in general as having a 'soft-adaptable' boundary.

A priori it is not clear whether it is better to have regular ('soft-resilient') or less regular (soft-adaptable) jets. In particular, regularity implies a certain rigidity in the jet algorithm's ability to adapt a jet to the successive branching nature of QCD radiation. On the other hand knowledge of the typical shape of jets is often quoted as facilitating experimental calibration of jets, and soft-resilience can simplify certain theoretical calculations, as well as eliminate some parts of the momentum-resolution loss caused by underlying-event and pileup contamination.

Examples of jet algorithms with a soft-resilient boundary are the plain "iterative cone" algorithm, as used for example in the CMS collaboration [6], and fixed-cone algorithms such as Pythia's [7] CellJet. The CMS iterative cone takes the hardest object (particle, calorimeter tower) in the event, uses it to seed an iterative process of looking for a stable cone, which is then called a jet. It then removes all the particles contained in that jet from the event and repeats the procedure with the hardest available remaining seed, again and again until no seeds remain. The fixed-cone algorithms are similar, but simply define a jet as the cone around the hardest seed, skipping the iterative search for a stable cone. Though simple experimentally, both kinds of algorithm have the crucial drawback that if applied at particle level they are collinear unsafe, since the hardest particle is easily changed by a quasi-collinear splitting, leading to divergences in higher-order perturbative calculations.[1]

In this paper it is not our intention to advocate one or other type of algorithm in the debate concerning soft-resilient versus soft-adaptable algorithms. Rather, we feel that this debate can be more fruitfully served by proposing a simple, IRC safe, soft-resilient jet algorithm, one that leads to jets whose shape is not influenced by soft radiation. To do so, we take a quite non-obvious route, because instead of making use of the concept of a stable cone, we start by generalising the existing sequential recombination algorithms, k_t [1] and Cambridge/Aachen [2].

As usual, one introduces distances d_{ij} between entities (particles, pseudojets) i and j and d_{iB} between entity i and the beam (B). The (inclusive) clustering proceeds by identifying the smallest of the distances and if it is a d_{ij} recombining entities i and j, while if it is d_{iB} calling i a jet and removing it from the list of entities. The distances are recalculated and the procedure repeated until no entities are left.

The extension relative to the k_t and Cambridge/Aachen algorithms lies in our definition of the distance measures:

$$d_{ij} = \min(k_{ti}^{2p}, k_{tj}^{2p}) \frac{\Delta_{ij}^2}{R^2}, \tag{1a}$$

$$d_{iB} = k_{ti}^{2p}, \tag{1b}$$

where $\Delta_{ij}^2 = (y_i - y_j)^2 + (\phi_i - \phi_j)^2$ and k_{ti}, y_i and ϕ_i are respectively the transverse momentum, rapidity and azimuth of particle i. In addition to the usual radius parameter R, we have added a parameter p to govern the relative power of the energy versus geometrical (Δ_{ij}) scales.

For $p = 1$ one recovers the inclusive k_t algorithm. It can be shown in general that for $p > 0$ the behaviour of the jet algorithm with respect to soft radiation is rather similar to that observed for the k_t algorithm, because what matters is the ordering between particles and for finite Δ this is maintained for all positive values of p. The case of $p = 0$ is special and it corresponds to the inclusive Cambridge/Aachen algorithm.

[1] This is discussed in the appendix in detail for the iterative cone, and there we also introduce the terminology iterative cone with split–merge steps (IC-SM) and iterative cone with progressive removal (IC-PR), so as to distinguish the two broad classes of iterative cone algorithms.

The ingredients and the method - 2

Negative values of p might at first sight seem pathological. We shall see that they are not.[2] The behaviour with respect to soft radiation will be similar for all $p < 0$, so here we will concentrate on $p = -1$, and refer to it as the "anti-k_t" jet-clustering algorithm.

2 Characteristics and properties

2.1 General behaviour

The functionality of the anti-k_t algorithm can be understood by considering an event with a few well-separated hard particles with transverse momenta k_{t1}, k_{t2}, ... and many soft particles. The $d_{1i} = \min(1/k_{t1}^2, 1/k_{ti}^2)\Delta_{1i}^2/R^2$ between a hard particle 1 and a soft particle i is exclusively determined by the transverse momentum of the hard particle and the Δ_{1i} separation. The d_{ij} between similarly separated soft particles will instead be much larger. Therefore soft particles will tend to cluster with hard ones long before they cluster among themselves. If a hard particle has no hard neighbours within a distance $2R$, then it will simply accumulate all the soft particles within a circle of radius R, resulting in a perfectly conical jet.

If another hard particle 2 is present such that $R < \Delta_{12} < 2R$ then there will be two hard jets. It is not possible for both to be perfectly conical. If $k_{t1} \gg k_{t2}$ then jet 1 will be conical and jet 2 will be partly conical, since it will miss the part overlapping with jet 1. Instead if $k_{t1} = k_{t2}$ neither jet will be conical and the overlapping part will simply be divided by a straight line equally between the two. For a general situation, $k_{t1} \sim k_{t2}$, both cones will be clipped, with the boundary b between them defined by $\Delta R_{1b}/k_{t1} = \Delta_{2b}/k_{t2}$.

Similarly one can work out what happens with $\Delta_{12} < R$. Here particles 1 and 2 will cluster to form a single jet. If $k_{t1} \gg k_{t2}$ then it will be a conical jet centred on k_1. For $k_{t1} \sim k_{t2}$ the shape will instead be more complex, being the union of cones (radius $< R$) around each hard particle plus a cone (of radius R) centred on the final jet.

The key feature above is that the soft particles do not modify the shape of the jet, while hard particles do. I.e. the jet boundary in this algorithm is resilient with respect to soft radiation, but flexible with respect to hard radiation.[3]

The behaviours of different jet algorithms are illustrated in fig. 1. We have taken a parton-level event together with $\sim 10^4$ random soft 'ghost' particles (as in [4]) and then clustered them with 4 different jet algorithms. For each of the partonic jets, we have shown the region within which the random ghosts are clustered into that jet. For the k_t and Cambridge/Aachen algorithms, that region depends somewhat on the specific set of ghosts and the jagged borders of the jets are a consequence of the randomness of the ghosts — the jet algorithm is adaptive in its response to soft particles, and that adaptiveness applies also to the ghosts which take part in the clustering. For SISCone one sees that single-particle jets are regular (though with a radius $R/2$ — as pointed out in [4]), while composite jets have more varied shapes. Finally with the anti-k_t algorithm, the hard jets are all circular with a radius R, and only the softer jets have more complex shapes. The pair of jets near $\phi = 5$ and $y = 2$ provides an interesting example in this respect. The left-hand one is much softer than the right-hand one. SISCone (and Cam/Aachen) place the boundary between

[2] Note that, for $p < 0$, $\min(k_{ti}^{2p}, k_{tj}^{2p})$ differs from another possible extension, $|\min(k_{ti}^2, k_{tj}^2)|^p$, which can lead to strange behaviours.

[3] For comparison, IC-PR algorithms behave as follows: with $R < \Delta_{12} < 2R$, the harder of the two jets will be fully conical, while the softer will be clipped regardless of whether p_{t1} and p_{t2} are similar or disparate scales; with $\Delta_{12} < R$ the jet will be just a circle centred on the final jet.

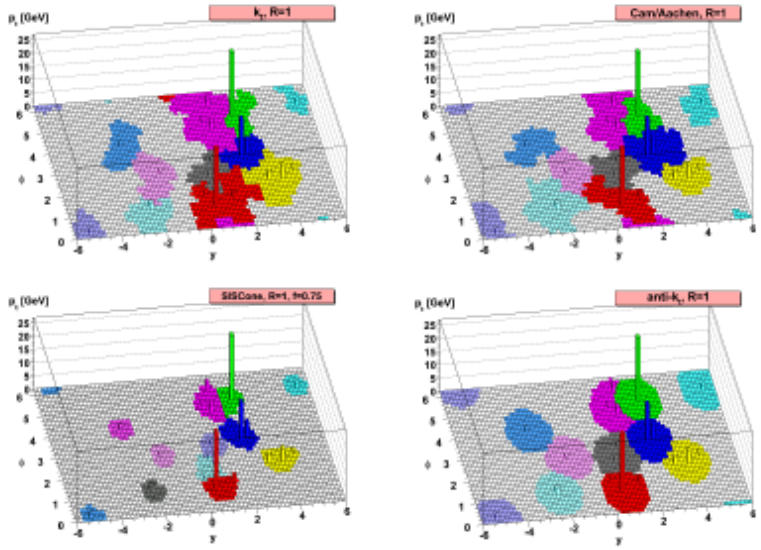

Figure 1: A sample parton-level event (generated with Herwig [8]), together with many random soft "ghosts", clustered with four different jets algorithms, illustrating the "active" catchment areas of the resulting hard jets. For k_t and Cam/Aachen the detailed shapes are in part determined by the specific set of ghosts used, and change when the ghosts are modified.

the jets roughly midway between them. Anti-k_t instead generates a circular hard jet, which clips a lens-shaped region out of the soft one, leaving behind a crescent.

The above properties of the anti-k_t algorithm translate into concrete results for various quantitative properties of jets, as we outline below.

2.2 Area-related properties

The most concrete context in which to quantitatively discuss the properties of jet boundaries for different algorithms is in the calculation of jet areas.

Two definitions were given for jet areas in [4]: the passive area (a) which measures a jet's susceptibility to point-like radiation, and the active area (A) which measures its susceptibility to diffuse radiation. The simplest place to observe the impact of soft resilience is in the passive area for a jet consisting of a hard particle p_1 and a soft one p_2, separated by a $y - \phi$ distance Δ_{12}. In usual IRC safe jet algorithms (JA), the passive area $a_{\mathrm{JA},R}(\Delta_{12})$ is πR^2 when $\Delta_{12} = 0$, but changes when Δ_{12} is increased. In contrast, since the boundaries of anti-k_t jets are unaffected by soft radiation,

The ingredients and the method - 1

$$d_{ij} = \min(k_{ti}^{2p}, k_{tj}^{2p}) \frac{\Delta_{ij}^2}{R^2},$$
$$d_{iB} = k_{ti}^{2p},$$

d_{ij} distance between objects ij

d_{iB} distance between object i and beam

- k_{ti} is the transverse momentum
- $\Delta_{ij}^2 = (y_i - y_i)^2 + (\phi_i - \phi_i)^2$
- y_i is the rapidity (use also η)
- ϕ_i is the azimuthal angle
- R is a parameter → opening of the jet
- p is a parameter of the algorithm → energy hierarchy
  - p = -1, 0, 1

p=1 is the k_t algo, p=0 is the Cambridge/Aachen algo, p=-1 is the anti-k_t algo

The distance d_{ij}

$$d_{ij} = \min(k_{ti}^{2p}, k_{tj}^{2p}) \frac{\Delta_{ij}^2}{R^2},$$ $k_t = p_T$, R^2 algorithm parameter

p=0 is the Cambridge/Aachen $\rightarrow d_{ij} = \frac{\Delta_{ij}^2}{R^2}$

$$\Delta_{ij}^2 = (y_i - y_j)^2 + (\phi_i - \phi_j)^2$$

Object i : k_i, ϕ_i, η_i

Object j : k_{tj}, ϕ_j, η_j

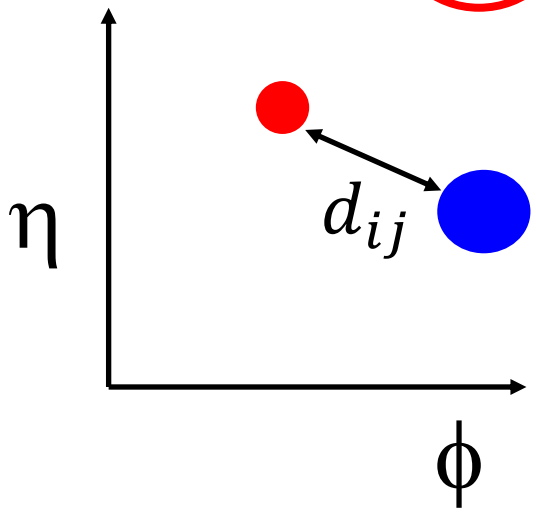

Jets for different k_T algos

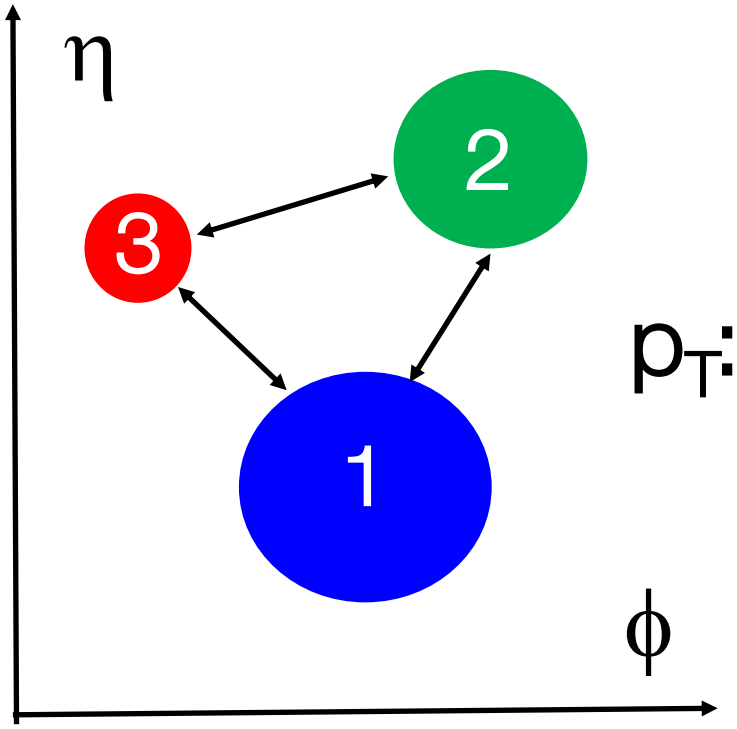

$$\Delta_{ij}^2 = (y_i - y_j)^2 + (\phi_i - \phi_j)^2$$

p_T: 1 > 2 > 3

$$d_{ij} = \min(k_{ti}^{2p}, k_{tj}^{2p}) \frac{\Delta_{ij}^2}{R^2},$$
$$d_{iB} = k_{ti}^{2p},$$

$\min(k_1^2, k_2^2)$

k_T ~p^2	anti-k_T ~p^{-2}
$d_{13}<d_{23}<d_{12}$	$d_{13}<d_{23}<d_{32}$

$\min(\frac{1}{k_1^2}, \frac{1}{k_2^2})$

The distance d_{ij} anti-k_T

$$d_{ij} = \min(k_{ti}^{2p}, k_{tj}^{2p}) \frac{\Delta_{ij}^2}{R^2}$$

$k_t = p_T$, R^2 algorithm parameter

p=-1 is anti-k_T algorithm $\rightarrow$ $d_{ij} = \frac{\Delta_{ij}^2}{R^2} \cdot \min(k_{ti}^{-2}, k_{tj}^{-2})$

$$\Delta_{ij}^2 = (y_i - y_j)^2 + (\phi_i - \phi_j)^2$$

Object i : k_{ti}, ϕ_i, η_i

Object j : k_{tj}, ϕ_j, η_j

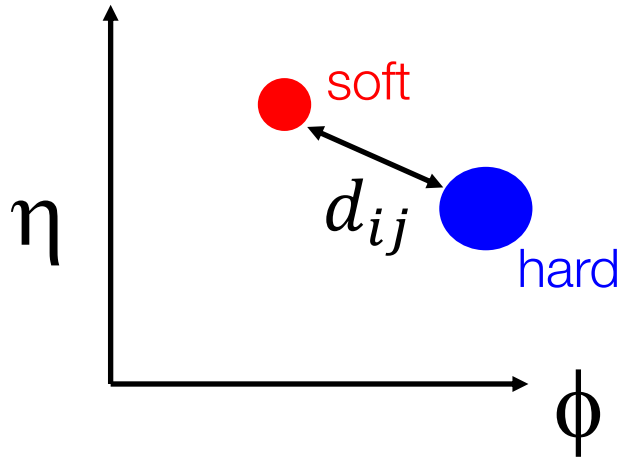

d_{ij} is determined by hard particles $\rightarrow$ soft particles cluster around hard ones!

The distance d_{ij} k_T

$$d_{ij} = \min(k_{ti}^{2p}, k_{tj}^{2p}) \frac{\Delta_{ij}^2}{R^2},$$ $k_t = p_T$, R^2 algorithm parameter

p=1 is k_T algorithm $\rightarrow d_{ij} = \frac{\Delta_{ij}^2}{R^2} \cdot \min(k_{ti}^2, k_{tj}^2)$

$$\Delta_{ij}^2 = (y_i - y_j)^2 + (\phi_i - \phi_j)^2$$

Object i : k_{ti}, ϕ_i, η_i

Object j : k_{tj}, ϕ_j, η_j

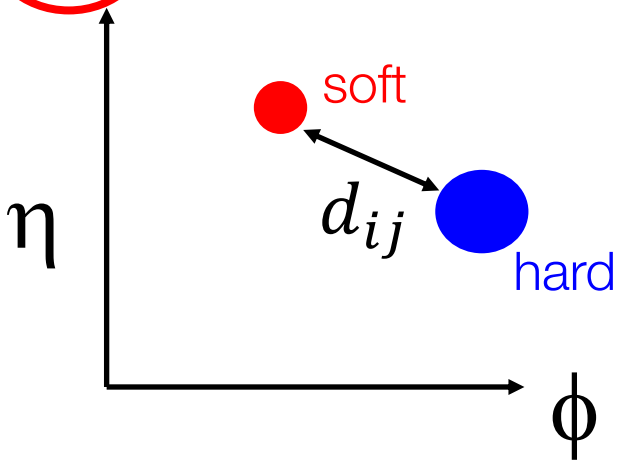

d_{ij} is determined by soft particles → soft particles cluster first!

Jets look different in different algos

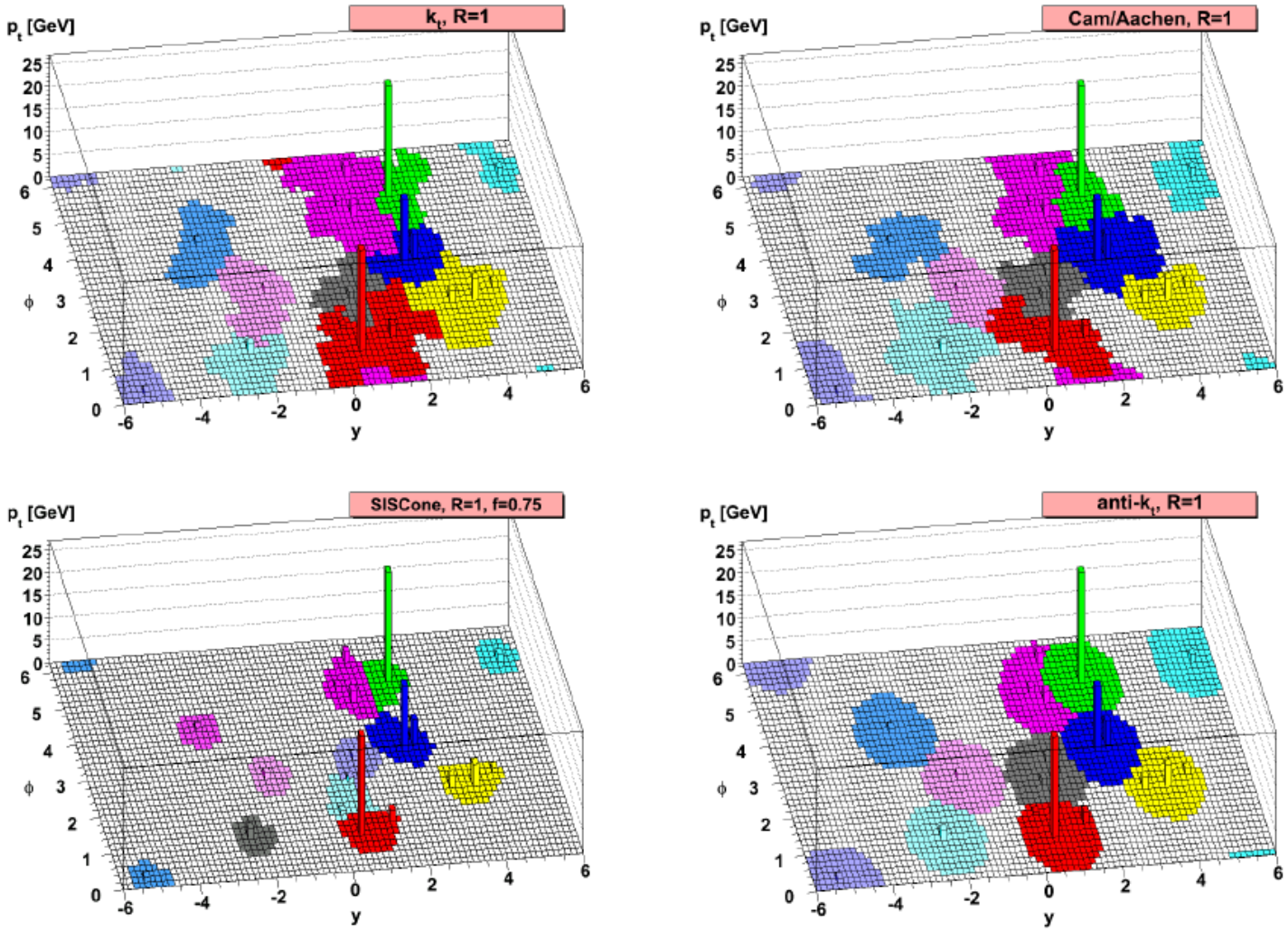

Jet Energy Calibration

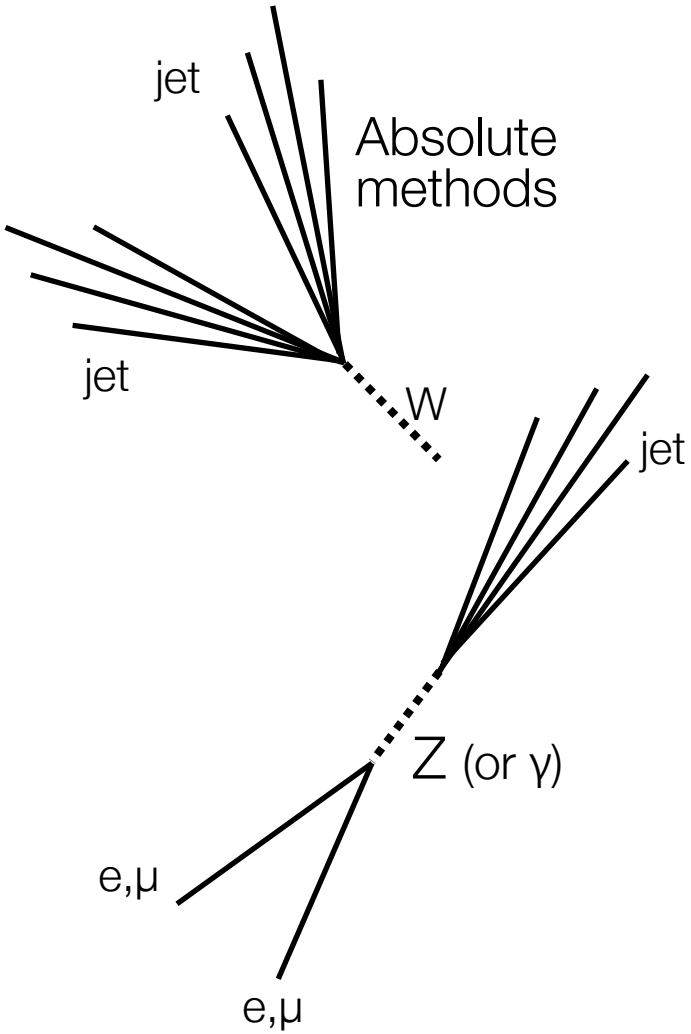

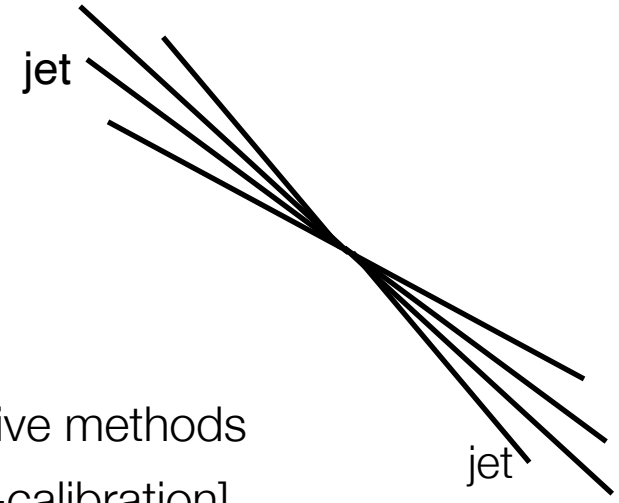

Relative methods
[Inter-calibration]

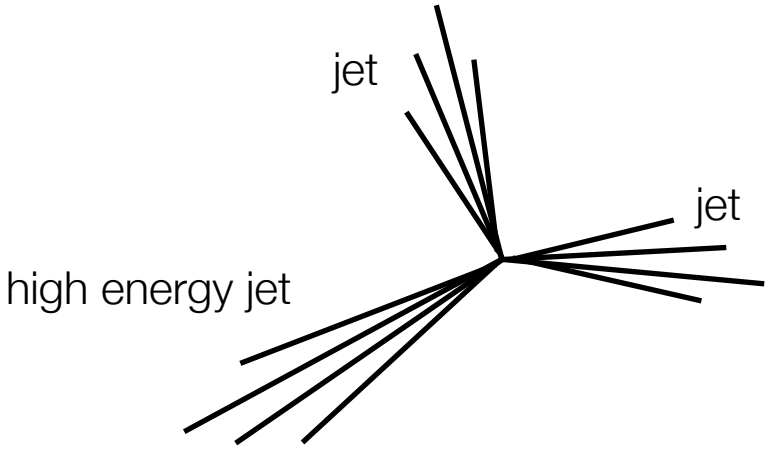

Jet Energy Calibration

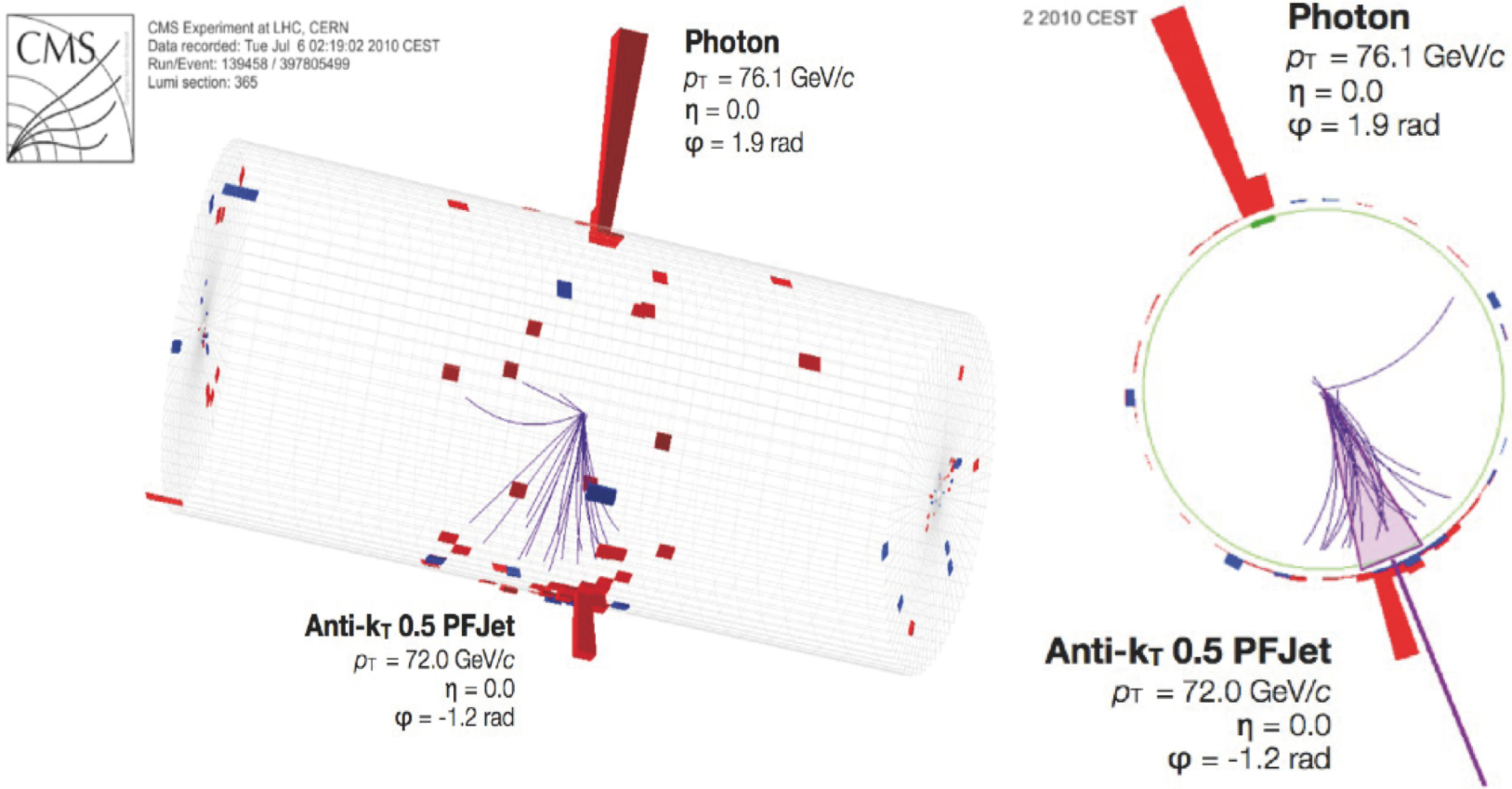

Absolute Method Uses p_t balance in back-to-back photon+jet events

Jets & Boosted Objects

X ATLAS Italia Workshop
10/02/2015
Matteo Franchini

Jets

- Jets are composite objects used to represent the final state partons clustering together their decay products → best jet definition can change depending on its purpose.
- Different jet types exist depending on:
  - jet-clustering algorithm used(*Anti-k_T* k_T, Cambridge / Aachen *C/A*);
  - jet constituent (truth particle, tracks, topo-cluster);
  - radius parameter, influencing the width of the jet;
- Jets are the basic ingredients for many analyses (di-jets, top, exotics…). **Accurate measurements of jet 4-momenta are required.**
- Raw detector (calorimeter) signals need to be **precisely calibrated combining MC and in-situ** (using data) calibration techniques.

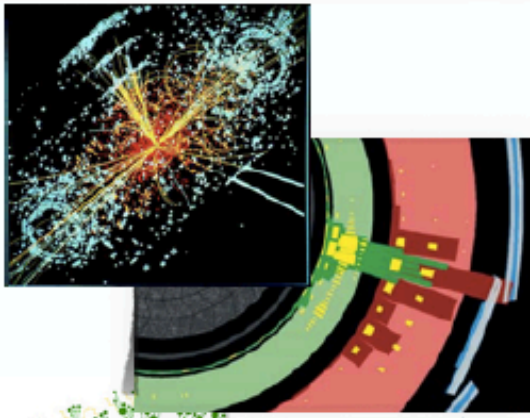
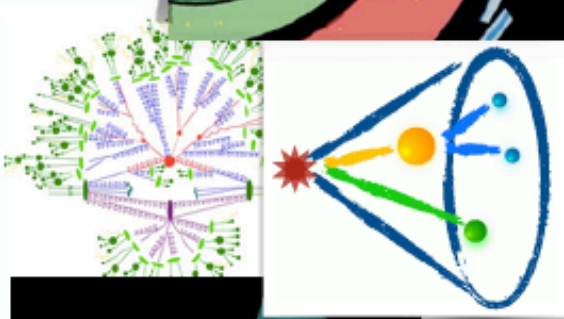
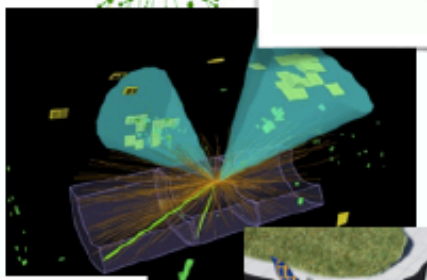

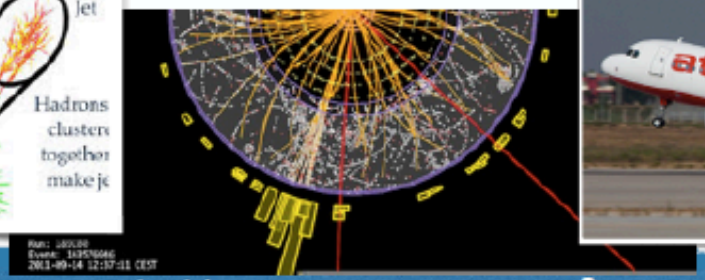


Jet reconstruction

Calorimeter jets

are → were!

Units in $|E|/\sigma_{noise}$

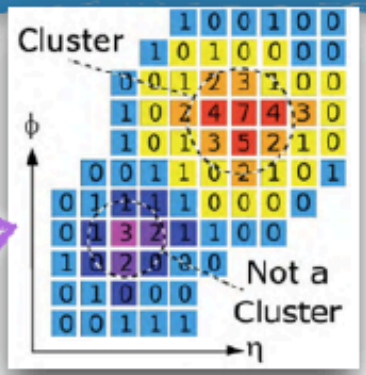

- Calo jets are the standard jets used in ATLAS;
- **Components**: 3D clusters of energy deposits in the calorimeter (***topo-clusters***).
- Topo-cluster are built from topologically connected calorimeter cells with noise-threshold requirements.
- Jet reconstruction uses different **sequential algorithms**. Input topo-clusters are iteratively merged minimising the distance ρ_{ij}. The **radius parameter** R is proportional to jet dimension.

$$\rho_{ij} = \min\left(p_{Ti}^{2p}, p_{Tj}^{2p}\right)\frac{(\Delta R_{ij})^2}{R^2} \qquad \Delta R_{ij}^2 = (\eta_i - \eta_j)^2 + (\varphi_i - \varphi_j)^2$$

AntiKt (p=-1) | **Cambridge/Aachen (p=0)** | **Kt (p=1)**

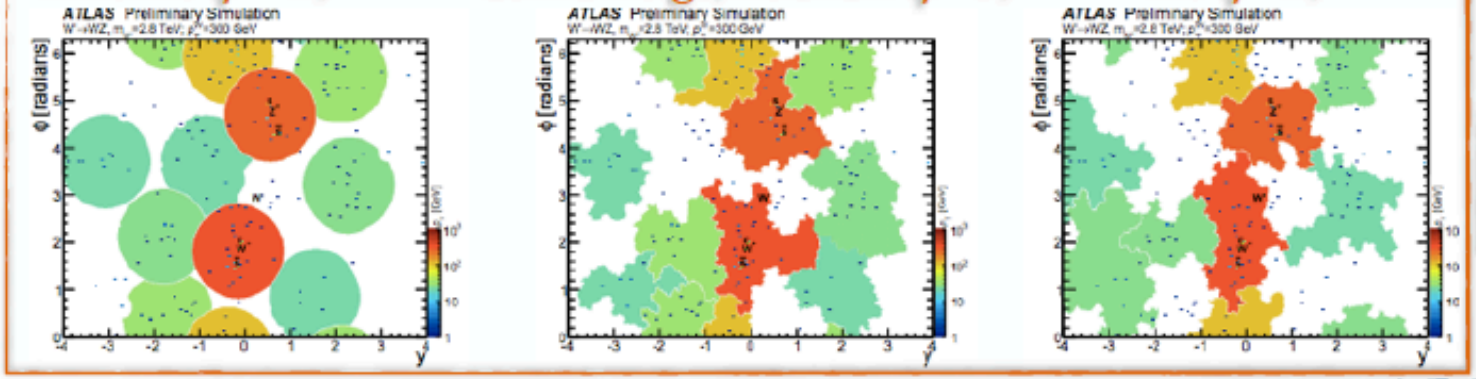

Different algorithms produce different jets

Jet reconstruction

Track jets

- Same reconstruction algorithms as for calo jets but ID tracks from the primary vertex are used as constituents.
  - Mainly used for calibration and CP tests;
  - Have better resolution (<~500 GeV)and pile-up stability. Can be matched with topo-clusters.

Combined Performance

Truth jets

- **Constituents:** all MC truth stable particles (*HepMC status code=1 and* $c \cdot t > 10mm$) that are not:
  - Neutrinos and dressed electrons & muons not from hadrons; including photons is analysis dependent;
  - B-tagging done using b-meson ghost matching.

Dressing: add the photons in a small cone around the particle to the particle itself.

- Used in energy calibration, MC performance studies and fiducial phase-space analyses (*particle level*).

Particle level object definition note ATL-COM-PHYS-2014-439

Jet calibration

Calo jets (EM or LCW) → Pileup Correction → Origin Correction → Energy & η Calibration → GS Calibration → In-situ Correction

LCW → Local Calibration Weight

- Topo-clusters are divided in 2 categories primarily depending on measured **energy density** and **longitudinal shower depth**.
  - **EM scale (default)** which correctly measures the energy deposited in the calorimeter by particles produced in electromagnetic showers (in EM case, the calorimeter is compensating);
  - **Had.** or **Local Calibration Weight (LCW) scale**: LCW algorithm calibrates topo-clusters in order to correctly reproduce the hadronic shower energy (compensating correction) as a function of η, ρ and E.
- Both energy corrections are derived from single charged and neutral pion MC simulations.

$$\text{Weight} = \frac{E_{visible}(\text{topo-cl})}{E_{true}(\text{topo-cl})}$$

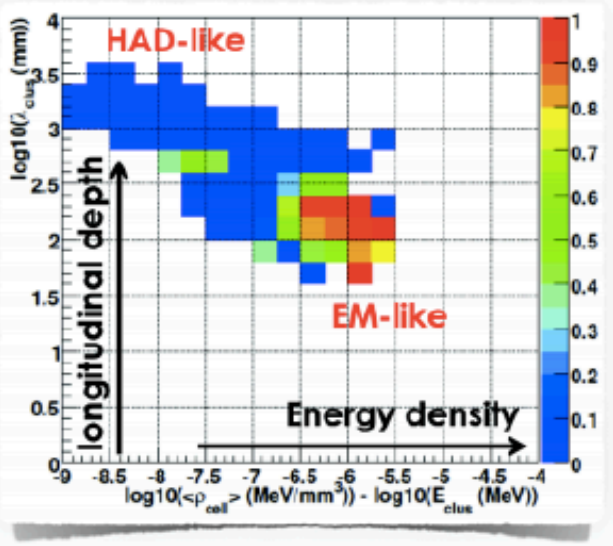

Mention to pile-up

N_{PV} =# reconstructed primary vertices

$\langle\mu\rangle$ = expected average # interactions

pile-up = proton-proton collisions in addition to the collision of interest

25 ns, which is the interval between proton-proton bunch crossings

In the ATLAS detector many of the subsystems have sensitivity windows longer 25 ns.

→ every physics object is affected by pile-up in some way

- from additional energy contributions in jets to
- mis-reconstruction of background as high-momentum muons.

In-time pile-up: additional proton-proton collisions occurring in the same bunch crossing as the collision of interest;

Out-of-time pile-up: additional proton-proton collisions occurring in bunch-crossings just before and after the collision of interest. When detectors are sensitive to several bunch-crossings or their electronics integrate over more than 25 ns, these collisions can affect the signal in the collision of interest;

Pileup

- Correction accounting for the **energy excess** due to pile-up interactions (both in-time and out-of-time ones);

- Derived from MC simulations as a function of the **number of primary vertices** (N_{PV}) and the **expected average number of interactions** ($<\mu>$) in bins of jet η and p_T.

- Improve the energy resolution and decrease pile-up fluctuations

$$p_T^{Corrected} = p_T - \underbrace{\rho \cdot A_T}_{\text{Area correction}} - \underbrace{\alpha \cdot (N_{PV} - 1) - \beta \cdot <\mu>}_{\text{Residual correction}}$$

$\alpha \propto$ in-time pileup
$\beta \propto$ out-time pileup

- Two method used:
  - **Jet area correction:** pile up p_T density ρ is evaluated depending on the jet area;
  - **Residual pile-up correction:** 2 different coefficients depending on $<\mu>$ and N_{PV} respectively.

Origin Correction

- Corrects the calorimeter jet direction making it **point back to the primary event vertex** instead of the nominal centre of the ATLAS detector.
- Energy of the reconstructed jet is not affected by origin correction;
- Improves jet angular resolution, with small improvements to p_T response

RunII:
latest news: manpower needed, migration not yet completed.

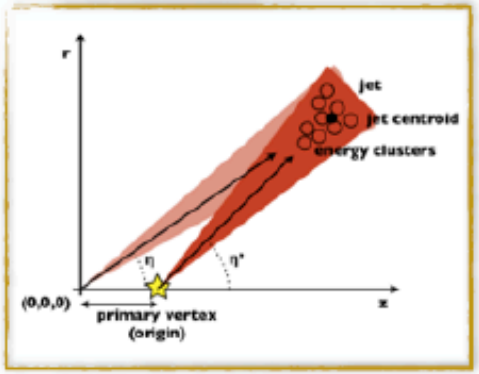

- Calo jets
- Track jets
- Calo jets + corr

RMS

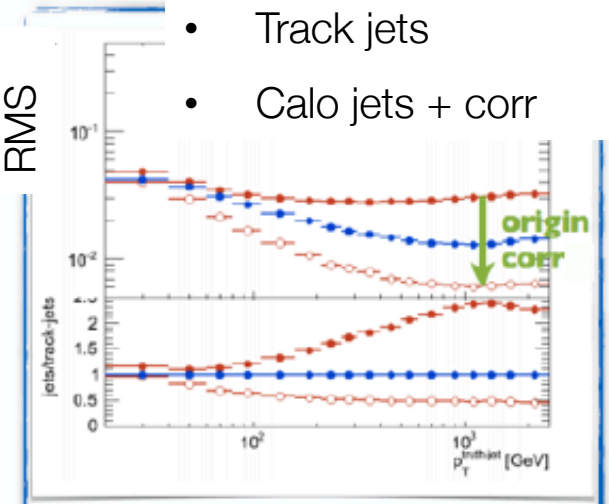

The plot shows **jet η resolution** for:
- Calorimeter jets;
- Track jets;
- Calorimeter jets after origin correction.

Angular resolution improved.

In-Situ Calibration

- In-situ calibrations use well measurable objects or quantities from data in order to validate and to correct MC calibrations. Different techniques exists.

Direct p_T balance (DB): The transverse momentum of the jet with the highest p_T is corrected to the transverse momentum of the reference Z boson or photon, balancing the total p_T.

RunII: Z+jet: code to be tested, V+jet and other: work still ongoing.

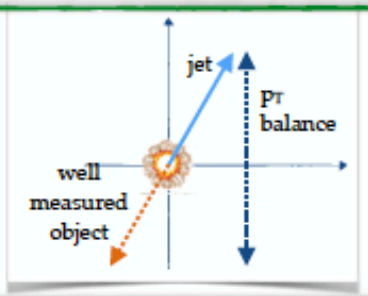

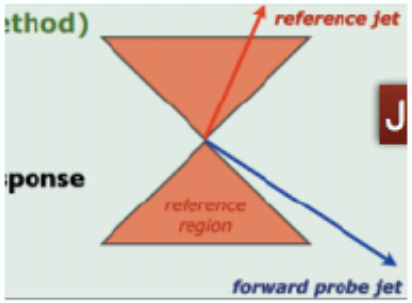

η-intercalibration: A relative calibration technique using the matrix method to correct high-η jets with low-η in data (forward jets with $|\eta| > 0.8$). The response is found solving a linear system for all jet pairs.

$$\mathcal{R} = \frac{p_T^{\text{left}}}{p_T^{\text{right}}} = \frac{c^{\text{right}}}{c^{\text{left}}} = \frac{2+\langle\mathcal{A}\rangle}{2-\langle\mathcal{A}\rangle} \qquad \mathcal{A} = \frac{p_T^{\text{left}} - p_T^{\text{right}}}{p_T^{\text{avg}}}, \quad \eta^{\text{left}} < \eta^{\text{right}}$$

RunII: Code migrated but not finalised yet.

RunII: overall timescale = start of data taking.
some ideas about giving more importance to in-situ calibration wrt MC dependent ones.

Boosted

Boosted Jets

- **What are boosted jets?** Standard jets characterised by high p_T. (> ~200-300 GeV)
- **Why?** LHC energies allows to investigate new energy regions once forbidden and high p_T jets are the key for this unexplored physics.
- **Yes, but why different?** High Lorenz boost brings decay products closer one each other as their parton showers merge together. Impossible to distinguish in separate jets.
- **Solution:** include all the decay product' showers in a single (larger) jet.
- **Moreover:** decrease combinatorial (and physical) bkg.

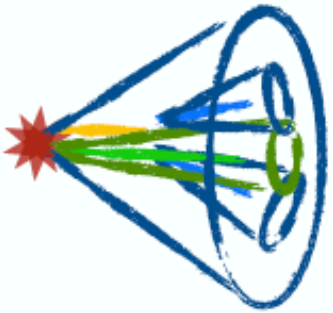

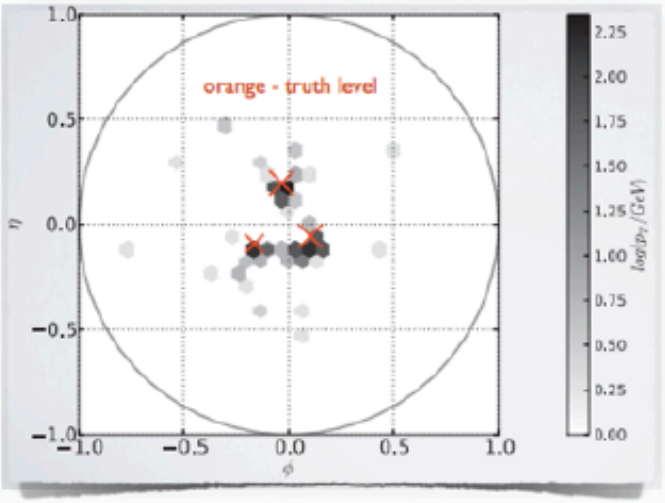

$\Delta R \approx 2m/p_T$

top with $p_T > 350$ GeV have $\Delta R < 1.0$.

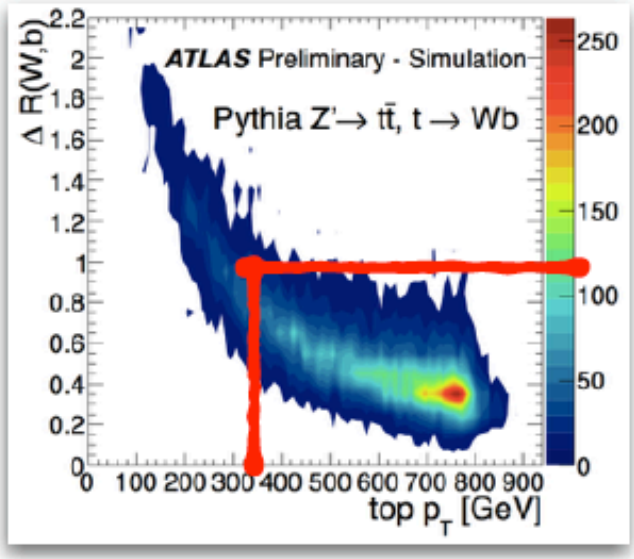

Boosted Jets

- Since standard techniques are not efficient in boosted topologies —> new identification algorithms developed. From "simple" *grooming+variable-cut* to complex algorithms.
- Boosted regime very diffused in **exotics searches** but also **top measurements** (cross section, charge asymmetry) and starting in **ttH (interest from Bologna)**.
- Boosted objects are mainly **top quarks** and **Z/W bosons**. Start looking at boosted Higgs, many theoretical papers.

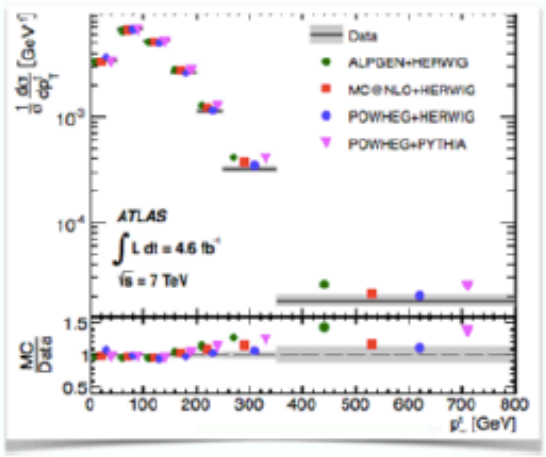

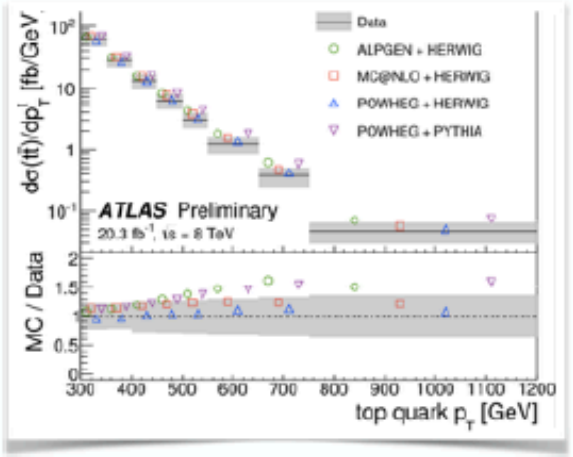

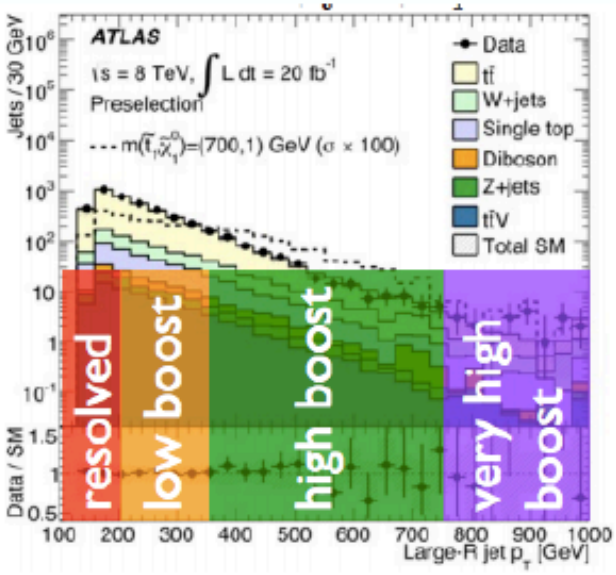

Not easy to find a definite boundary between resolved and boosted. One of the main future challenges will be to merge coherently the 2 results.

Boosted jets divided in low, high and very high boosted depending on jet p_T. Algorithms performances change among these regions.

Jets grooming - 1

Introduction to grooming

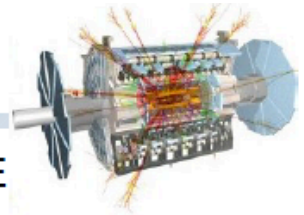

- **Jet grooming:** seeks to get rid of softer components in a jet from UE or pileup and leave constituents from the hard scatter behind
  - Better mass resolution expected after grooming
  - Great for searching for boosted objects contained in a large-R jet!
  - Is especially important to have these studies now so that we are prepared as LHC ramps up luminosity

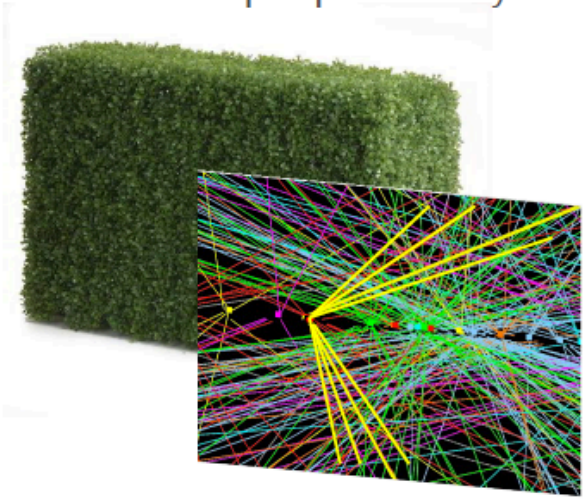

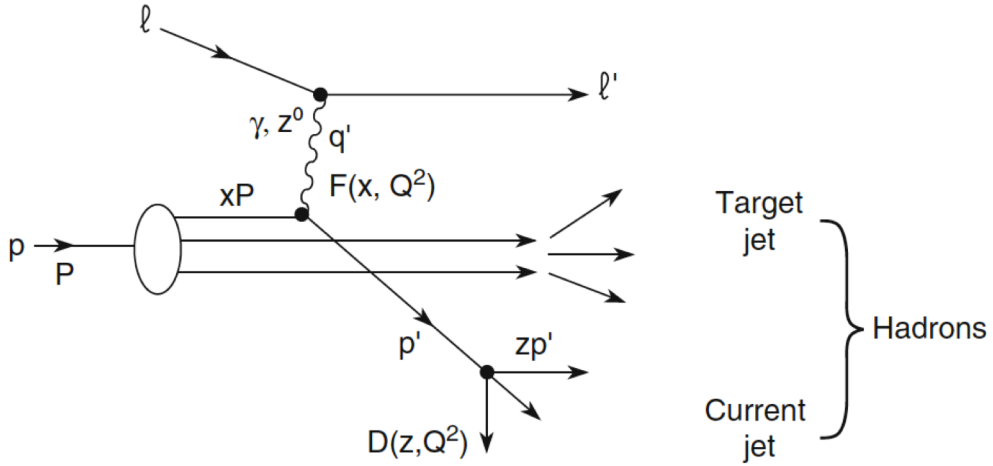

- Three algorithms studied: mass-drop/filtering, pruning, trimming
- **ATLAS results shown today:** summarize the performance between various tunes of groomed algorithms

Jets grooming - 2

Jet grooming

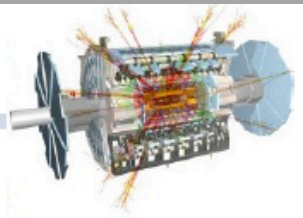

- **"Mass drop/filtering"** http://arxiv.org/abs/0802.2470
  (J. Butterworth, A. Davidson, M. Rubin, G. Salam)
  - Identify relatively symmetric subjets, each with significantly smaller mass than their sum
  - Was optimized for H→bb search using C/A jets...**not applied to anti-kt jets!**

Mass drop: create 2 subjets

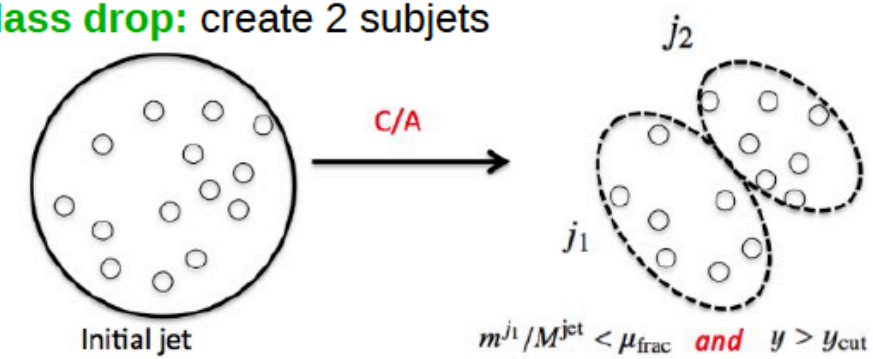

$$\frac{\min[(p_T^{j_1})^2, (p_T^{j_2})^2]}{(M^{\text{jet}})^2} \times \Delta R_{j_1,j_2}^2 > y_{\text{cut}}.$$

Tuned parameter: μ_{frac} (y_{cut} set to 0.09)

Filtering: constituents of j1, j2 are reclustered using C/A

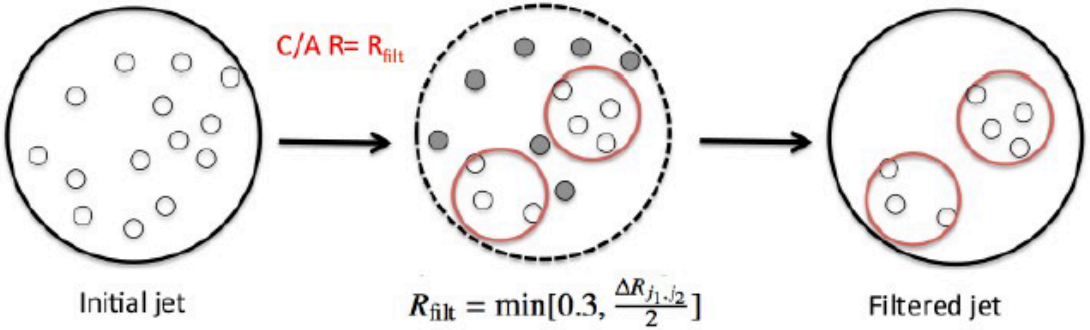

CA = Cambridge/Achen jet algorithm

Jets grooming - 3

Jet grooming

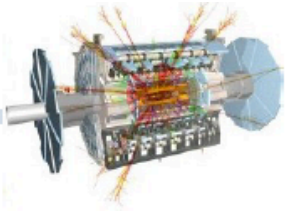

- **"Trimming"** http://arxiv.org/abs/0912.1342 (D. Krohn, J. Thaler, L. Wang)
  - uses k_t algorithm to create subjets of size R_{sub} from the constituents of the large-R jet: any subjets failing $p_T i / p_T < f_{cut}$ are removed

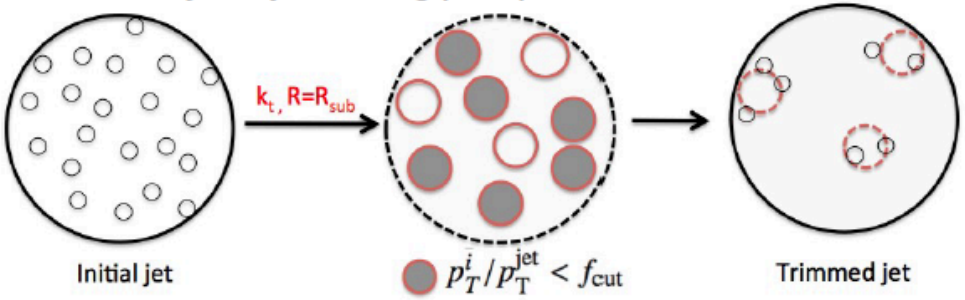

Tuned parameters: f_{cut} and R_{sub}

- **"Pruning"** http://arxiv.org/abs/0912.0033 (S. Ellis, C. Vermilion, J. Walsh)
  - Recombine jet constituents with C/A or kt while vetoing wide angle (R_{cut}) and softer (z_{cut}) constituents. Does not recreate subjets but prunes at each point in jet reconstruction

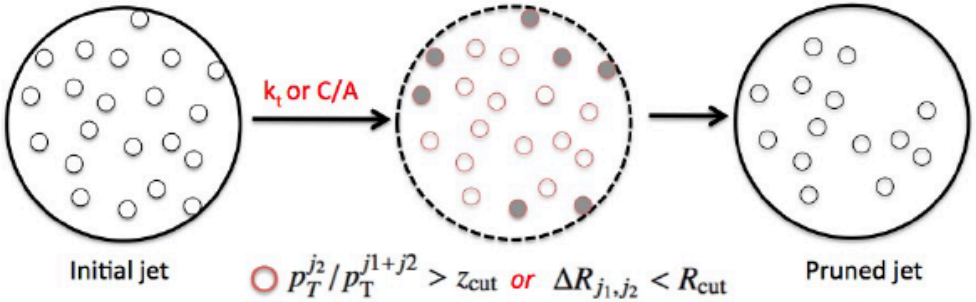

Tuned parameters: R_{cut} and z_{cut}

Jet Grooming

Trimming

- Re-cluster using the *k_T algorithm* to create smaller sub-jets.
  Remove each sub-jets satisfying the p_T criteria:

$$p_{Ti}/p_T^{\text{jet}} < f_{\text{cut}}$$

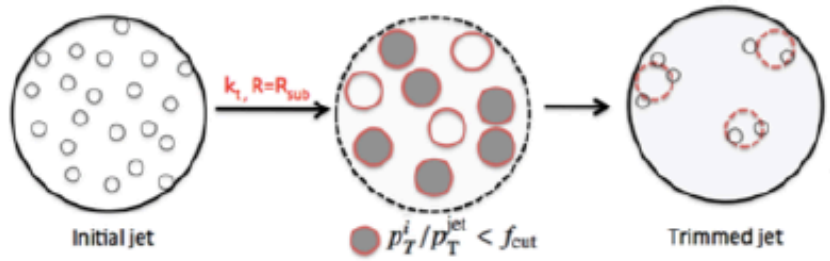

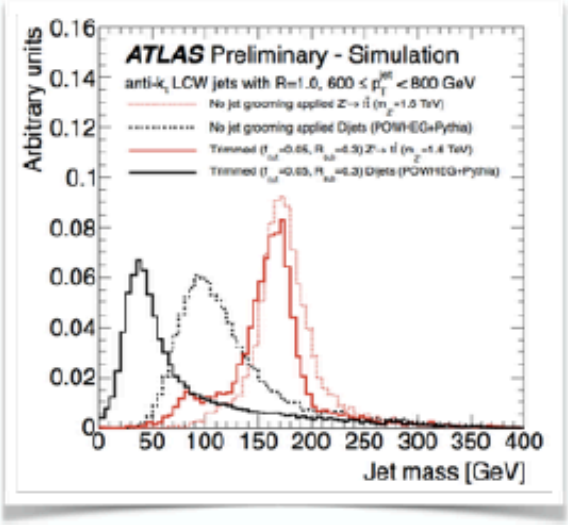

The trimming improves the discrimination between top quark jets and light quark jets.

Mass Drop Filtering

- Divide the jet in two, j_1 and j_2, where $m_{j1} > m_{j2}$;
- ask for mass symmetry and angular asymmetry criteria (*mass drop*);

$$m^{j_1}/m^{\text{jet}} < \mu_{\text{frac}}, \qquad \frac{\min[(p_T^{j_1})^2,(p_T^{j_2})^2]}{(m^{\text{jet}})^2} \times \Delta R_{j_1,j_2}^2 > y_{\text{cut}},$$

- re-cluster (*C/A*) with $R = dR\ (j_1, j_2)$ and taking only 3 most energetic sub-jets (*filtering*);

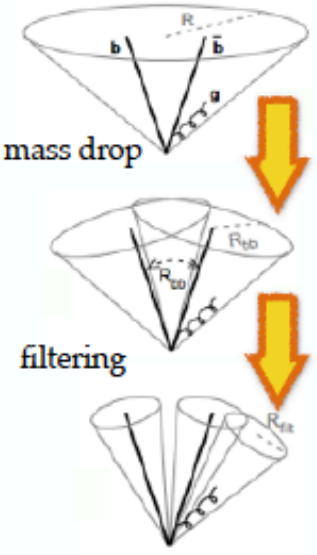

HEPTopTagger

- An algorithm combining **grooming** (mass drop filtering) and **substructure variable selection** (jet mass) specifically tuned to tag top jets.
- Older ATLAS top tagging algorithm. *C/A* **jets** used. Possible tuning of the parameters.

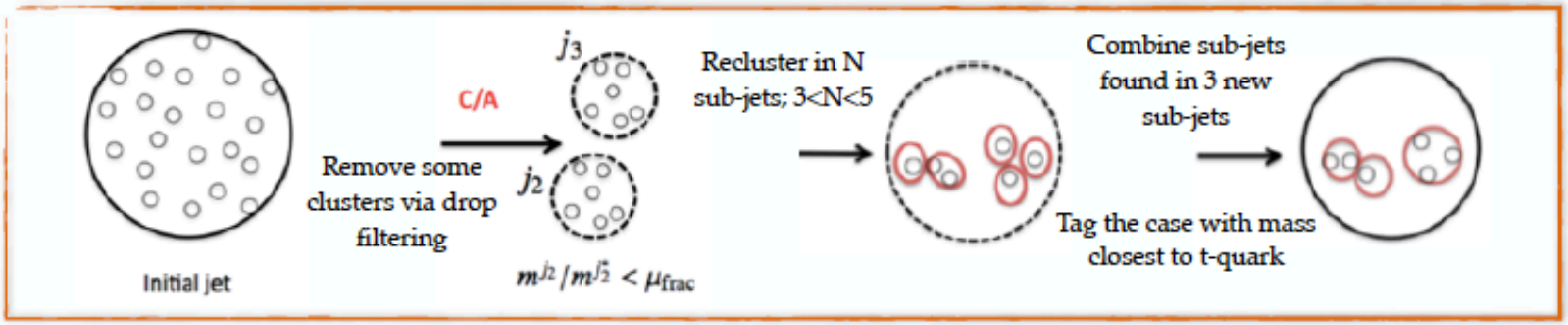

- HEPTopTagger tagging efficiency on MC ttbar sample;
- **Tuning:** default-025

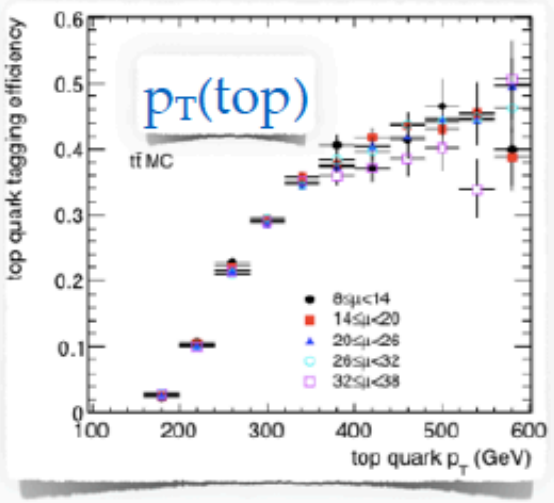

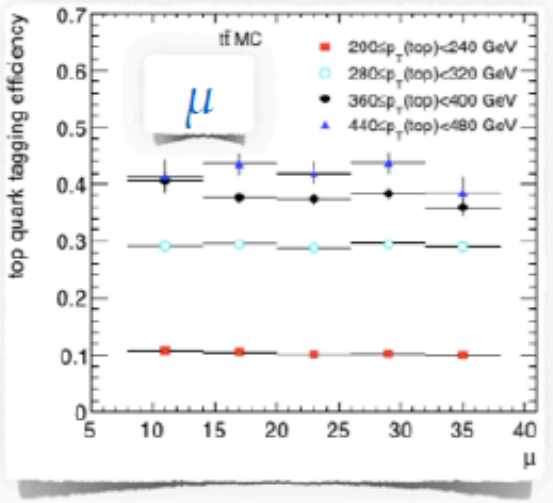

Boosted Boson Tagging

- Studies involved mainly hadronic decaying W bosons.
- Concentrating on *grooming +variable-cut* techniques; lots of substructure variables considered (Planar flow, z-splitting, sphericity, Fox-Wolfram momentum, …);
- **BDRS** (Butterworth,Davison,Rubin, Salam): a mass-drop filtering specifically tuned for boson jets.

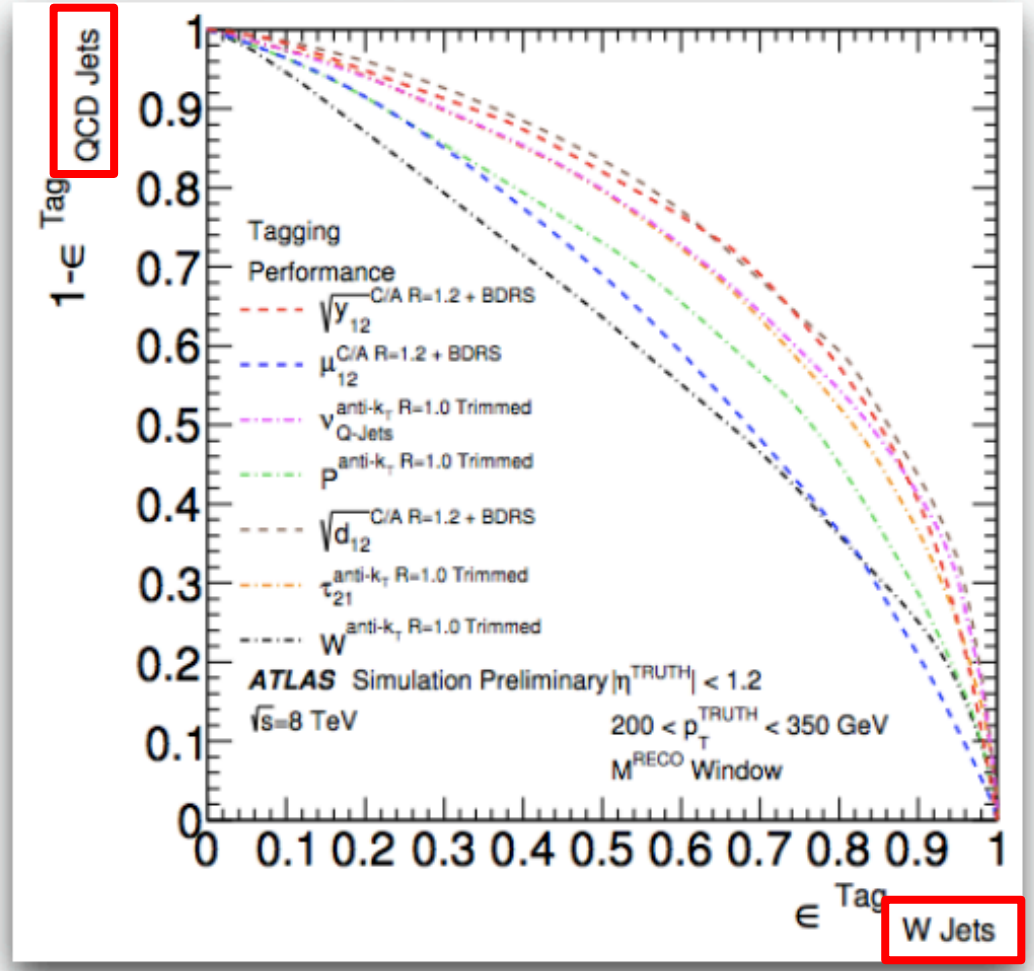

Pisa using boson tagging in WV -> *lvjj & lvJ* analysis

See Margherita's talk

https://cds.cern.ch/record/1967511/files/ATL-COM-PHYS-2014-1450.pdf

Boosted Top Tagging

- Many analysis still using simple *grooming+variable-cut* techniques (tt resonance, tt cross section l+jets, …);

Bologna's working on that!

- Other taggers also used, especially HEPTopTagger (tt cross section full-had [TOM+HEPTT], 4th generation quark [HEPTT], …)

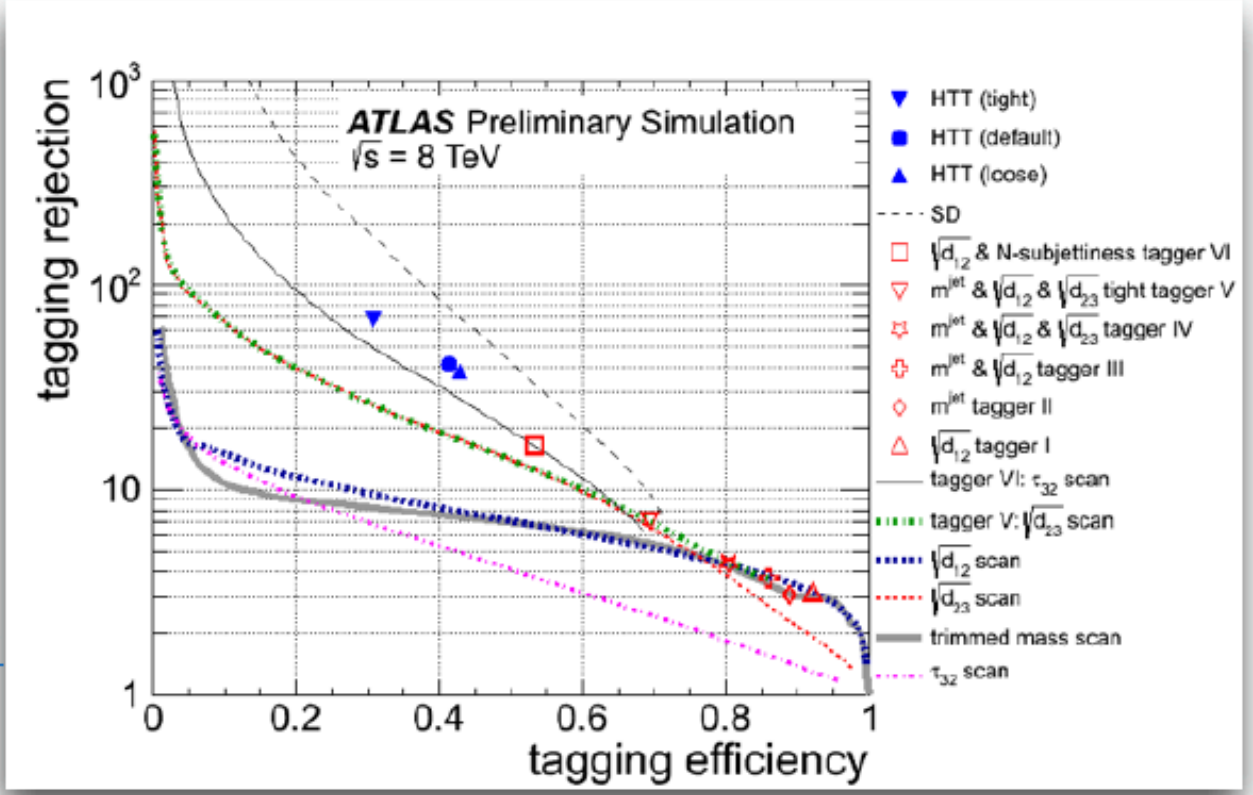

https://cds.cern.ch/record/1571040/files/ATLAS-CONF-2013-084.pdf

Muon Systems

Alignment and Resolution Determination

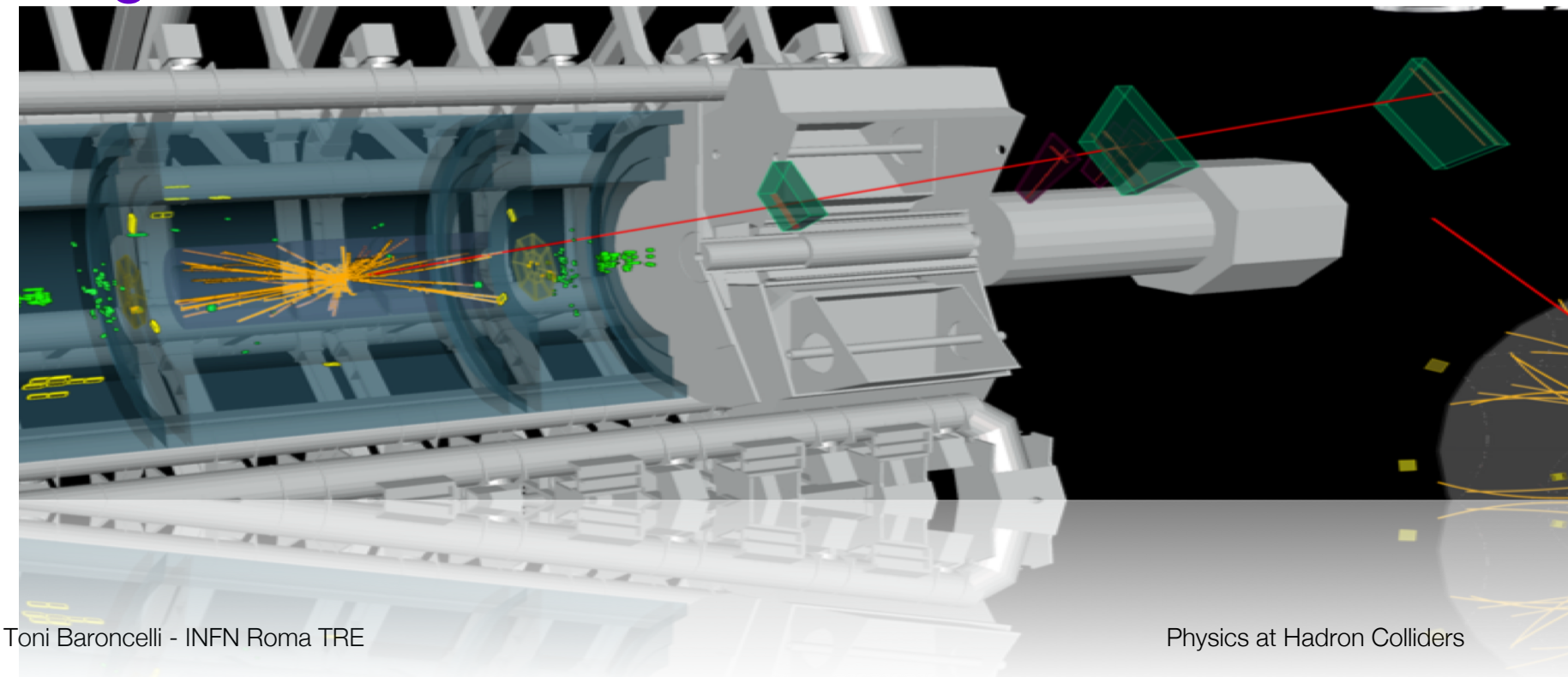

Muon Systems

Design goals:

Reconstruct high-p_T muons over large η-range

Trigger on high-p_T muons

Needs:

Very good spatial resolution

Hermetic detector ("no holes")

Fast detector response

ATLAS & CMS:

Combination of muon system & magnet drove detector layout

ATLAS: standalone muon reconstruction (toroid magnets)

CMS: muon detection in iron flux return

Both: large scale precision detectors with excellent alignment

[precision mechanics & optical alignment system]

Muon Systems

Issue	ATLAS	CMS
Design	Air-core toroid magnets Standalone muon reconstruction	Flux return instrumented Tracks point back to collision point
Barrel Tracking	Drift tubes Precision: 30–50 μm	Drift tubes Precision: 100–500 μm
End-cap Tracking	Cathode strip chambers High rate capability	Cathode strip chambers High rate capability
Barrel Trigger	Resistive plate chambers Fast response [5 ns]	Resistive plate chambers Fast response [5 ns]
End-cap Trigger	Thin gap chambers Fast response, high rates	

ATLAS Muon Spectrometer

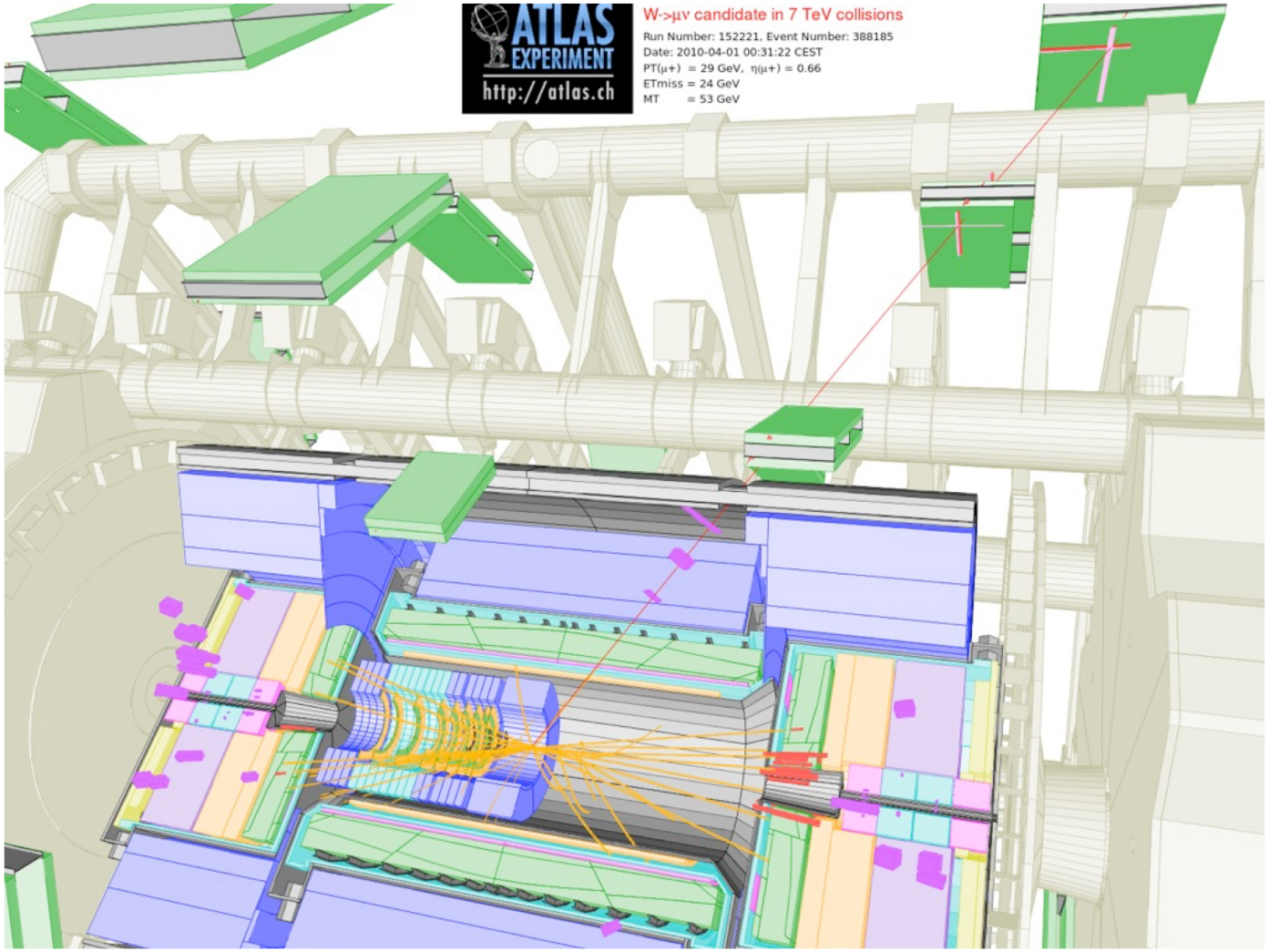

Muon Performance

TABLE 12 Main parameters of the ATLAS and CMS muon measurement systems as well as a summary of the expected combined and stand-alone performance at two typical pseudorapidity values (averaged over azimuth)

Parameter	ATLAS	CMS
Pseudorapidity coverage		
-Muon measurement	$\|\eta\| < 2.7$	$\|\eta\| < 2.4$
-Triggering	$\|\eta\| < 2.4$	$\|\eta\| < 2.1$
Dimensions (m)		
-Innermost (outermost) radius	5.0 (10.0)	3.9 (7.0)
-Innermost (outermost) disk (z-point)	7.0 (21–23)	6.0–7.0 (9–10)
Segments/superpoints per track for barrel (end caps)	3 (4)	4 (3–4)
Magnetic field B (T)	0.5	2
-Bending power (BL, in T· m) at $\|\eta\| \approx 0$	3	16
-Bending power (BL, in T· m) at $\|\eta\| \approx 2.5$	8	6
Combined (stand-alone) momentum resolution at		
-p = 10 GeV and $\eta \approx 0$	1.4% (3.9%)	0.8% (8%)
-p = 10 GeV and $\eta \approx 2$	2.4% (6.4%)	2.0% (11%)
-p = 100 GeV and $\eta \approx 0$	2.6% (3.1%)	1.2% (9%)
-p = 100 GeV and $\eta \approx 2$	2.1% (3.1%)	1.7% (18%)
-p = 1000 GeV and $\eta \approx 0$	10.4% (10.5%)	4.5% (13%)
-p = 1000 GeV and $\eta \approx 2$	4.4% (4.6%)	7.0% (35%)

ATLAS: larger coverage

ATLAS: better standalone perf.

CMS: better combined perf.

[Froidevaux, Sphicas]

Overview of Muon Reconstruction in ATLAS

μ-rec = ID + Calo + MS

MS : 3 stations

Muon reconstruction using information from tracking sub-detectors (ID, MS) and calorimeter:

- **Combined (CB):** ID + MS hits with full track re-fit. Main reconstruction type, bulk of the muons
- **Stand-alone (SA):** MS-only track identification and reconstruction. Recovers muon reconstruction for $|\eta| > 2.5$
- **Segment-tagged (ST):** muon tag with MS segment, momentum reconstructed with ID. Recovers regions of poor coverage + low pt muons. Good purity
- **CaloTag:** reconstruction with ID and calorimetric MIP only. Used mostly for efficiency studies. Low purity, fills MS gap at $\eta \approx 0$.

Rough relative acceptances of reco-algorithms:

- MuIDCo: CB outside-in, $\approx$ 96%
- MuGirl: CB inside-out, $\approx$ 1%
- CaloTag calo-tagger, $\approx$ 1.5%
- MuTagIMO: segment-tagger, $\approx$ 0.5%
- MuIDSA: MS SA reconstruction, $\approx$ 1%

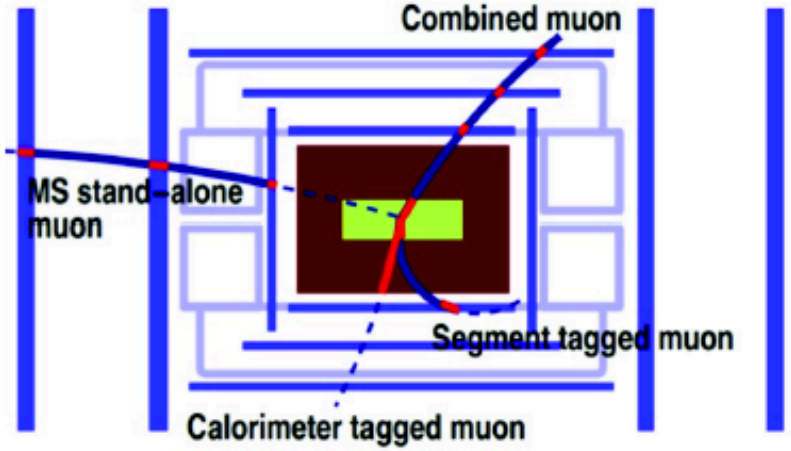

Muon Types in ATLAS

4 different types of reconstructed muons in ATLAS depending on which detector(s) is (are) used

SA, CB, ST, CaloTag

One muon traverses ID, Calorimeters, Muon Spectrometer

– Stand-Alone (SA) muons: the muon trajectory is reconstructed only in the MS. The parameters of the muon track at the interaction point are determined by extrapolating the track back to the point of closest approach to the beam line, taking into account the estimated energy loss of the muon in the calorimeters. In general the muon has to traverse at least two layers of MS chambers to provide a track measurement. SA muons are mainly used to extend the acceptance to the range $2.5 < |\eta| < 2.7$ which is not covered by the ID;

– Combined (CB) muon track reconstruction is performed independently in the ID and MS, and a combined track is formed from the successful combination of a MS track with an ID track. This is the main type of reconstructed muons;

– Segment-tagged (ST) muons: a track in the ID is classified as a muon if, once extrapolated to the MS, it is associated with at least one local track segment in the MDT or CSC chambers. ST muons can be used to increase the acceptance in cases in which the muon crossed only one layer of MS chambers, either because of its low p_T or because it falls in regions with reduced MS acceptance;

– Calorimeter-tagged (CaloTag) muons: a track in the ID is identified as a muon if it could be associated to an energy deposit in the calorimeter compatible with a minimum ionizing particle. This type has the lowest purity of all the muon types but it recovers acceptance in the uninstrumented regions of the MS. The identification criteria of this muon type are optimized for a region of $|\eta| < 0.1$ and a momentum range of $25 \lesssim p_T \lesssim 100$ GeV.

Muon Selection Working Points for Physics Analysis == Quality

Goal: optimal and easy-to-use muon selection Working Points (WP):

- *Initial situation:* knowledge of reconstruction algorithms, Run I analysis experience
- WP optimization to be performed well before data-taking:
  - ⇒ Usage by early analysis
  - ⇒ Performance measurement
- Studied background discriminating variables:
  - ⇒ *ROC curves, tests on partially reprocessed Run I data*
- Efficiency/rejection ratios of ID-tracks for *truth-classified* simulated muons (signal or K/π backgrounds)

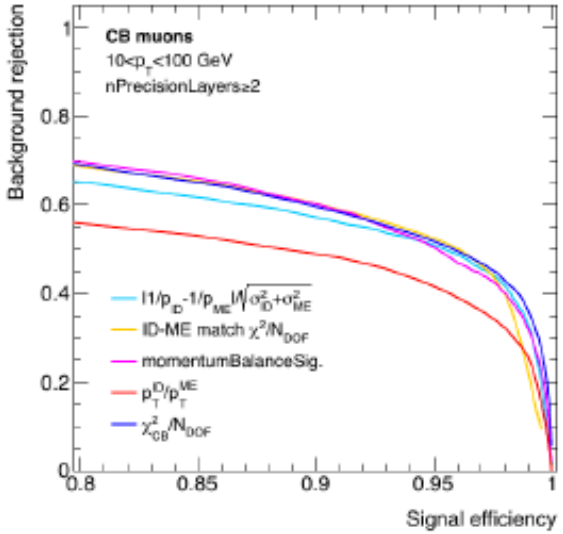

WP definition for Run II analysis:

Good signal/background separation power from *1/p significance*: $\frac{|1/p_{ID}-1/p_{MS}|}{\sqrt{\sigma^2_{ID}+\sigma^2_{MS}}} < 7$

- **Loose:** all muon algorithms, using calo/segment-tagged in $|\eta| < 0.1$ ($H \to ZZ$ Run-I-like)
- **Medium:** CB muons (SA in $2.5 < |\eta| < 2.7$), ≥ 2 stations (or > 1 in $|\eta| < 0.1$),
- **Tight:** ≥ 2 stations, $1/p$ significance<5, $\chi^2_{CB} < 8$

Muon WPs: Expected Efficiencies and Fake Rates

Fake muon → muon from HF or wrong reconstruction

- Expected efficiencies and fake rates from $t\bar{t}$ simulation
- Analysis of performance with 50 ns or 25 ns running conditions

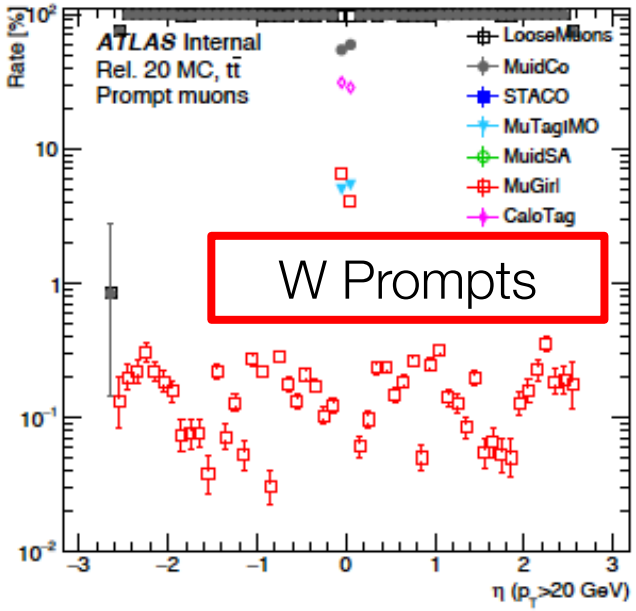

Prompt μ from W: $p_T > 20$ GeV

p_T in [4, 100]	50 ns	25 ns
All Muons	99.60 ± 0.01	99.59 ± 0.01
Loose	98.68 ± 0.01	97.88 ± 0.01
Medium	96.78 ± 0.02	96.00 ± 0.01
Tight	96.10 ± 0.02	95.34 ± 0.02

*Quoted uncertainties are statistical only

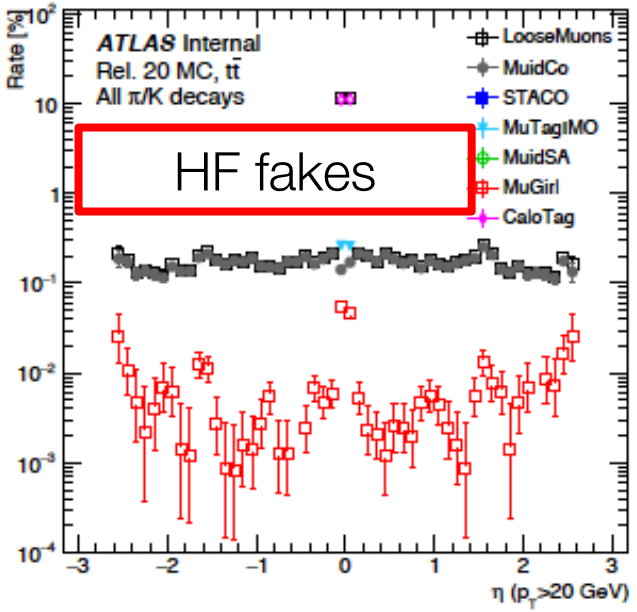

Fake μ from Hadrons: $p_T > 20$ GeV

p_T in [4, 100]	50 ns	25 ns
All Muons	8.62 ± 0.01	9.19 ± 0.01
Loose	0.61 ± 0.01	0.64 ± 0.01
Medium	0.37 ± 0.01	0.39 ± 0.01
Tight	0.31 ± 0.01	0.32 ± 0.01

Tag & Probe method

Total reconstruction efficiency

$$\varepsilon = \varepsilon(ID) \times \varepsilon(MS) \times \varepsilon(comb)$$

- $\varepsilon(ID)$: Inner tracker reconstruction efficiency
- $\varepsilon(MS)$: Muon Spectrometer reconstruction efficiency
- $\varepsilon(comb)$: Combination efficiency

The muon reconstruction efficiency is measured with respect to Inner Detector tracks

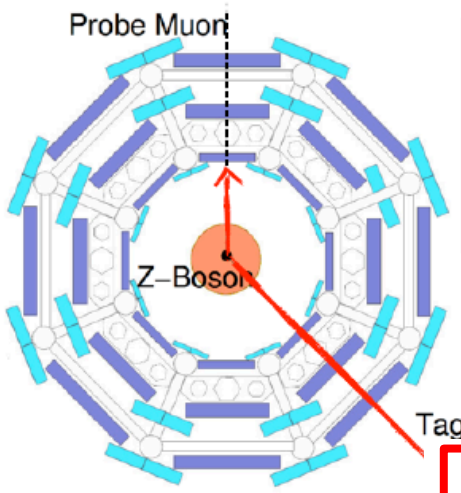

$$SF = \frac{\varepsilon^{\mathrm{Data}}(\mathrm{Type})}{\varepsilon^{\mathrm{MC}}(\mathrm{Type})}.$$

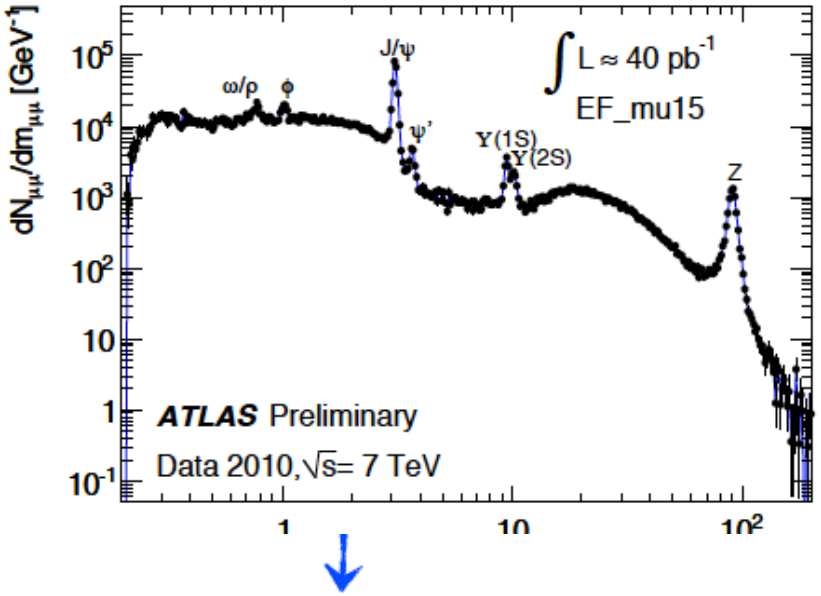

The $J/\psi \to \mu^+\mu^-$ decay is used to obtain a sample of low-p_T probes, while the $Z \to \mu^+\mu^-$ decay provides high p_T probes

In-situ measurement of muon reconstruction efficiency using well known resonances. Requires

1. A combined muon "**Tag**"
2. the tag is paired with an ID track giving an invariant mass close to the considered resonance mass
3. the fraction of reconstructed signal "**Probes**" measures the muon identification efficiency

Reconstruction efficiency of muons

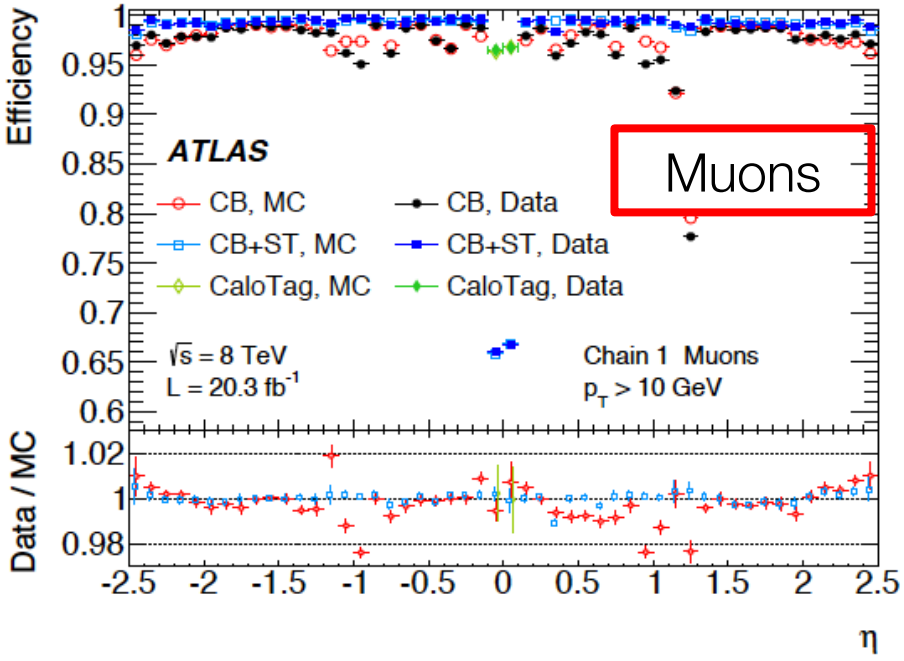

Fig. 3. Muon reconstruction efficiency as a function of η measured in $Z \to \mu\mu$ events for muons with $p_{\mathrm{T}} > 10$ GeV and different muon reconstruction types. CaloTag muons are only shown in the region $|\eta| < 0.1$, where they are used in physics analyses. The error bars on the efficiencies indicate the statistical uncertainty. The panel at the bottom shows the ratio between the measured and predicted efficiencies. The error bars on the ratios are the combination of statistical and systematic uncertainties.

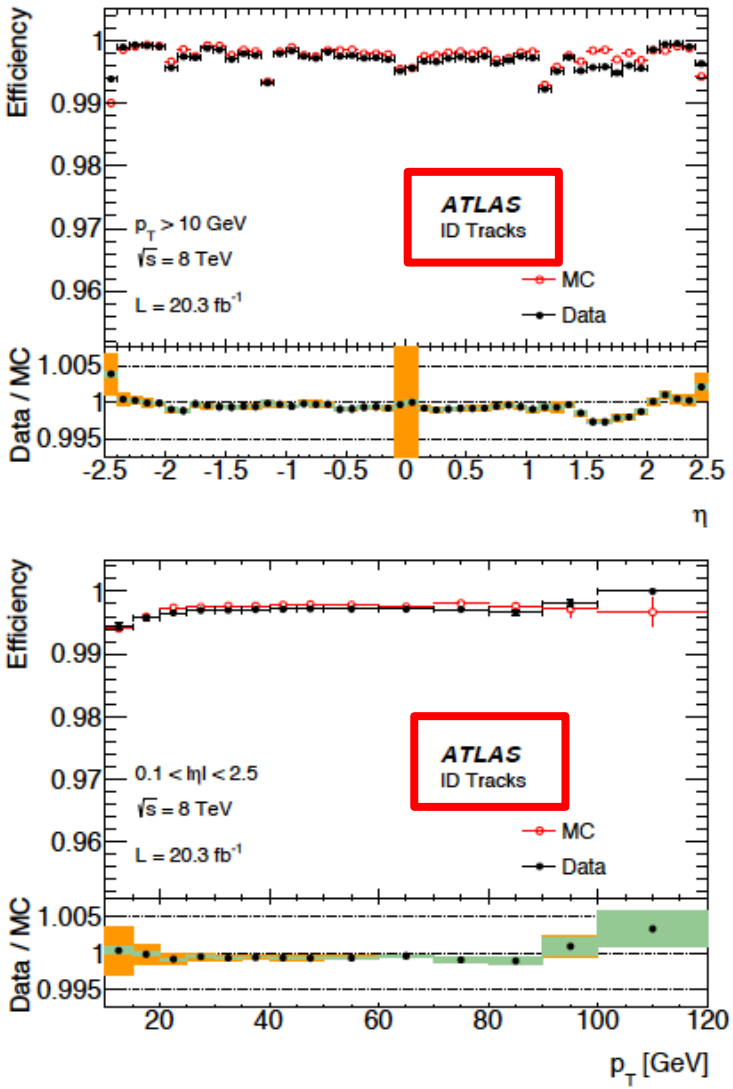

MC and data

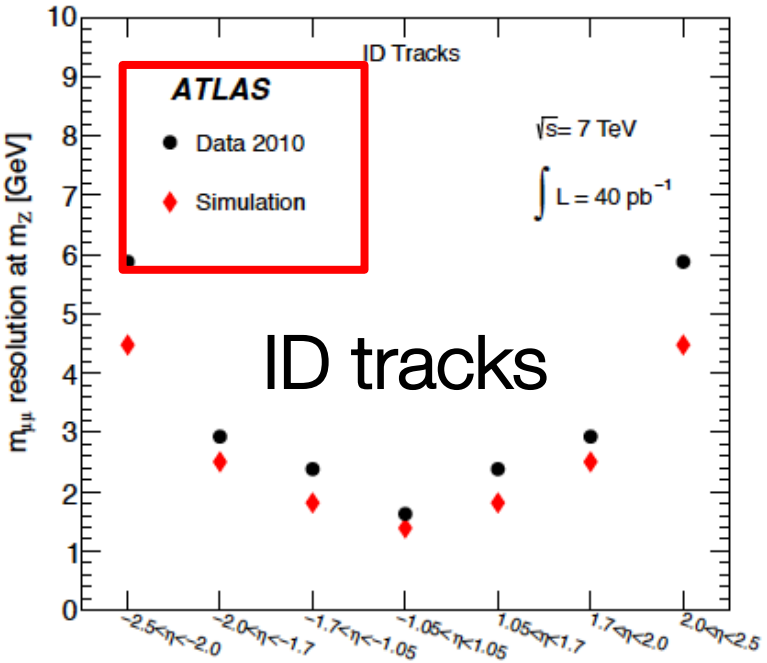

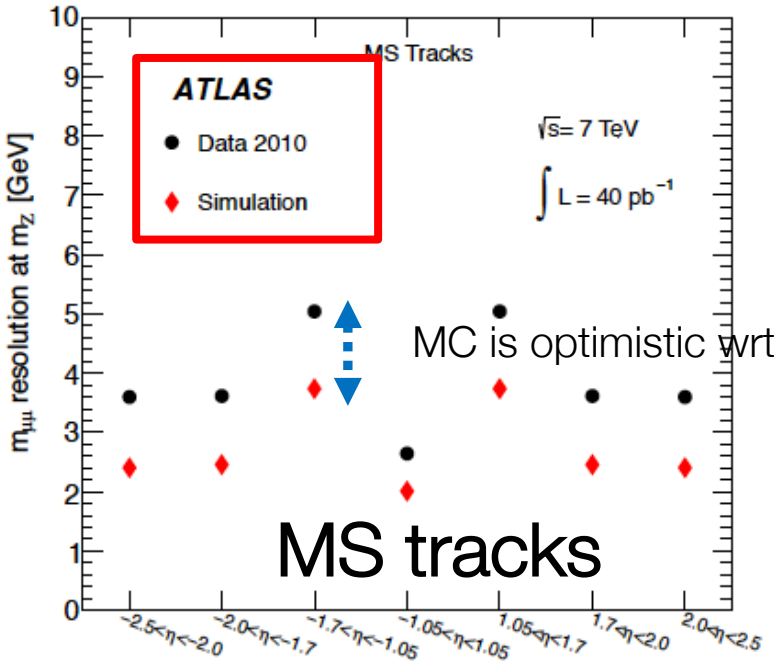

MC is optimistic wrt data

Monte Carlo is most of the time too optimistic. Since simulation is a fundamental ingredient of modern analysis we need to apply additional smearing and/or scale factors to the ideal resolution / response of the simulation. This is less obvious than it seems, degradation is often due to several effects (mis-alignment, additional material, not only worse resolution).

What do we want to do?

We want p_T from simulation to be as close to data as possible in terms of

- Scale
- Resolution

Parametrization of ID & MS resolutions

ID, Inner Detector

$$\frac{\sigma_{\mathrm{ID}}(p_{\mathrm{T}})}{p_{\mathrm{T}}} = a_{\mathrm{ID}}(\eta) \oplus b_{\mathrm{ID}}(\eta) \cdot p_{\mathrm{T}} \qquad \text{for } 0 < |\eta| < 2.0 \text{ ;}$$

$$\frac{\sigma_{\mathrm{ID}}(p_{\mathrm{T}})}{p_{\mathrm{T}}} = a_{\mathrm{ID}}(\eta) \oplus \frac{b_{\mathrm{ID}}(\eta) \cdot p_{\mathrm{T}}}{\tan^2(\theta)} \qquad \text{for } 2.0 < |\eta| < 2.5 \text{ .} \qquad (2)$$

The first term describes the multiple scattering contribution, whilst the second term describes the intrinsic resolution caused by the imperfect knowledge of the magnetic field in the ID, by the spatial resolution of the detector components, and by any residual misalignment of the detector components.

MS, Muon Spectrometer

The stand-alone muon resolution can be parameterised as follows:

$$\frac{\sigma_{\mathrm{SA}}(p_{\mathrm{T}})}{p_{\mathrm{T}}} = a_{\mathrm{MS}}(\eta,\phi) \oplus b_{\mathrm{MS}}(\eta,\phi) \cdot p_{\mathrm{T}} \oplus \frac{c(\eta,\phi)}{p_{\mathrm{T}}} \text{ ,} \qquad (3)$$

where the first two terms parameterise the effect of the multiple scattering and the contribution of the intrinsic momentum resolution of the MS, respectively. The third term parameterises the effect of the fluctuations of the muon energy loss in the calorimeters, but this is small for the momentum range under consideration.

Corrections to muon momentum resolution and scale in MC

Samples of J/Psi, Upsilon and Z decays are used to study the muon momentum scale and resolution. The (ATLAS) simulation includes the best knowledge of the geometry, material distribution, and physics of the muon interaction. Additional corrections are needed to reproduce the muon momentum resolution and scale of experimental data at the level of precision that can be obtained using high statistics samples of dimuon resonances.

s_0 scale, Δr_o additional smearing

Det = MS, ID

depends on η, ϕ

$$p_{\mathrm{T}}^{\mathrm{Cor,Det}} = \frac{p_{\mathrm{T}}^{\mathrm{MC,Det}} + \sum_{n=0}^{1} s_n^{\mathrm{Det}}(\eta,\phi)\left(p_{\mathrm{T}}^{\mathrm{MC,Det}}\right)^n}{1 + \sum_{m=0}^{2} \Delta r_m^{\mathrm{Det}}(\eta,\phi)\left(p_{\mathrm{T}}^{\mathrm{MC,Det}}\right)^{m-1} g_m}$$

$$(\text{with } s_0^{\mathrm{ID}} = 0 \text{ and } \Delta r_0^{\mathrm{ID}} = 0),$$

powers of p_T :

0 energy loss fluctuations

1. mult. scattering, B inhomogeneities, mis-alignments

2. Intrinsic resolution

$$\frac{\sigma(p_{\mathrm{T}})}{p_{\mathrm{T}}} = r_0/p_{\mathrm{T}} \oplus r_1 \oplus r_2 \cdot p_{\mathrm{T}},$$

g_m gaussian distribution

Corrections to muon momentum resolution and scale in MC

s_i scale, Δr_i additional smearing

powers of p_T (0,1,2):

1. energy loss fluctuations
2. mult. scattering, B inhomogeneities, mis-alignments
3. Intrinsic resolution

Changes scale of p_T

$$p_{\mathrm{T}}^{\mathrm{Cor,Det}} = \frac{p_{\mathrm{T}}^{\mathrm{MC,Det}} + \sum_{n=0}^{1} s_n^{\mathrm{Det}}(\eta,\phi)\left(p_{\mathrm{T}}^{\mathrm{MC,Det}}\right)^{n+1}}{1 + \sum_{m=0}^{2} \Delta r_m^{\mathrm{Det}}(\eta,\phi)\left(p_{\mathrm{T}}^{\mathrm{MC,Det}}\right)^{m-1} g_m}$$

Worsens resolution

$$\frac{\sigma(p_{\mathrm{T}})}{p_{\mathrm{T}}} = r_0/p_{\mathrm{T}} \oplus r_1 \oplus r_2 \cdot p_{\mathrm{T}},$$

g_m gaussian distribution

$$p_T^{MC,Corrected} = \frac{p_T^{MC,Original} + Correction}{1+}$$

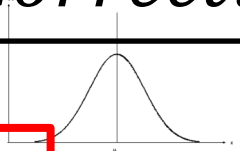

→ Find best correction that 'degrades' MC to 'Data'

Corrections: results

ID tracks

Region	Δr_1^{ID}	Δr_2^{ID} [TeV^{-1}]	s_1^{ID}
$\lvert\eta\rvert < 1.05$	$0.0068^{+0.0010}$	$0.146^{+0.039}$	$-0.92^{+0.26}_{-0.22} \times 10^{-3}$
$1.05 \leq \lvert\eta\rvert < 2.0$	$0.0105^{+0.0018}$	$0.302^{+0.046}$	$-0.86^{+0.30}_{-0.35} \times 10^{-3}$
$\lvert\eta\rvert \geq 2.0$	$0.0069^{+0.0121}$	$0.088^{+0.084}$	$-0.49^{+1.17}_{-1.63} \times 10^{-3}$

Δr can only fluctuate up!

Table 1. Summary of ID muon momentum resolution and scale corrections used in Eq. 9, averaged over three main detector regions. The corrections are derived in 18 η detector regions, as described in Sect. 5.1.1, and averaged according to the η width of each region. The uncertainties are the result of the sum in quadrature of the statistical and systematic uncertainties. Only upper uncertainties are reported for the Δr parameters; lower uncertainties are evaluated by symmetrization, as described in Sect. 5.1.2.

Region	Δr_0^{MS} [GeV]	Δr_1^{MS}	Δr_2^{MS} [TeV^{-1}]	s_0^{MS} [GeV]	s_1^{MS}
$\lvert\eta\rvert < 1.05$ (small)	$0.115^{+0.083}$	$0.0030^{+0.0079}$	$0^{+0.21}$	$-0.035^{+0.017}_{-0.011}$	$+3.57^{+0.38}_{-0.60} \times 10^{-3}$
$\lvert\eta\rvert < 1.05$ (large)	$0.101^{+0.090}$	$0.0034^{+0.0081}$	$0^{+0.11}$	$-0.022^{+0.007}_{-0.014}$	$-0.22^{+0.37}_{-0.24} \times 10^{-3}$
$1.05 \leq \lvert\eta\rvert < 2.0$ (small)	$0^{+0.080}$	$0.0171^{+0.0059}$	$0^{+0.22}$	$-0.032^{+0.017}_{-0.016}$	$-1.07^{+0.77}_{-0.93} \times 10^{-3}$
$1.05 \leq \lvert\eta\rvert < 2.0$ (large)	$0^{+0.080}$	$0.0190^{+0.0047}$	$0^{+0.17}$	$-0.026^{+0.009}_{-0.017}$	$-1.46^{+0.45}_{-0.57} \times 10^{-3}$
$\lvert\eta\rvert \geq 2.0$ (small)	$0^{+0.080}$	$0.0022^{+0.0075}$	$0^{+0.06}$	$-0.031^{+0.029}_{-0.031}$	$-0.91^{+1.63}_{-0.91} \times 10^{-3}$
$\lvert\eta\rvert \geq 2.0$ (large)	$0^{+0.080}$	$0.0171^{+0.0052}$	$0^{+0.29}$	$-0.057^{+0.019}_{-0.021}$	$+0.40^{+1.22}_{-0.50} \times 10^{-3}$

Table 2. Summary of MS momentum resolution and scale corrections for small and large MS sectors, averaged over three main detector regions. The corrections for large and small MS sectors are derived in 18 η detector regions, as described in Sect. 5.1.1, and averaged according to the η width of each region. The parameters Δr_0^{MS}, for $\lvert\eta\rvert > 1.05$, and Δr_2^{MS}, for the full η range, are fixed to zero. The uncertainties are the result of the sum in quadrature of the statistical and systematic uncertainties. Only upper uncertainties are reported for the Δr parameters; lower uncertainties are evaluated by symmetrization, as described in Sect. 5.1.2.

MS tracks

Reconstruction Efficiencies with 50 ns and 25 ns Datasets

- Data-driven reco-efficiencies are a test of our detector understanding
- Do them as soon as data is available ⇒ reliable tools and very quick turnaround from MCP

50 ns dataset

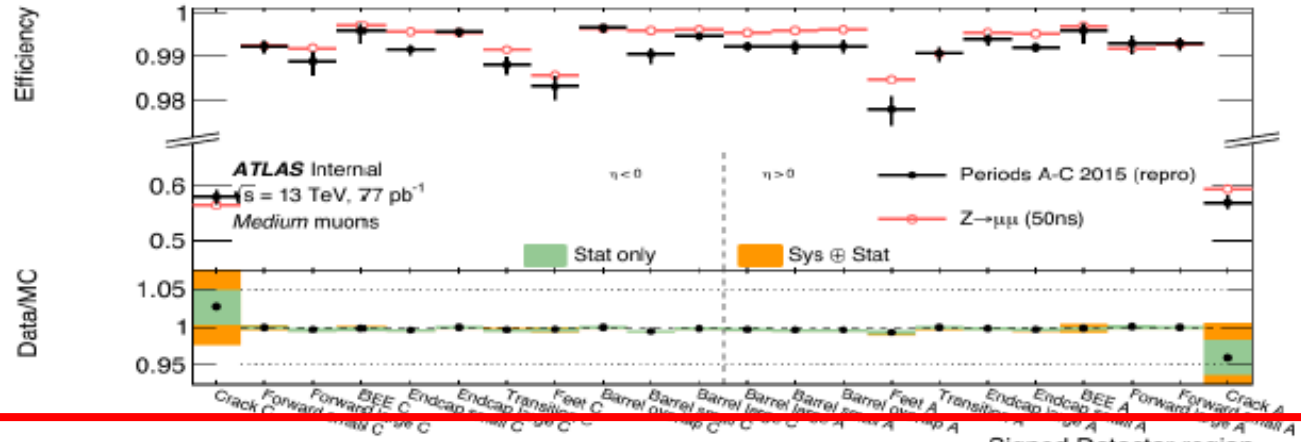

Recent 25 ns data

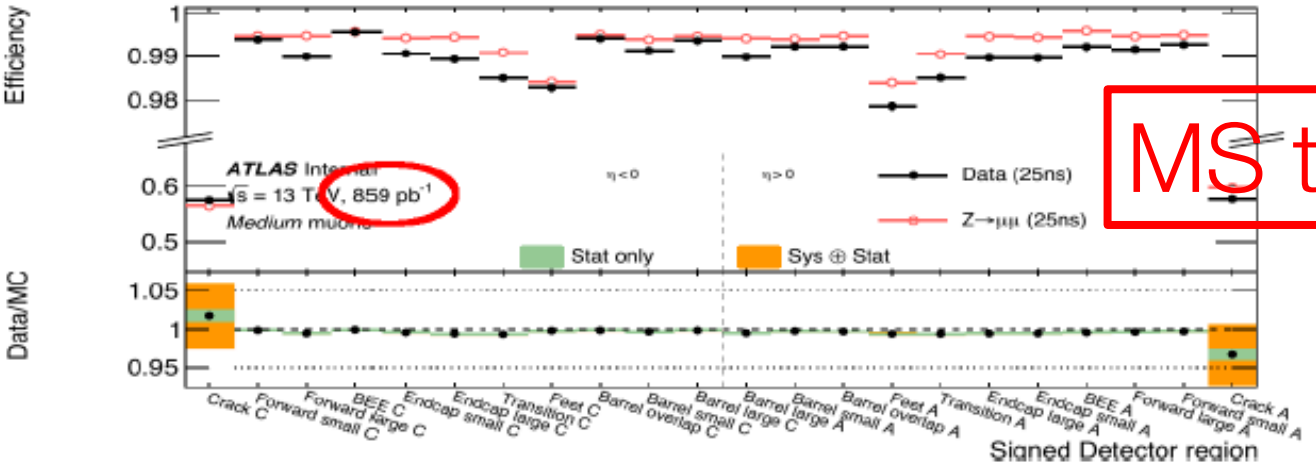

MS tracks

- Slight efficiency drop in 25ns dataset quickly identified and understood (thanks to tracking-CP experts) to be due to TRT occupancy

Recap

- Calorimeters, EM, HC
- Jets (with calorimeter objects!)
  - Building Jets (→ definition of distance → Achen, k_T, anti-k_T algorithms)
  - Boosted Jets
- Muons
  - Different types of reconstructed muons
  - Tuning MC to make it look like data → scale factors, additional smearings
- MET: combination of Calorimeter objects + Muons
- → can we do better??

MET studies

Missing Transverse Momentum Measurement using the ATLAS Detector

The ATLAS Collaboration

LHCC Poster Session, 4 March, 2015, CERN

Bo Liu (Academia Sinica/Shandong University) on behalf of ATLAS $E_{\mathrm{T}}^{\mathrm{miss}}$ group

E_T^{miss} and Particle-Flow

Marianna Testa (LNF-INFN)

Performance of missing transverse momentum reconstruction in ATLAS studied in proton-proton collisions in 2012 at 8 TeV

Luis March
School of Physics, University of the Witwatersrand, Johannesburg 2050, South Africa
E-mail: lmarch@cern.ch

arXiv:1802.08168v2 [hep-ex] 13 Dec 2018

understanding MET

MET is the undetected energy (may be carried away by non-interacting particles)(but also due to detector-effects like inefficiencies or cracks)

Not associated to a track

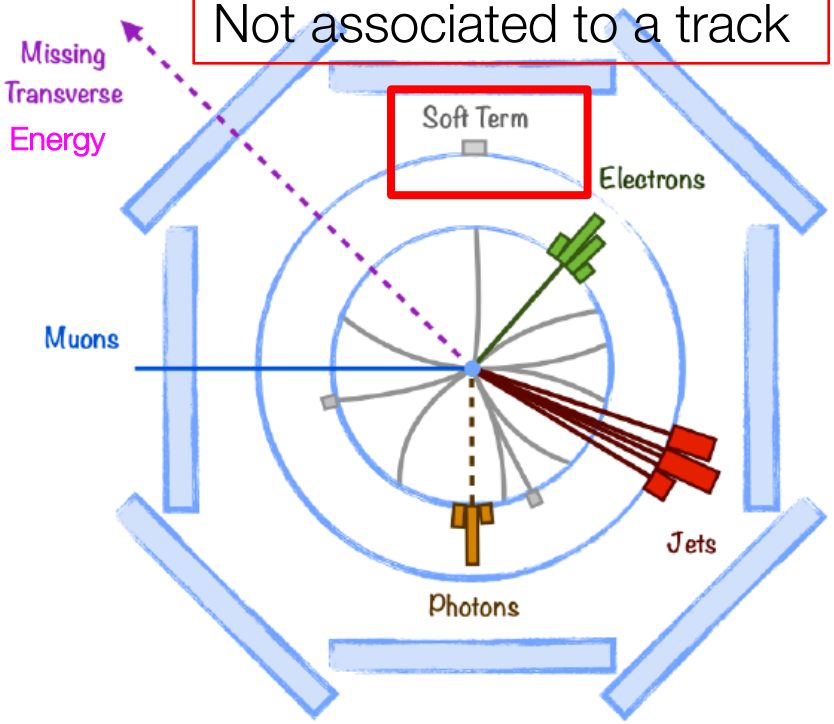

In this flavour

$$MET = \Sigma \text{ (calorimeters)} + \text{Muons}$$

MET is affected by PU pile-up

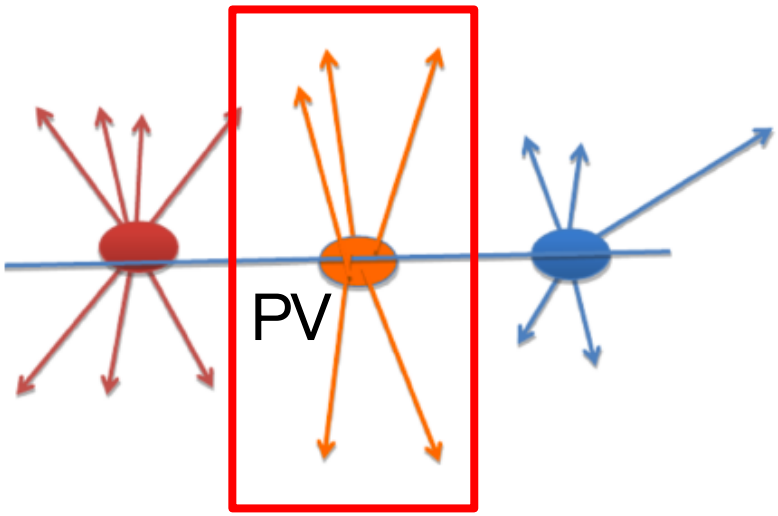

how to exclude non-PV objects from the calculation of the hard-scattering HS vertex?

E_T^{miss} Reconstruction

MET_RefFinal is the basic recommended reconstruction for E_T^{miss}.
It's the vectorial sum of high p_T objects + clusters/tracks not associated to them.
The sequence of high-p_T objects is by determined by the reconstruction quality of the object:

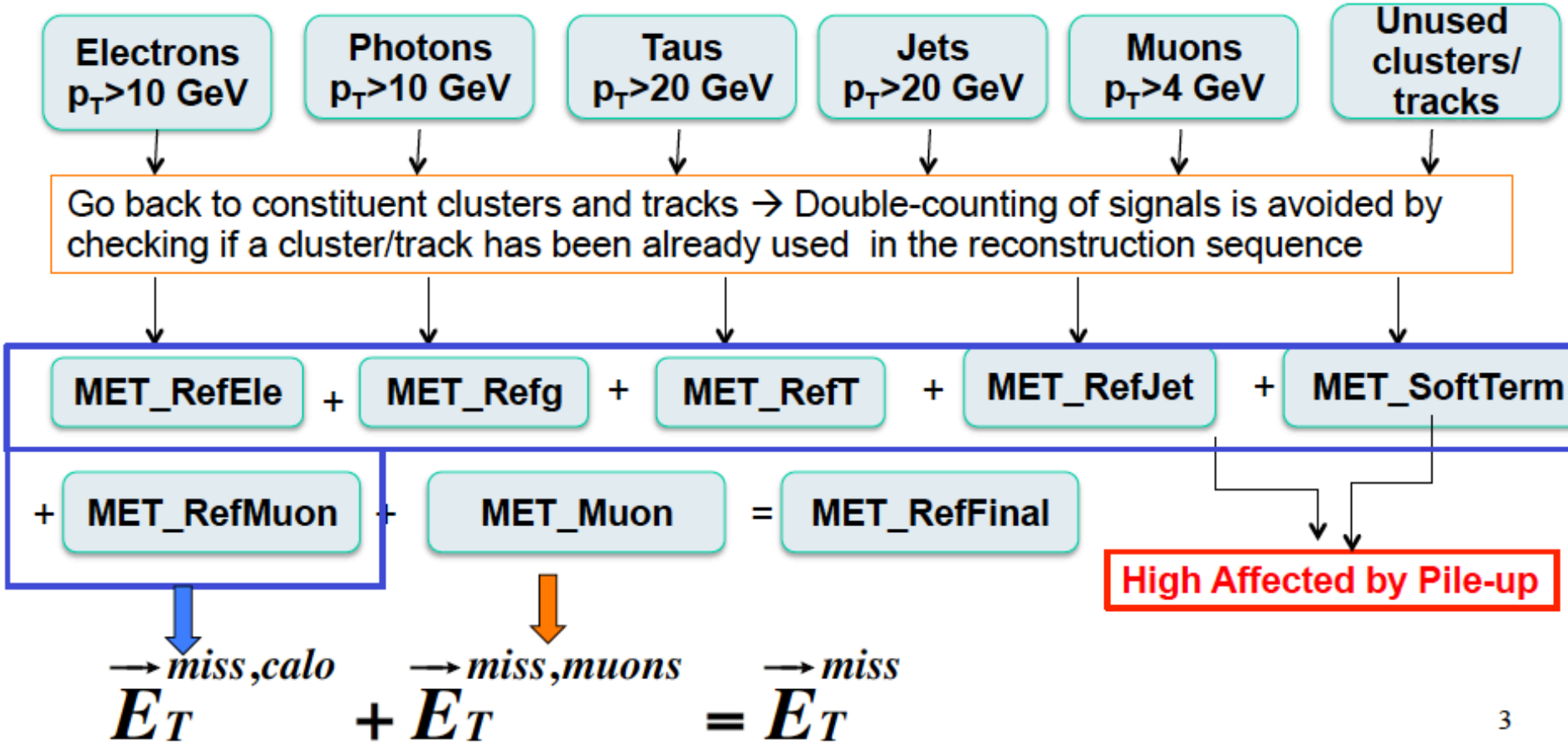

Pile-up, suppression (mitigation) in Jets

To suppress pile-up jets cut on the Jet Vertex Fraction (JVF)

JVF = the fraction of momenta of tracks matched to the jet which are associated with the hard scattering vertex:

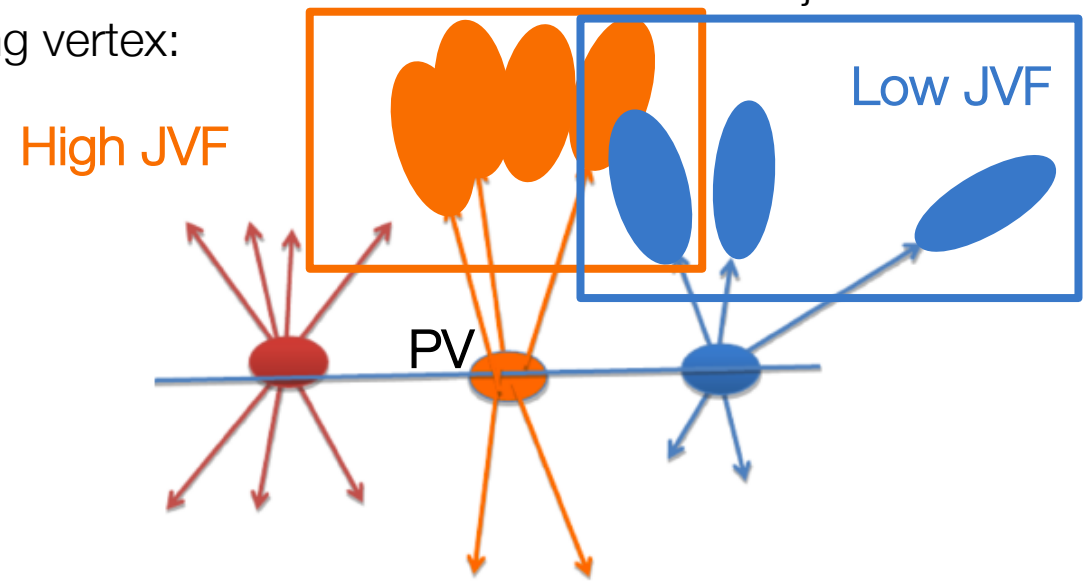

$$JVF = \sum_{tracks_{jets},PV} p_T \Big/ \sum_{tracks_{jets}} p_T$$

- Sums over the tracks matched to the jet
- PV denotes the tracks associated to the Primary Vertex (PV).

Remove Jets with JVF < cut

Correcting soft terms of MET

Two methods for suppressing the pile-up in the soft terms:

- use of tracks (associated with the primary vertex), similar to JVF:

$$STVF = \sum_{tracks_{SoftTerm},PV} p_T \Big/ \sum_{tracks_{SoftTerm}} p_T$$

Non associated to PV

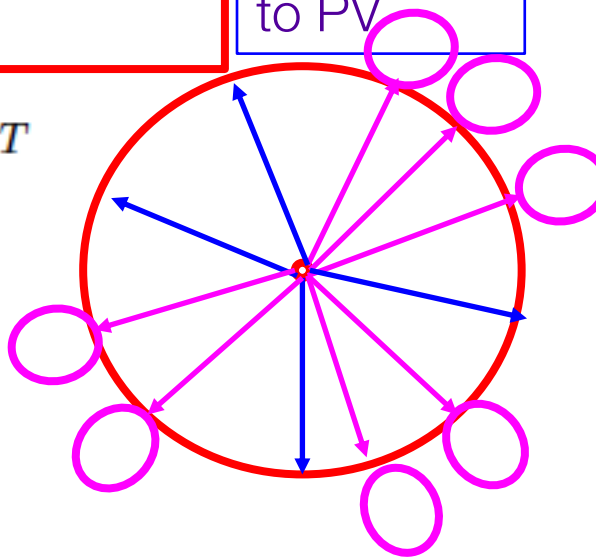

sums are taken over

- the tracks unmatched to physics objects
- tracks associated to the primary vertex.

The $E_T^{miss,SoftTerm}$ is multiplied by the STVF factor and the E^{miss}_T calculated, with this corrected soft term.

- jet area method.

➢The event transverse momentum density ρ is used $p_T^{jet,corr} = p_T^{jet} - \rho A^{jet}$

Comparison among different MET's

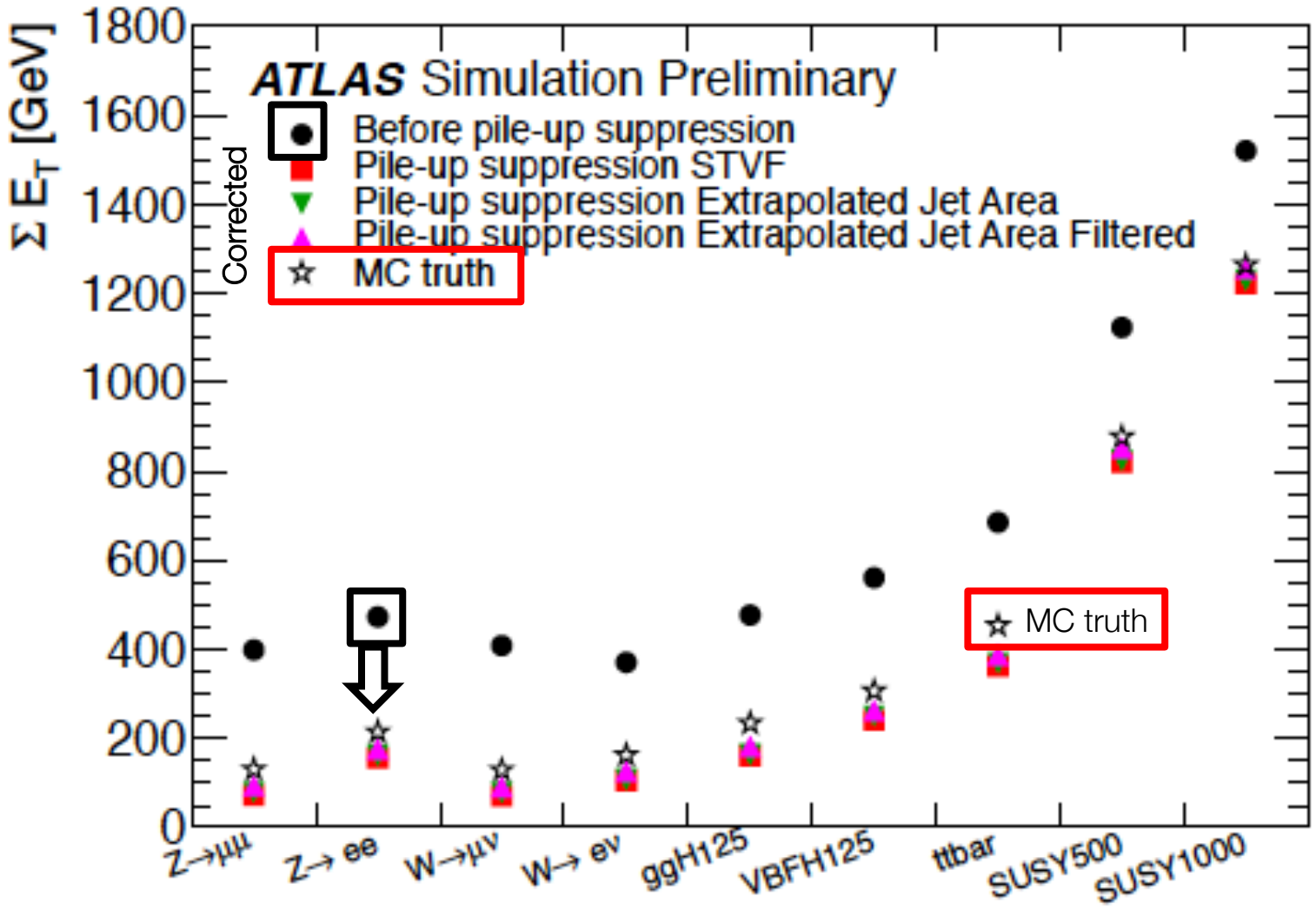

Beyond MET: Particle Flow?

Particle-Flow

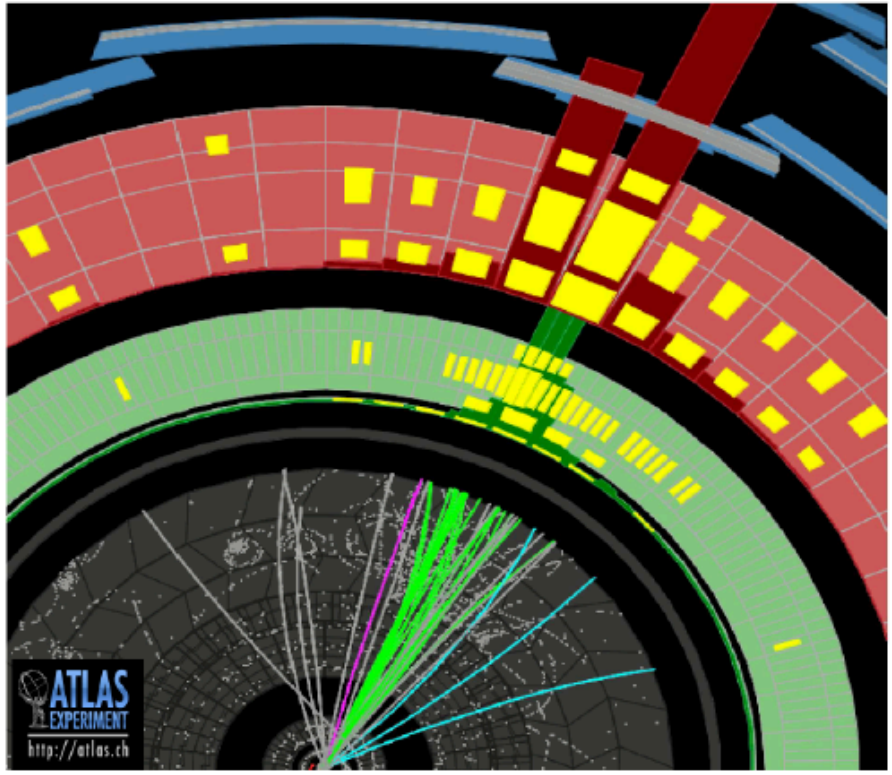

Particle-Flow: Introduction

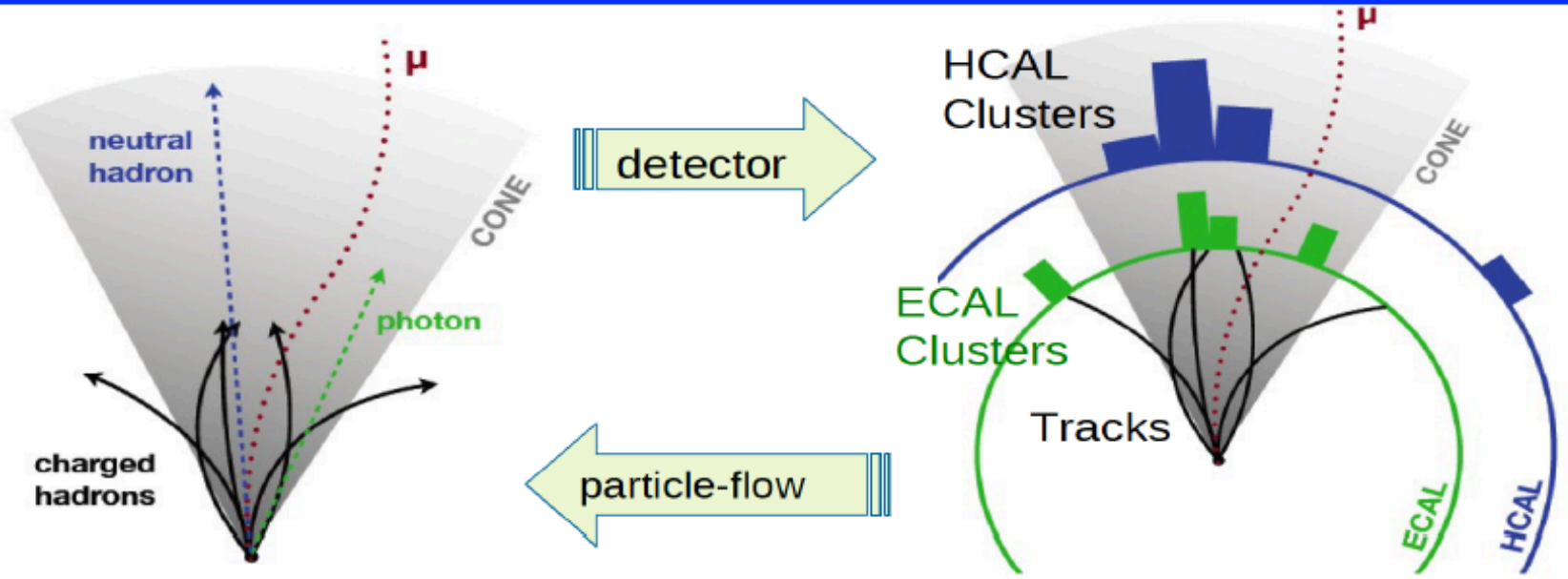

The Particle Flow algorithm aims at identifying and reconstructing individual particles from the collision by optimally combining the information from different subdetectors

List of individual particles is then used to reconstruct jets, determine E_T^{miss}, τ and tag b-jet

Through **combination of information Particle Flow allows to mitigate maximally Pile-up**

Particle-Flow paradigm

In a typical jet
- **60%** of jet energy in **charged hadrons**
- **30%** **in photons** mainly from $\pi^0 \rightarrow \gamma\gamma$
- **10%** **in neutral hadrony** mainly n and K_L

❖ **Traditional calorimetric approach**:
- Measure all components of jet in ECAL/HCAL

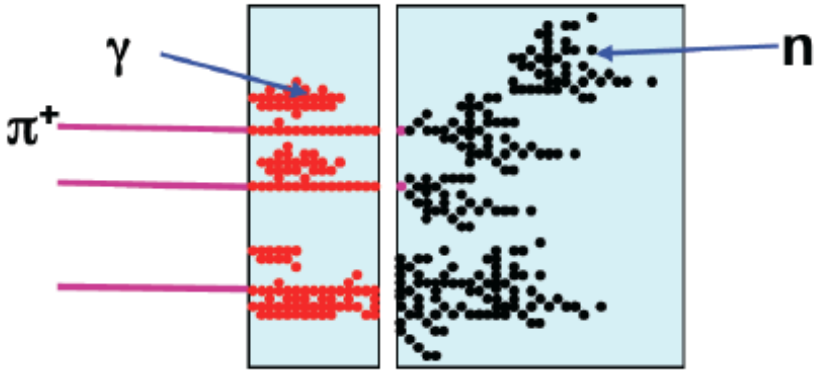

$$E_{JET} = E_{ECAL} + E_{HCAL}$$

❖ **Idealised PFlow approach**:
- Charged particles measured in the tracker
- Photons in ECAL
- Neutral hadrons in the HCAL

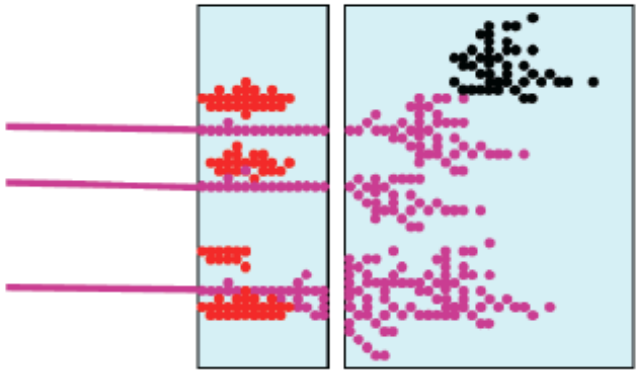

$$E_{JET} = E_{TRACK} + E_{\gamma} + E_{n}$$

Tracker vs Calorimeter

- The design of the ATLAS detector [8] specifies a calorimeter energy resolution for single charged pions in the centre of the detector of

$$\frac{\sigma(E)}{E} = \frac{50\,\%}{\sqrt{E}} \oplus 3.4\,\% \oplus \frac{1\,\%}{E}, \tag{1}$$

while the design inverse transverse momentum resolution for the tracker is

$$\sigma\left(\frac{1}{p_{\mathrm{T}}}\right) \cdot p_{\mathrm{T}} = 0.036\,\% \cdot p_{\mathrm{T}} \oplus 1.3\,\%, \tag{2}$$

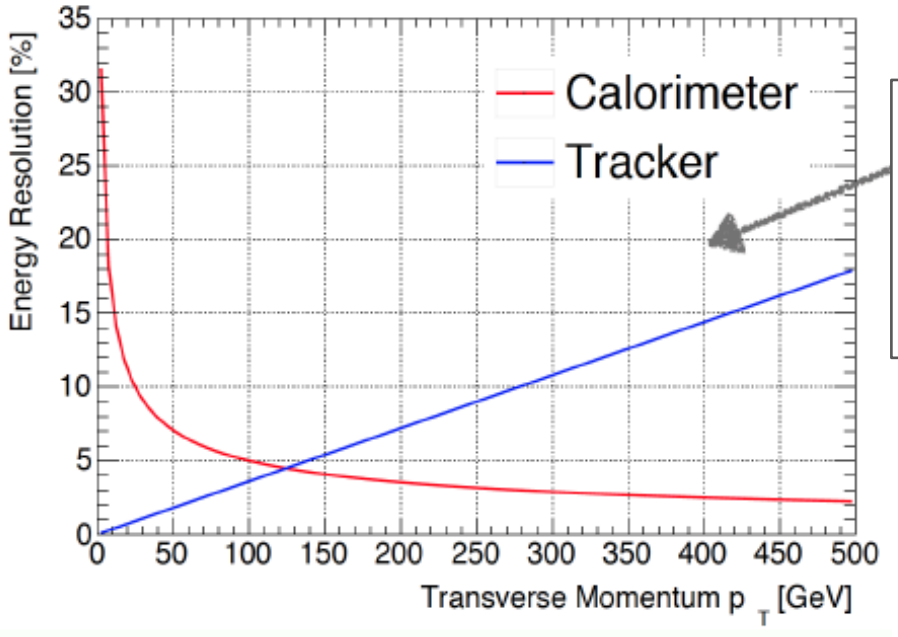

Above ~ 140 GeV the calorimeter has a better resolution than the tracker

Recent reference to PF in ATLAS

Eur. Phys. J. C (2017) 77:466
DOI 10.1140/epjc/s10052-017-5031-2

THE EUROPEAN PHYSICAL JOURNAL C

CrossMark

Regular Article - Experimental Physics

Jet reconstruction and performance using particle flow with the ATLAS Detector

ATLAS Collaboration*

CERN, 1211 Geneva 23, Switzerland

Received: 31 March 2017 / Accepted: 27 June 2017 / Published online: 13 July 2017

Jets with Particle-Flow

There are several benefits to use particle in Jet reconstruction

1) The **tracker** has a **better energy resolution** than the calorimeter at low p, in ATLAS for p_T<140 GeV
2) In a jet **soft charged particles** are swept away by the magnetic field, can be **recovered by the tracker**
3) Tracker can pick cup charged particles which would be below the calo noise threshold
4) The tracker has better η,Φ resolution
5) The tracker can tell which vertex the charged particles come from

Charged Hadron subtraction

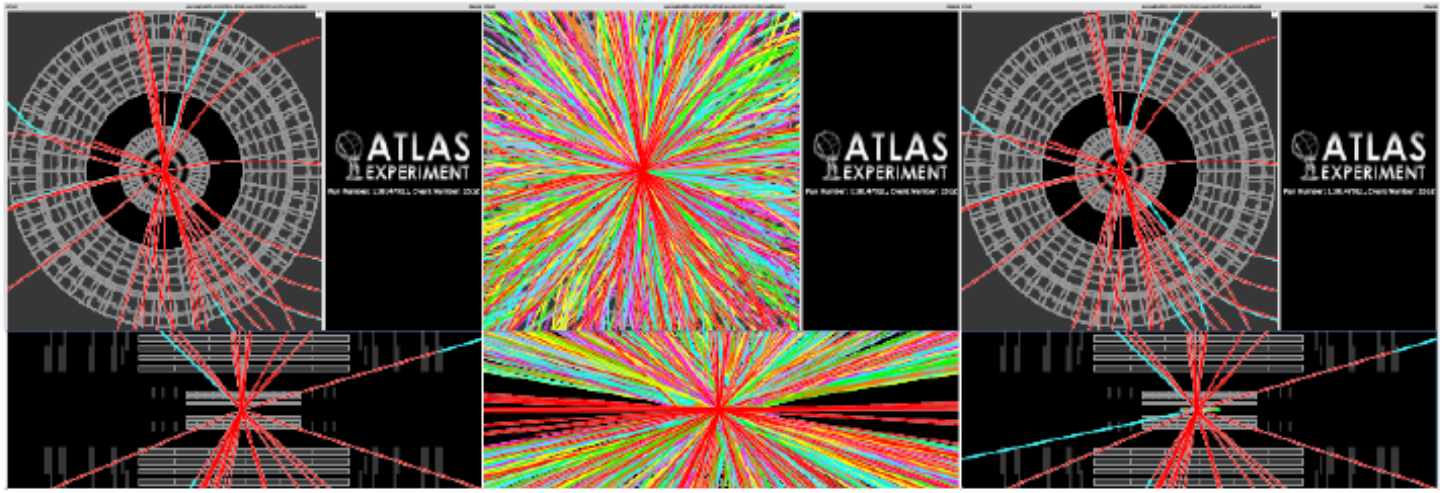

The same event with No pile-up (with z_0), $\mu = 40$ (without z_0), $\mu = 40$ (with z_0).

Particle-Flow in ATLAS

Match Tracks to Clusters

A cluster can contain a single, many or part of the shower

Does the cluster energy match the track (E/p)?

YES

NO

Match all clusters in ΔR<0.2 to recover split showers

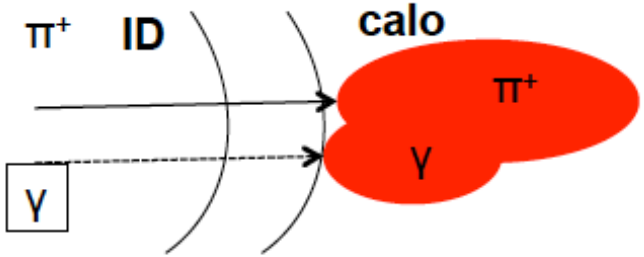

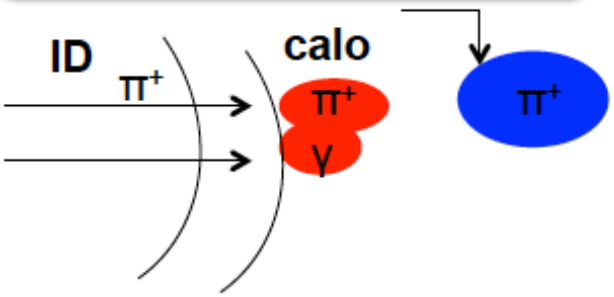

Subtract matched energy deposit cell-by-cell from the calorimeter

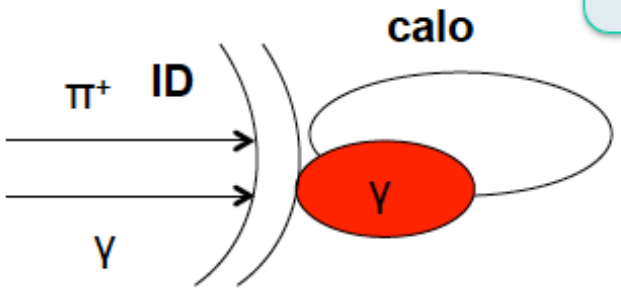

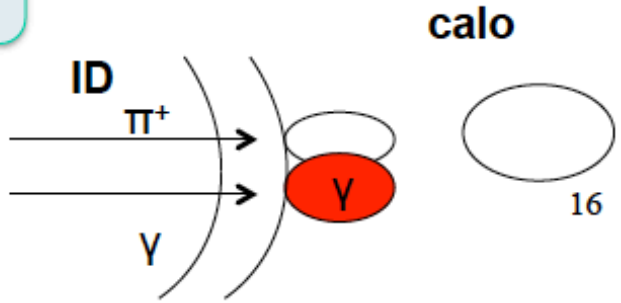

The Algorithm - Cell-By-Cell Subtraction

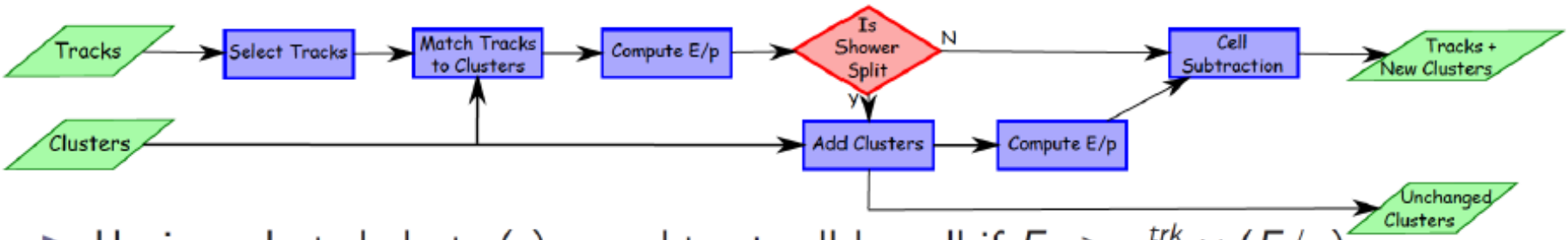

- Having selected cluster(s) we subtract cell-by-cell if $E_{cl} > p^{trk} \times (E/p)$.
- Each layer is split into rings around the extrapolated track.
- Shower profiles binned in E, $|\eta|$ and LHED are used to determine the ring with the highest expected energy density.
- These cells are removed and this is continued until $E_{sub} = p^{trk} \times (E/p)$.
- Only a fraction of the energy in the final ring will be removed.

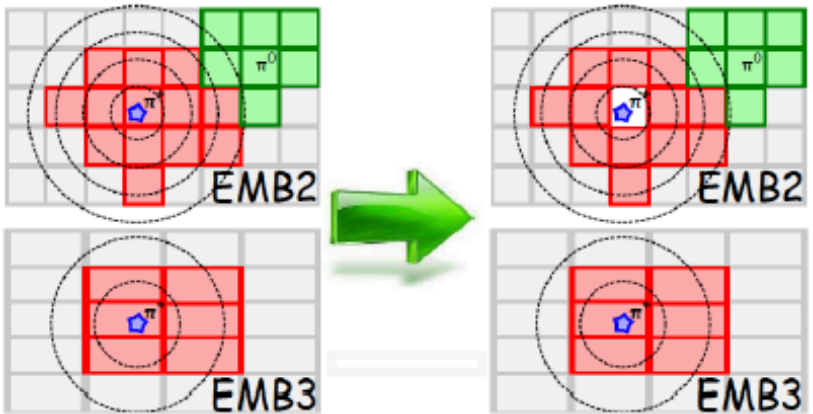

The Algorithm - Cell-By-Cell Subtraction

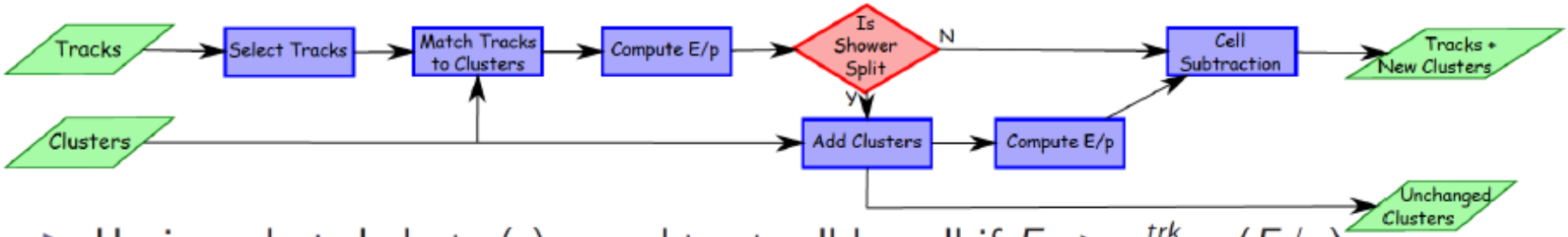

- Having selected cluster(s) we subtract cell-by-cell if $E_{cl} > p^{trk} \times (E/p)$.
- Each layer is split into rings around the extrapolated track.
- Shower profiles binned in E, $|\eta|$ and LHED are used to determine the ring with the highest expected energy density.
- These cells are removed and this is continued until $E_{sub} = p^{trk} \times (E/p)$.
- Only a fraction of the energy in the final ring will be removed.

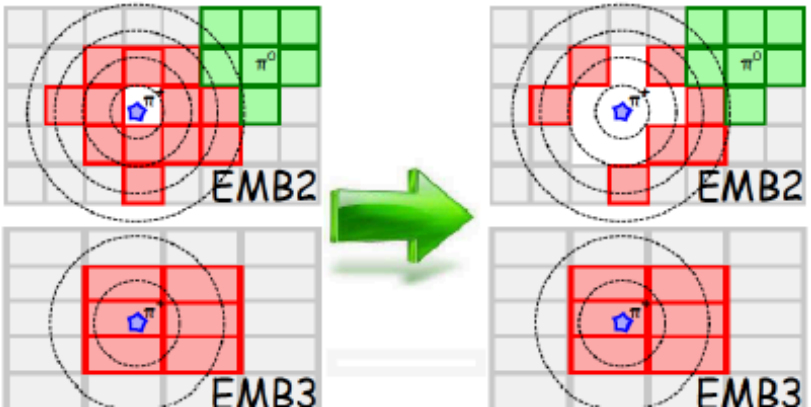

The Algorithm - Cell-By-Cell Subtraction

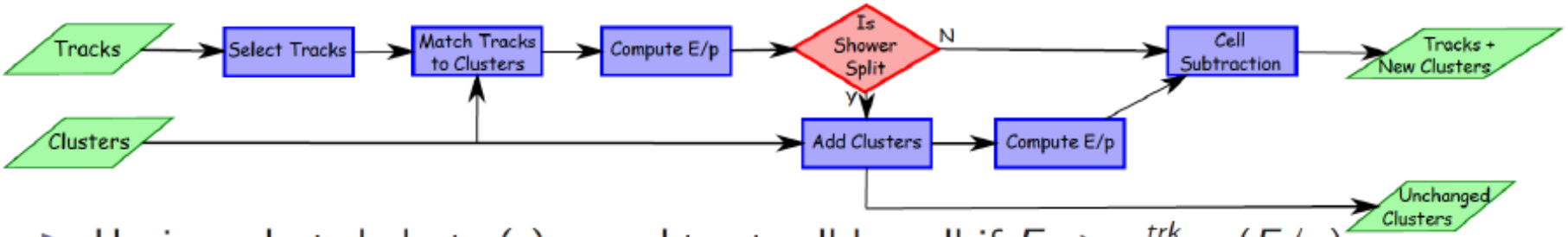

- Having selected cluster(s) we subtract cell-by-cell if $E_{cl} > p^{trk} \times (E/p)$.
- Each layer is split into rings around the extrapolated track.
- Shower profiles binned in E, $|\eta|$ and LHED are used to determine the ring with the highest expected energy density.
- These cells are removed and this is continued until $E_{sub} = p^{trk} \times (E/p)$.
- Only a fraction of the energy in the final ring will be removed.

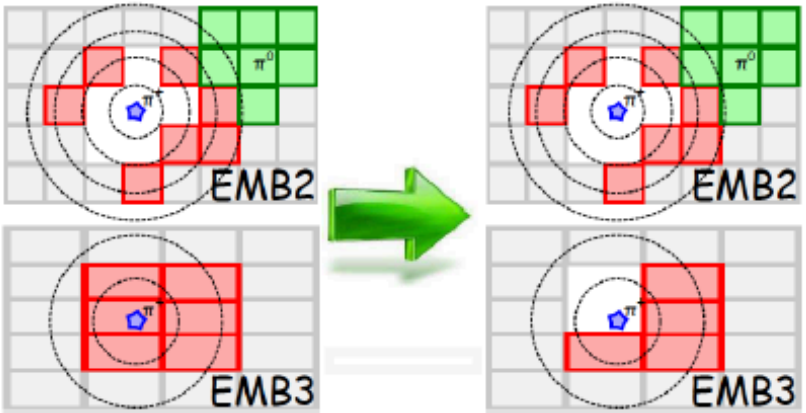

The Algorithm - Cell-By-Cell Subtraction

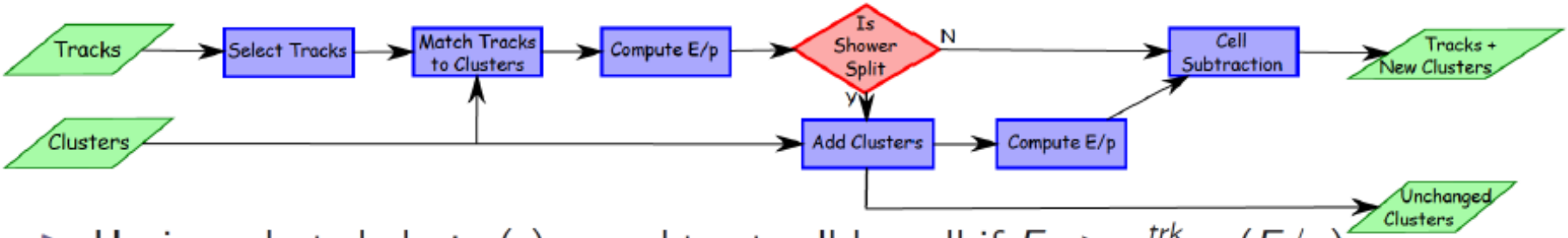

- Having selected cluster(s) we subtract cell-by-cell if $E_{cl} > p^{trk} \times (E/p)$.
- Each layer is split into rings around the extrapolated track.
- Shower profiles binned in E, $|\eta|$ and LHED are used to determine the ring with the highest expected energy density.
- These cells are removed and this is continued until $E_{sub} = p^{trk} \times (E/p)$.
- Only a fraction of the energy in the final ring will be removed.

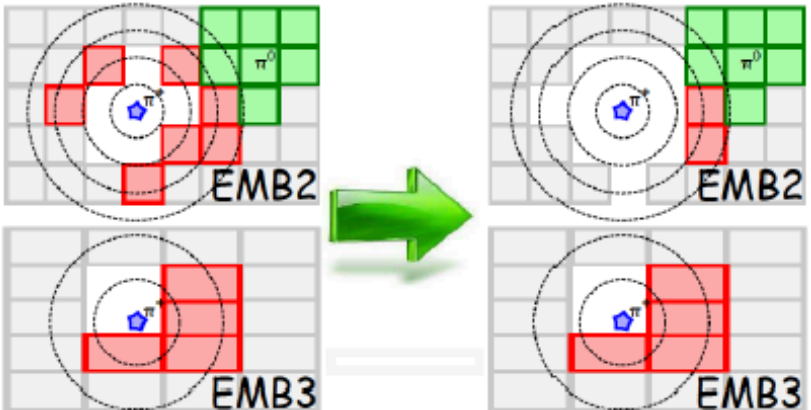

The Algorithm - Cell-By-Cell Subtraction

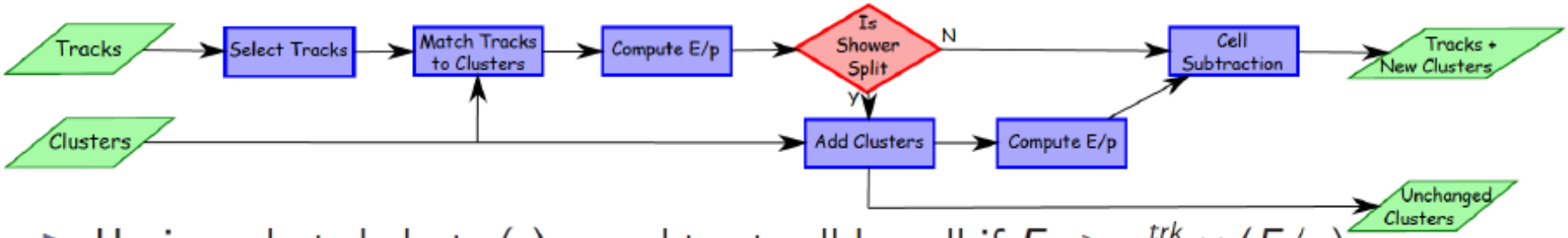

- Having selected cluster(s) we subtract cell-by-cell if $E_{cl} > p^{trk} \times (E/p)$.
- Each layer is split into rings around the extrapolated track.
- Shower profiles binned in E, $|\eta|$ and LHED are used to determine the ring with the highest expected energy density.
- These cells are removed and this is continued until $E_{sub} = p^{trk} \times (E/p)$.
- Only a fraction of the energy in the final ring will be removed.

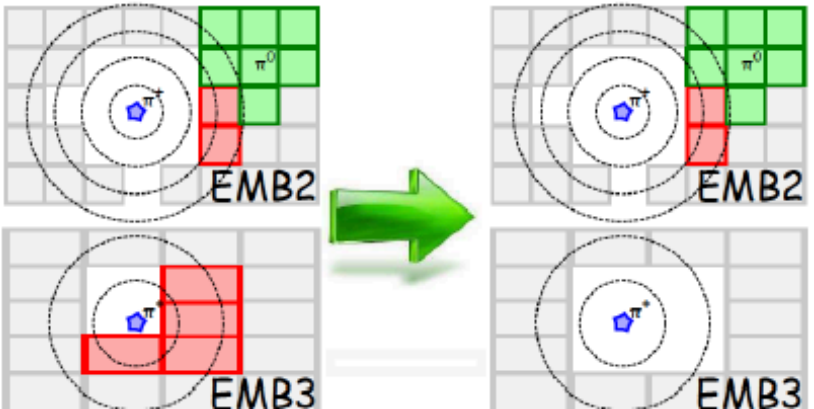

The Algorithm - Cell-By-Cell Subtraction

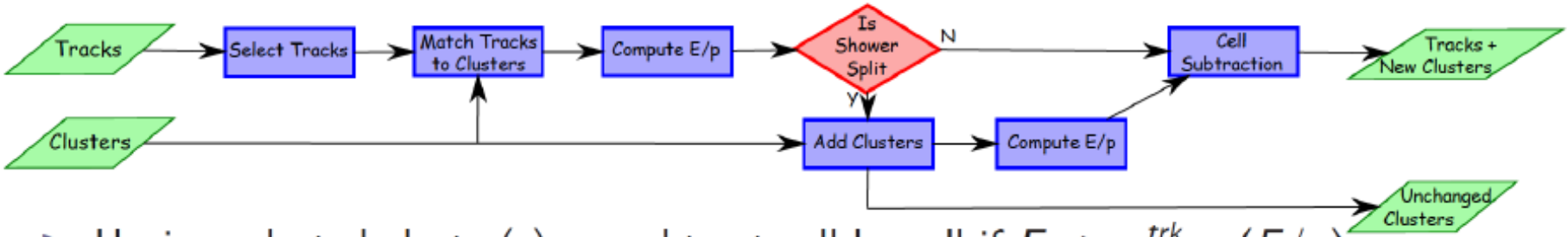

- Having selected cluster(s) we subtract cell-by-cell if $E_{cl} > p^{trk} \times (E/p)$.
- Each layer is split into rings around the extrapolated track.
- Shower profiles binned in E, $|\eta|$ and LHED are used to determine the ring with the highest expected energy density.
- These cells are removed and this is continued until $E_{sub} = p^{trk} \times (E/p)$.
- Only a fraction of the energy in the final ring will be removed.

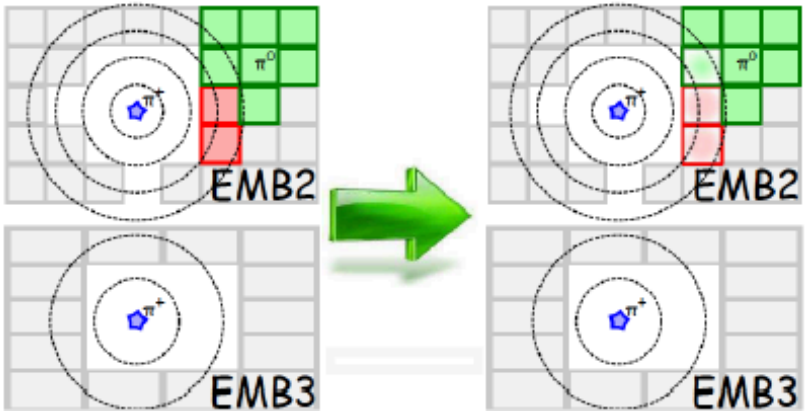

Examples

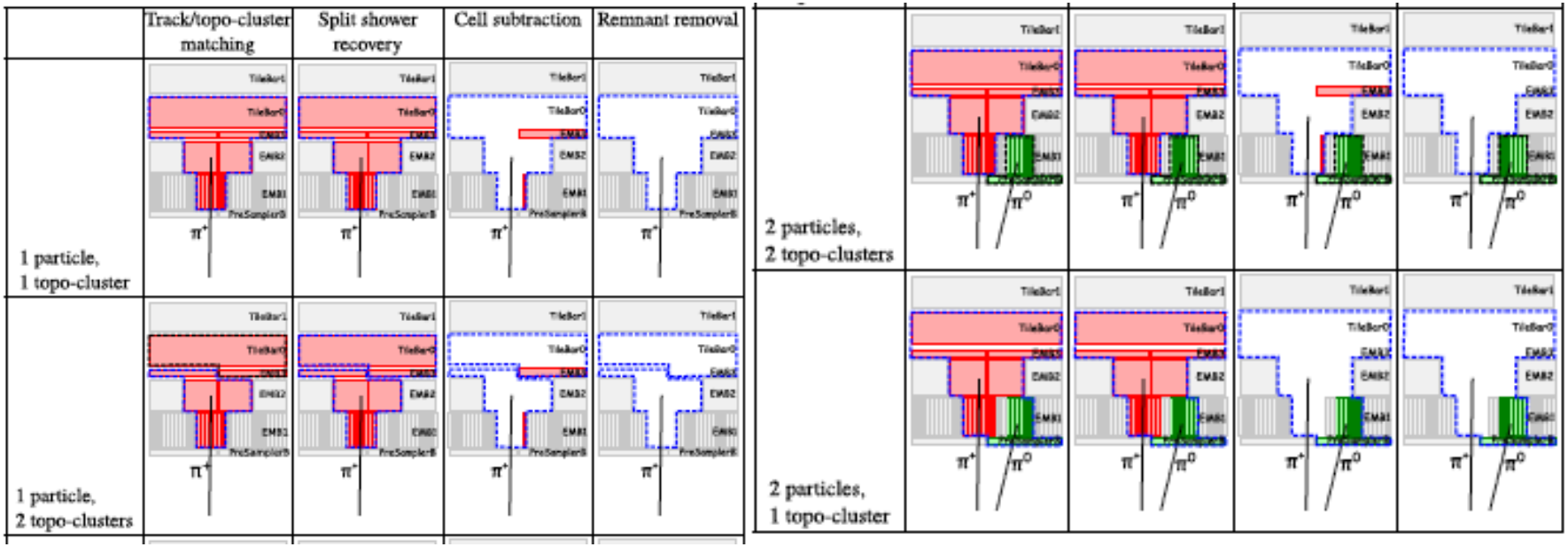

Idealised examples of how the algorithm is designed to deal with several different cases. The red cells are those which have energy from the π^+, the green cells energy from the photons from the π^0 decay, the dotted lines represent the original topo-cluster boundaries with those outlined in blue having been matched by the algorithm to the π^+, while those in black are yet to be selected. The different layers in the electromagnetic calorimeter (Presampler, EMB1, EMB2, EMB3) are indicated. In this sketch only the first two layers of the Tile calorimeter are shown (TileBar0 and TileBar1)

PFlow Jet p_T resolution

Much better resolution at low p_T

Two reasons:

1) Charged Hadron Subtraction:
removal of clusters associated to pile-up tracks in the event

2) Usage of (calibrated) track instead of clusters, which are under-calibrated at low energy
→ The constituent scale of the jets is raised

- At high p_T (> ~100 GeV) **the confusion in crowded environment** worsen the resolution

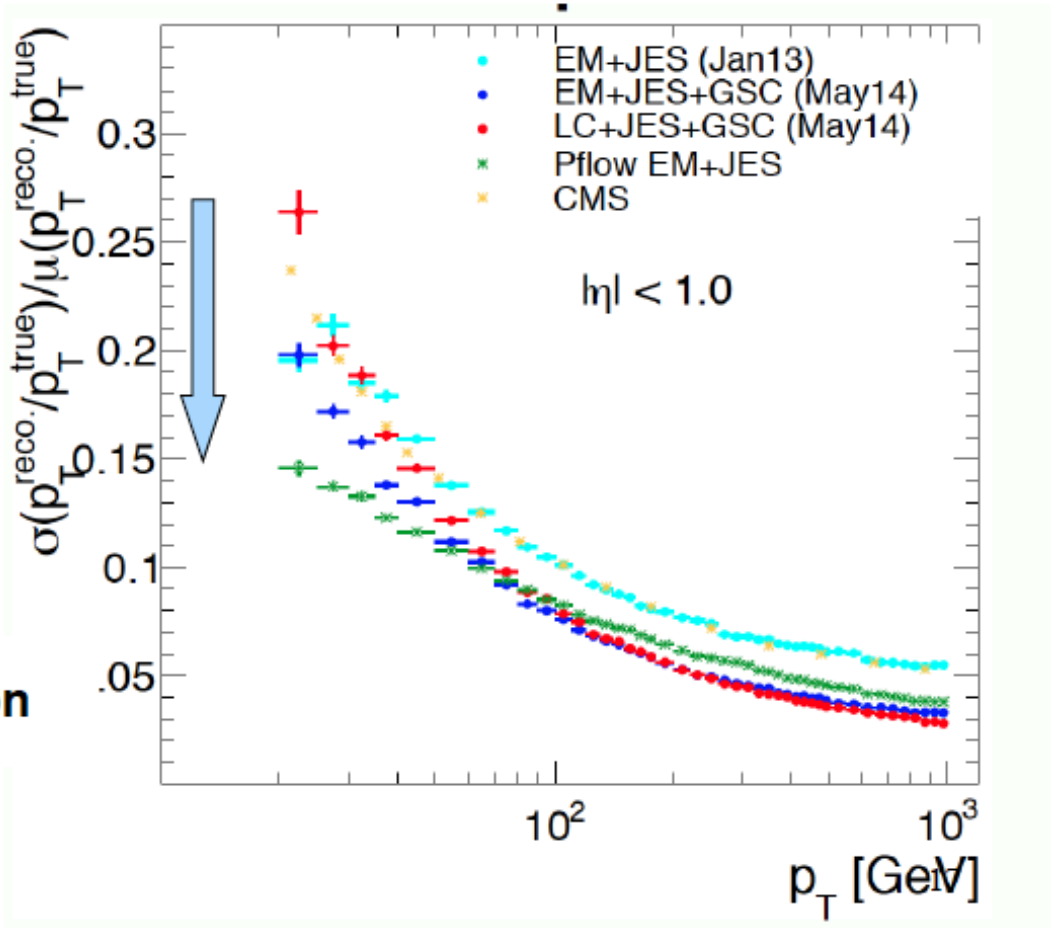

Checking Particle Flow

A sample of $Z \rightarrow \mu\mu$ events with a jet balancing the Z boson is used for the validation.

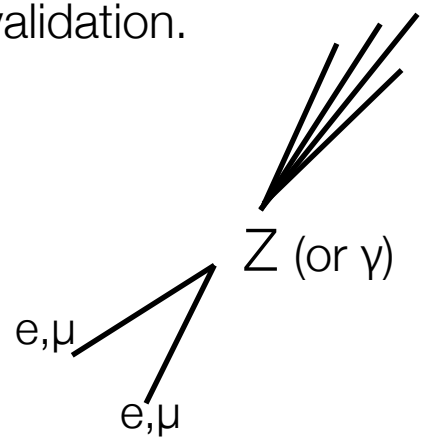

The particle flow algorithm is run on these events.

The jet with the highest p_T (j_1) and the reconstructed Z boson are required to be well separated in azimuthal angle, $\Delta\phi > \pi - 0.3$.

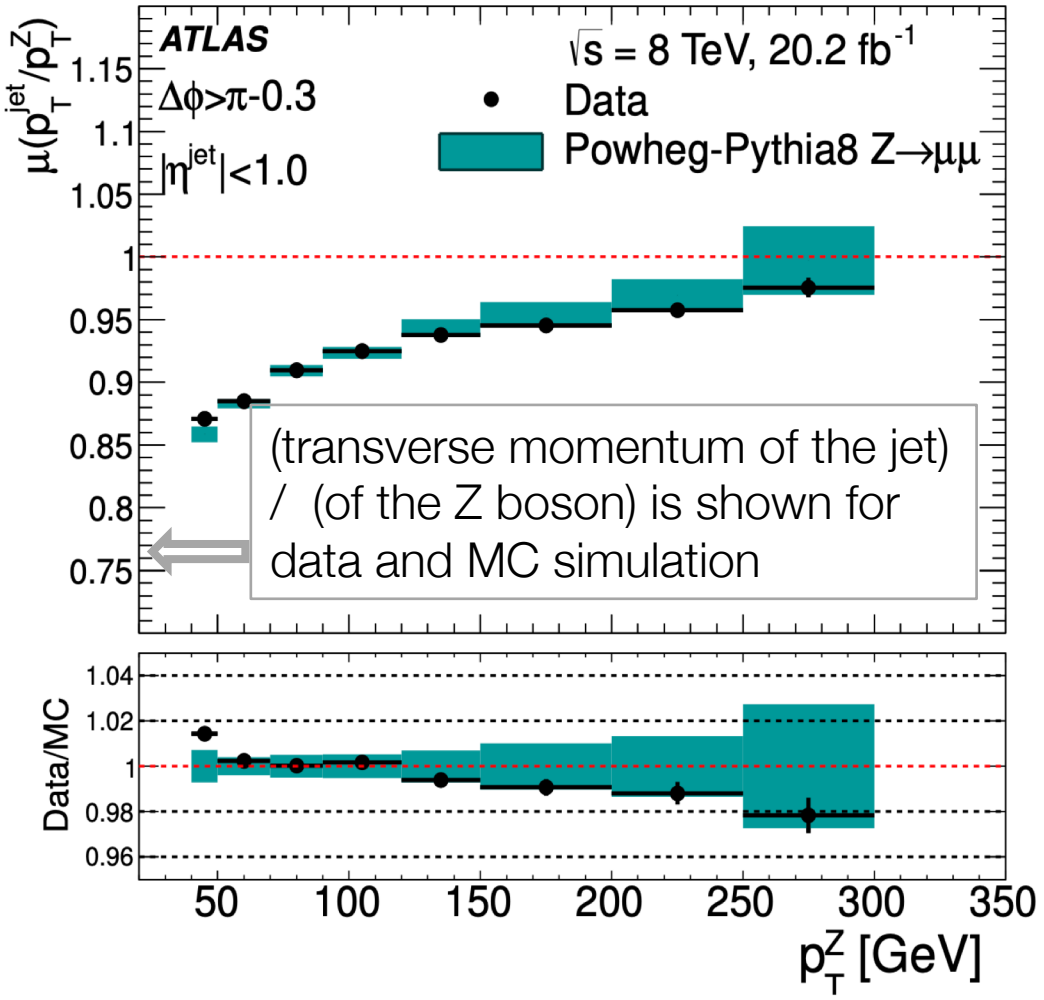

Improvement of Jet Resolution

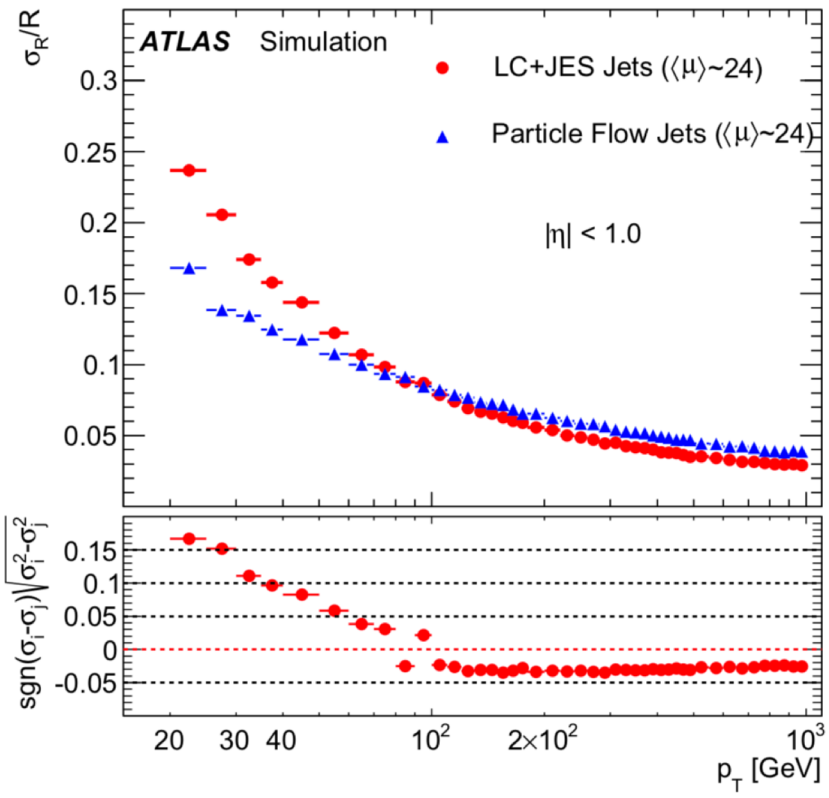

(a)

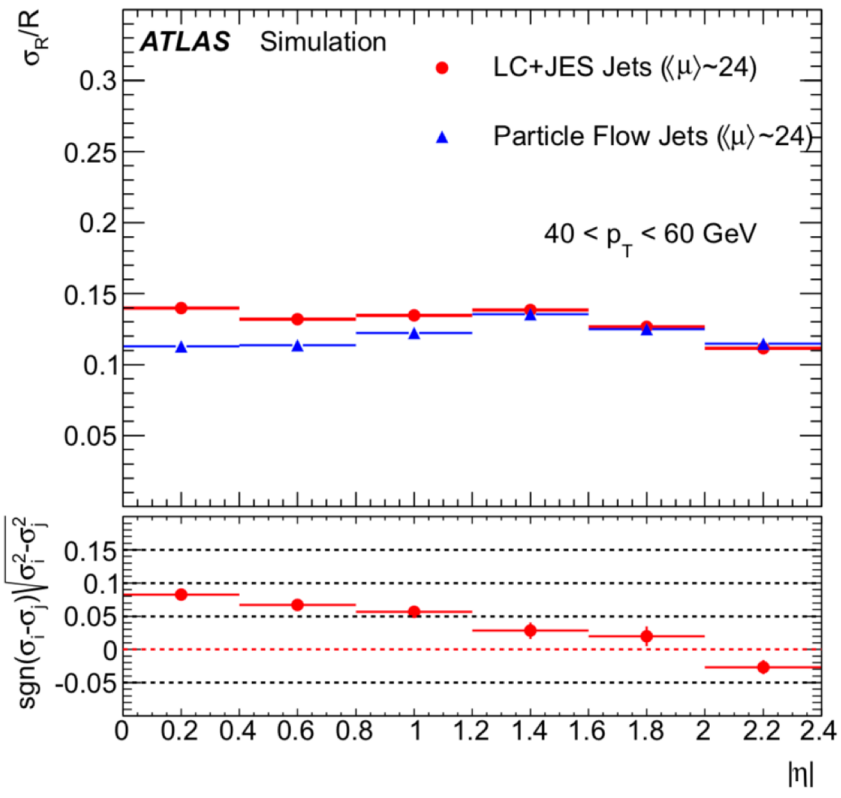

(b)

Fig. 26 The jet transverse momentum resolution as determined in dijet MC events for calorimeter jets and particle flow jets. Subfigure (**a**) shows the resolution as a function of p_{T} for jets with $|\eta| < 1.0$ and (**b**) shows the resolution as a function of $|\eta|$ for jets with $40 < p_{\mathrm{T}} < 60\,\mathrm{GeV}$. Simulated pile-up conditions are similar to the data-taking in 2012. To quantify the difference in resolution between particle flow and calorimeter jets, the *lower figure* shows the square root of the difference of the squares of the resolution for the two classes of jets

More on Resolution

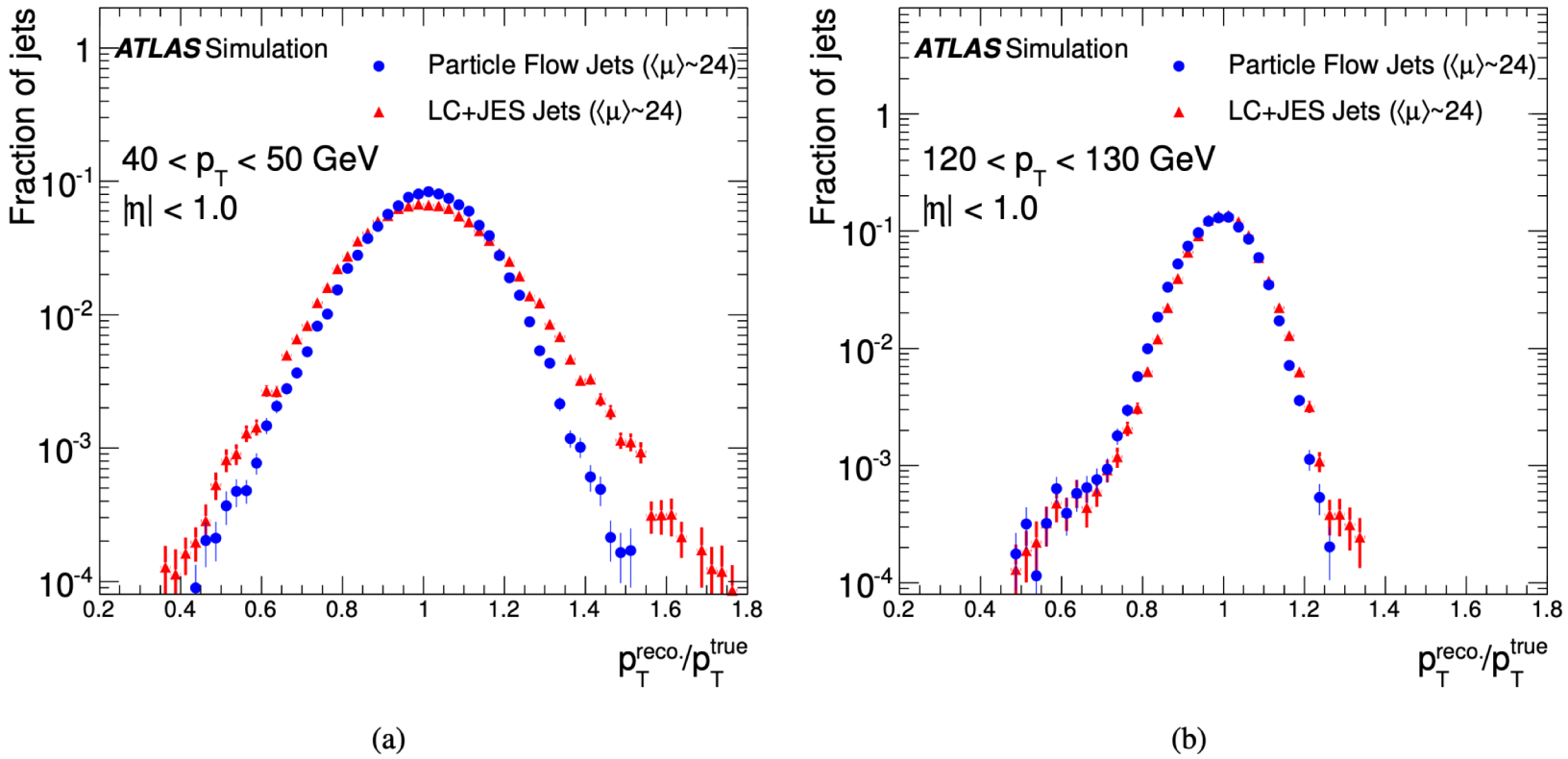

Figure 27: The jet transverse momentum response distribution as determined in dijet MC events for calorimeter jets and particle flow jets. Two different p_T bins as shown; (a) $40 < p_T < 50$ GeV and (b) $120 < p_T < 130$ GeV. Simulated pile-up conditions are similar to the data-taking in 2012.

Angular Resolution

Trackers reconstruct directions MUCH better than calorimeters (calorimeters → direction from vector (Primary Vertex) to (Vertex of Shower)

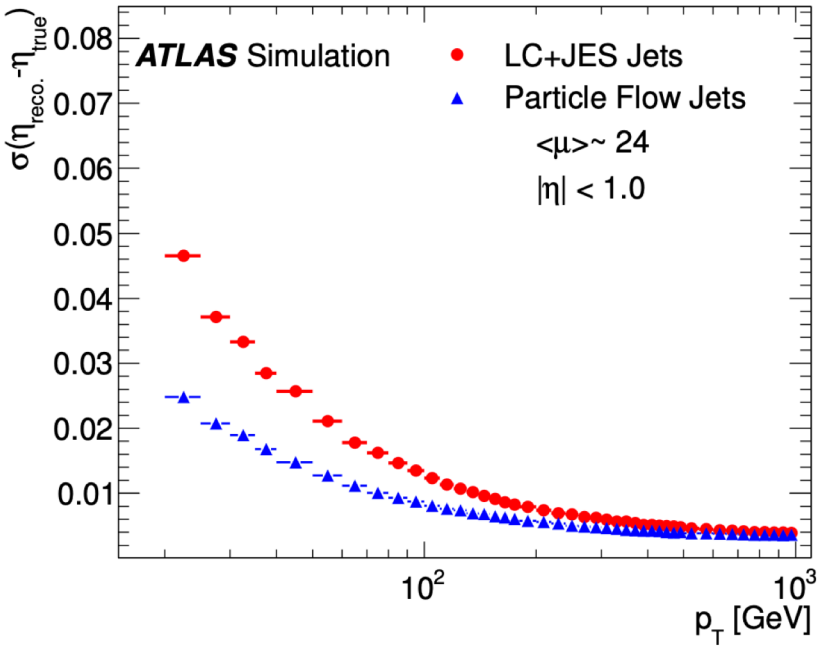

(a)

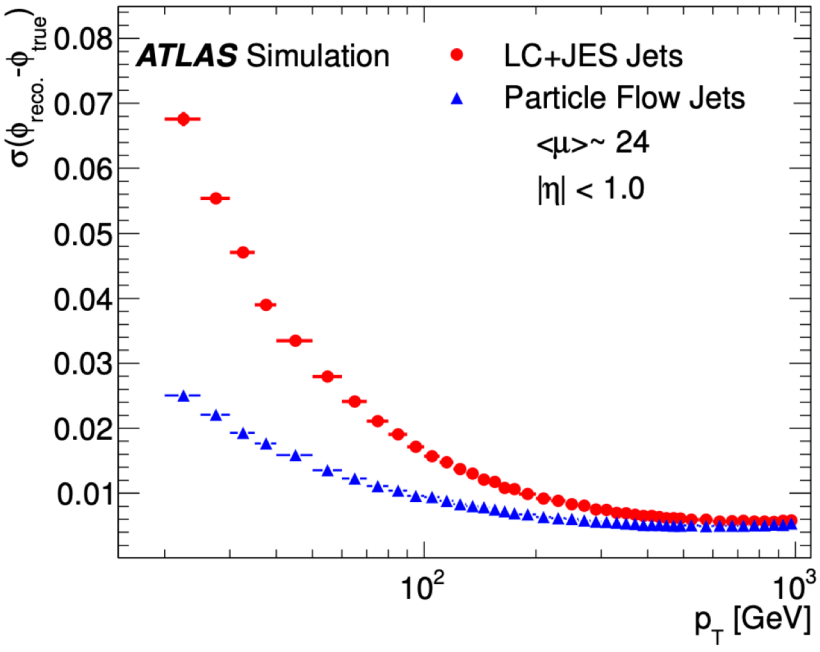

(b)

Figure 28: The angular resolution, (a) in η and (b) in ϕ, as a function of the jet p_{T}, determined in dijet MC simulation by fitting Gaussian functions to the difference between the reconstructed and truth quantities. Conditions are similar to the data-taking in 2012.

Fake Jets: JVF vs PF

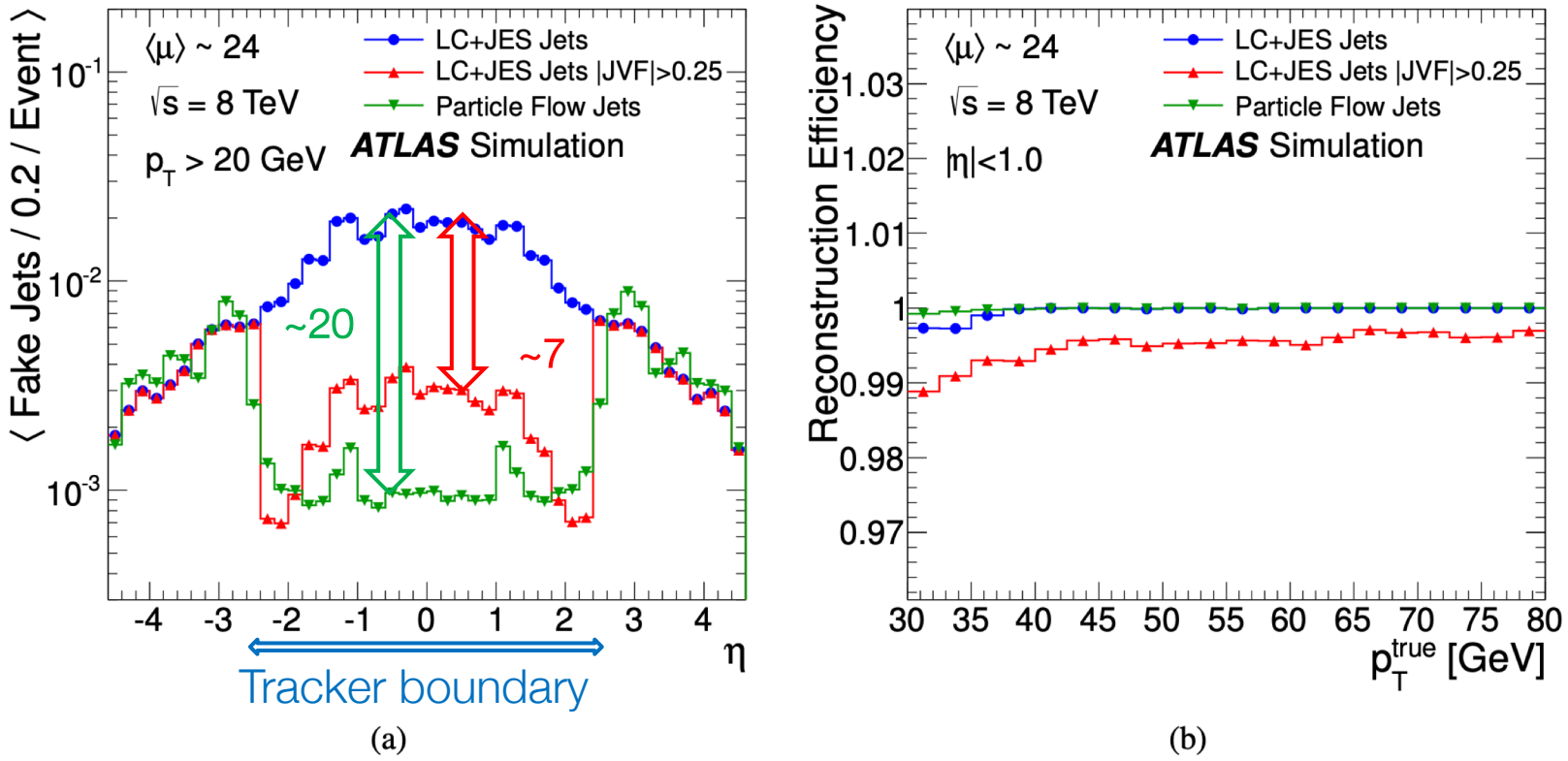

Figure 29: In the presence of pile-up, 'fake jets' can arise from particles not produced in the hard-scatter interaction. Subfigure (a) shows the number of fake jets (jets not matched to truth jets with $p_T > 4$ GeV within $\Delta R < 0.4$) and (b) the efficiency of reconstructing a hard-scatter jet (reconstructed jet found within $\Delta R < 0.4$ with $p_T > 15$ GeV) in dijet MC events. Simulated pile-up conditions are similar to the data-taking in 2012.

PF: Jets in High Pile-up

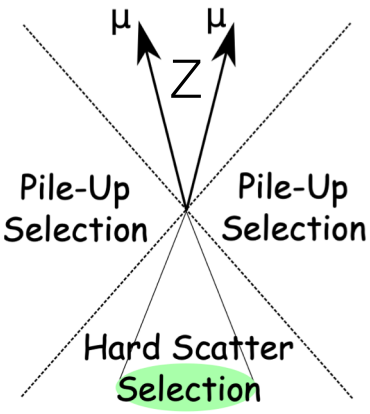

Regions of r–ϕ phase space which are expected to be dominated by hard-scatter jets (opposite in the η–ϕ plane to the Z → μμ decay) and where there is greater sensitivity to pile-up jet activity (perpendicular to the Z → μμ decay)

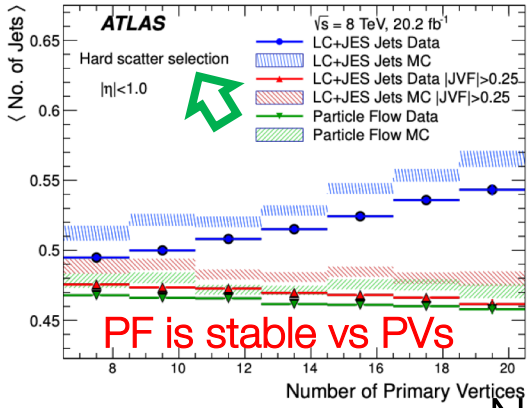

PF is stable vs PVs

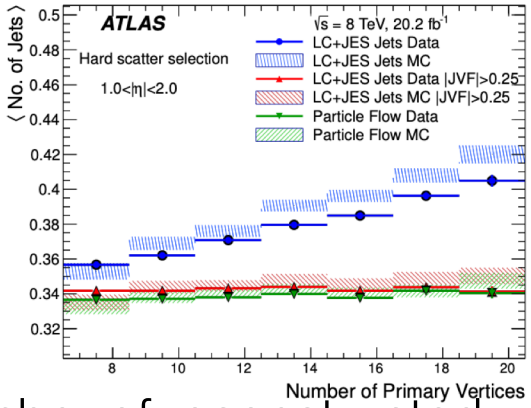

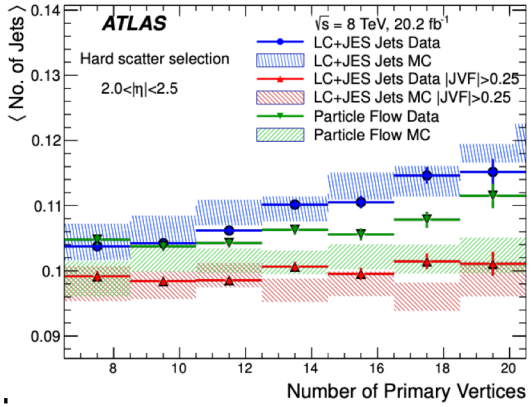

→ Number of reconstructed vertices

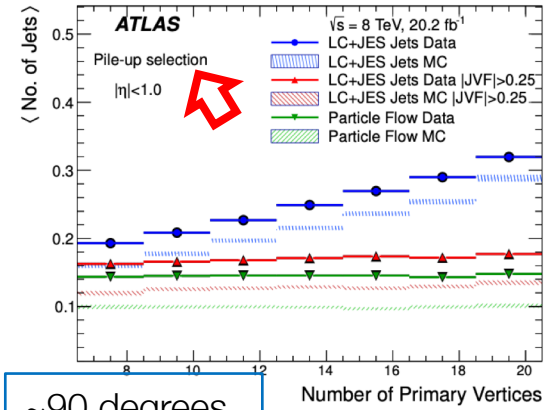

~90 degrees

(a) $|\eta| < 1.0$

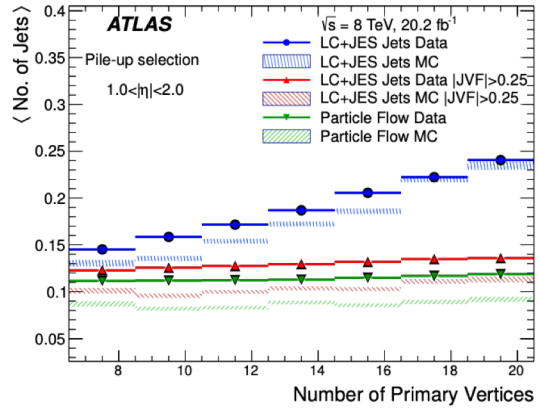

(b) $1.0 < |\eta| < 2.0$

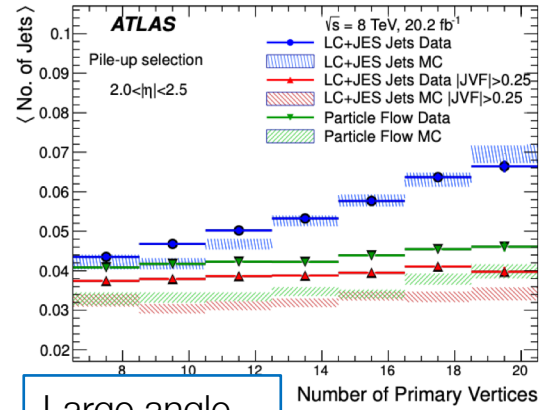

Large angle

(c) $2.0 < |\eta| < 2.5$

T

Resolution of PF

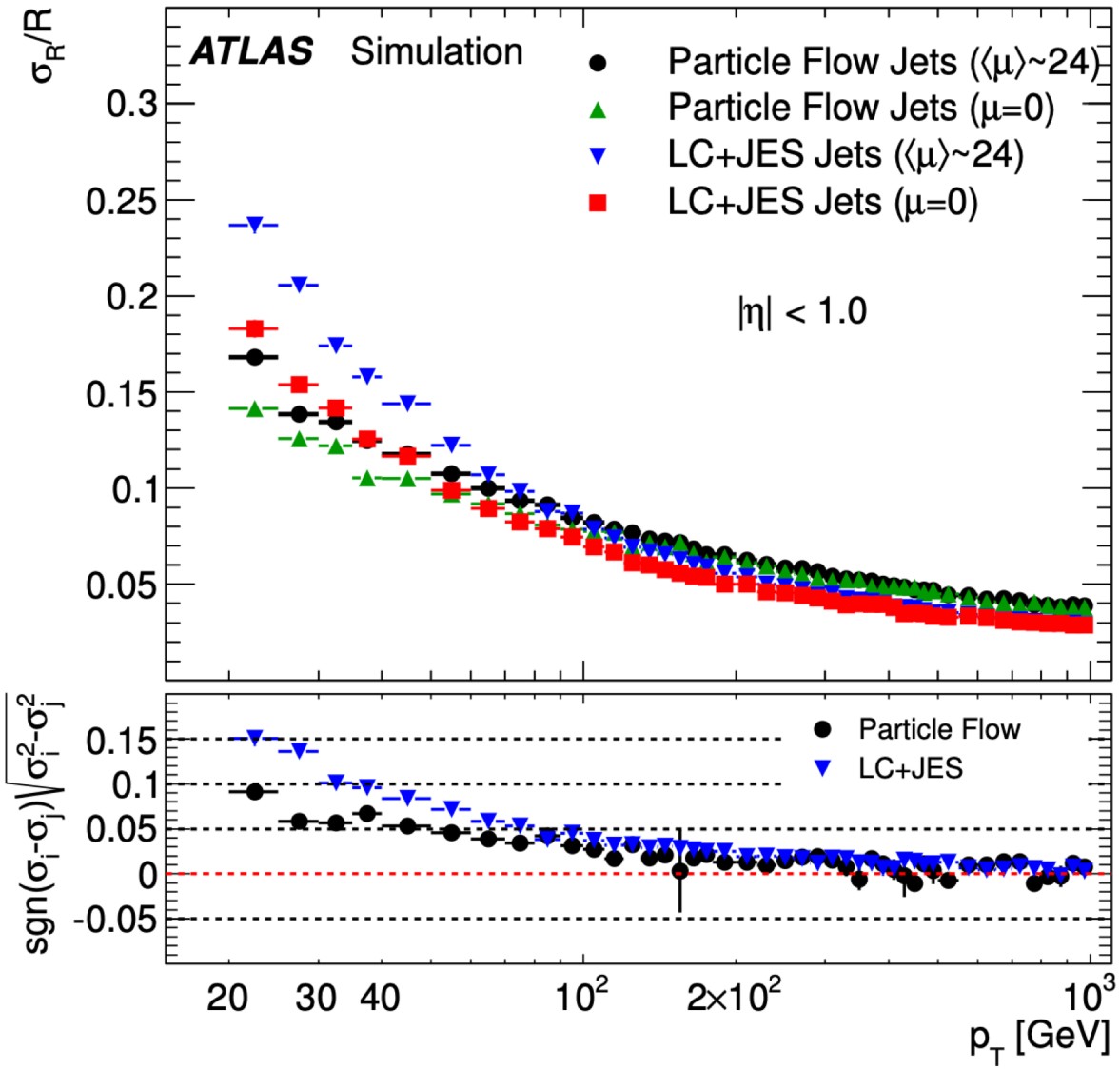

- Resolutions of calorimeter and PF jets as a function of p_T in di-jet simulation
- compared with pile-up μ=0 and μ=20 in the data.
- The quadratic difference in the resolution with and without pile-up is shown in the lower panel for LC+JES (blue) and particle flow (black) jets (what you have to add quadratically).